


UNIVERSITÀ DELLA CALABRIA

Dipartimento di Ingegneria Informatica, Modellistica,
Elettronica e Sistemistica

Scuola di Dottorato

Scienza e Tecnica "Bernardino Telesio"

XXVIII CICLO

Con il contributo della Regione Calabria

POR Calabria FSE 2007/2013 – Asse IV Capitale Umano

Obiettivo Operativo M.2

SURVEY, DIAGNOSIS AND MONITORING OF STRUCTURES AND LAND USING GEOMATICS TECHNIQUES: THEORETICAL AND EXPERIMENTAL ASPECTS

Settore Scientifico Disciplinare

ICAR/06

Direttore: Ch.mo Prof. Roberto Bartolino

Supervisore: Ch.mo Prof. Raffaele Zinno

Dottorando: Dott.ssa Serena Artese

SURVEY, DIAGNOSIS AND MONITORING OF STRUCTURES AND LAND USING GEOMATICS TECHNIQUES: THEORETICAL AND EXPERIMENTAL ASPECTS

RILIEVO, DIAGNOSI E MONITORAGGIO DI STRUTTURE E DEL TERRITORIO CON TECNICHE GEOMATICHE: ASPETTI TEORICI E SPERIMENTALI

La presente tesi è cofinanziata con il sostegno della Commissione Europea, Fondo Sociale Europeo e della Regione Calabria. L'autore è il solo responsabile di questa tesi e la Commissione Europea e la Regione Calabria declinano ogni responsabilità sull'uso che potrà essere fatto delle informazioni in essa contenute.

To my father

Abstract

The Geomatics techniques for the detection and representation of the land and objects have seen an exceptional development in recent years. The applications are innumerable and range from land planning to geophysics, from mitigation of landslide risk to monitoring of artifacts, from cultural heritage to medicine.

With particular regard to the structures and to the land, the technologies used can be divided into three categories: techniques based on the acquisition and processing of images, techniques based on the measurement of angles and distances, and combinations of the foregoing.

After an overview of Geomatics techniques and their basic theoretical concepts, a number of aspects have been thoroughly investigated. There follows a series of applications of the techniques described. Finally two new applications for deflection measurement of bridges under dynamic load are presented.

Riassunto

Le tecniche geomatiche per il rilievo e la rappresentazione del territorio e degli oggetti hanno avuto negli ultimi anni uno sviluppo eccezionale. Le applicazioni sono innumerevoli e spaziano dalla pianificazione del territorio alla geofisica, dalla mitigazione del rischio idrogeologico al monitoraggio di manufatti, dai beni culturali alla medicina.

Con particolare riguardo alle strutture e al territorio le tecnologie utilizzate possono essere distinte in tre categorie: tecniche basate sull'acquisizione ed il trattamento di immagini, tecniche basate sulla misura di angoli e distanze, combinazioni delle precedenti tecniche.

Dopo una panoramica delle tecniche geomatiche e dei rispettivi concetti teorici di base, alcuni aspetti sono approfonditi. Seguono una serie di applicazioni delle tecniche descritte. Infine vengono presentate due nuove applicazioni per la misura della deformazione di ponti sottoposti a carico dinamico.

Contents

Introduction

The continuing evolution of surveying techniques and 3D modeling, and, more generally, of Geomatic techniques based on sensors and the development of ever more efficient systems for the display of digital data, highlights the added value of the use of these methods in the field of evaluation, diagnosis and monitoring of structures and land.

In particular, there is a growing awareness about the active contribution that these technologies can provide in interpretation, storage, and data archiving and enhancement of detected objects.

The growing role of survey methods and digital three-dimensional modeling, in structural and territorial fields, is confirmed by the growth in demand, and their increasing use at different levels of scale and

resolution. Obviously the use of these instruments fits within the coding of a cognitive process, in which particular attention is paid to the integration of both traditional and innovative methods.

Some theoretical and experimental aspects related to surveying, diagnosis and monitoring of structures and land using geomatics techniques are described in this dissertation. Its structure and brief explanations of the chapters are presented as follows:

- **Chapter 1** explains the Geomatics techniques and the operating principles and the most common uses of the instruments for 3D data capture in the structural, cultural heritage and territorial fields.
- **Chapter 2** describes the case study of the Cavalcanti Palace. In order to evaluate the vulnerability of the building surveys on the building were carried out to define the state of degradation and the crack pattern. A special survey was carried out to check the verticality of the main facade using the total station.
- **Chapter 3** describes the survey of the Escuelas Pias Church in Valencia. The creation of the 3D model and results of some investigations has allowed the formulation of a hypothesis about the design of dome.

- **Chapter 4** describes the investigations carried out on the church of Santa Maria dei Longobardi, in San Marco Argentano, to understanding the structure of the facade.
- **Chapter 5** describes the activities, instruments and techniques used for surveying and modeling operations, along with the deviations between models and "as built", of ancient and modern bridges.
- **Chapter 6** describes the experiments conducted using the DIC method for the testing of some composite material specimens; the test has been integrated with an IR survey.
- **Chapter 7** describes the operations regarding the surveys of two landslides useful for evaluating dynamic and evolutionary mechanisms present in these areas and to predict possible scenarios of transformation.
- **Chapter 8** describes a new procedure to measure the dynamic deformation of a structure using a laser pointer.
- **Chapter 9** describes a new procedure to measure the dynamic deformation of a structure using laser scanner.
- **Chapter 10** presents the conclusions of this dissertation and recommendations for future research work.

1

Geomatics: techniques and tools for survey

Geomatics is a field of activity which,using a systematic approach, integrates all the means used to acquire and manage spatial data required as part of scientific, administrative, legal and technical operations involved in the process of production and management of spatial information. These activities include, but are not limited to, cartography, control surveying, digital mapping, geodesy, geographic information systems, hydrography, land information management, land surveying, mining surveying, photogrammetry and remote sensing.

Definition by the Canadian Institute of Geomatics in their quarterly journal "Geomatica"

Geomatics comes from the French word *gèomatique*. It comes from the greek *geo* (earth) and *informatics* (information + automation + ics) [Kemp, 2008].

The first use of this term is documented in the early 1970s, in France, when the Ministry of Equipment and Housing established the *Commission permanente de la géomatique*. After that this term was no longer used for several years.

In 1981, the term was reinvented by Michel Paradis, a French-speaking surveyor. He was a photogrammetrist working for the Ministry of Natural Resources in the Quebec Provincial Government, and used this term for a keynote paper he wrote for the 100th anniversary symposium of the Canadian Institute of Surveyng (which became the Canadian Institute of Geomatics)[Paradis, 1981].

With this term, he underlined the common aspects among the disciplines involved in data acquisition, processing, and dissemination of spatial data (surveying, photogrammetry, geodesy, hydrography, remote sensing, cartography, and GIS). In 1986, the Department of Surveyng at Laval University, driven by Pierre Gagnon, introduced the first academic program on geomatics in the world, thus replacing its surveying program [Bédard et al. 1987]. In 1989, the University changed the name of the Department (Geomatics Sciences), of the Faculty (Forestry and Geomatics) and

created the Centre for Geomatics.

Surveying departments at the University of Calgary and the University of New Brunswick also adopted this new name between the late 1980s and early 1990s, when they changed their identification as well as the titles of their degrees.

The term "geomatics" is nowadays widely used all around the world. It is commonly recognized that Canada is its motherland.

Geomatics includes the instruments and techniques used in land surveying, remote sensing, cartography, GIS (geographic information systems), GNSS (Global Navigation Satellite System), photogrammetry, geophysics, geography and mapping.

In a wider interpretation, Geomatics includes all techniques related to spatially referenced information.

There are many disciplines and techniques that constitute geomatics [Gomarasca, 2009]:

- Computer science: considered as a science of representation and the processing of applicable information through the development of technological tools (hardware) and of methods, models, algorithms and systems (software).
- Geodesy: the science that studies the shape and size of the Earth to define the reference surface in its complete form, the geoid, and in its simplified form, ellipsoid, and its external

gravitational field as a function of time.

- Topography: started with and as part of geodesy. It is the set of procedures of direct land surveying. Topography is a combination of methods and instruments to measure and represent the details of the Earth's surface by planimetry, altimetry, tachymetry and land surveying.
- Cartography: the description of the shape and dimension of the Earth and its natural and artificial details, by means of graphical or numerical representation of more or less wide areas, following fixed rules.
- Photogrammetry: the science that determines the position and shapes of objects by measuring them from photographic images.
- Remote sensing: the remote capture of data relating to territorial and environmental data, and the set of methods and techniques for their subsequent processing and interpretation.
- Global Positioning System (GPS): this is used to determine the three-dimensional (3D) position of fixed or moving objects, in space and time, all over the Earth’s surface, under any meteorological conditions and in real time.
- Laser scanning: this is used for the identification of subjects and the measurement of their shape and dimensions by means of the incident radiation in

the optical frequencies (0.3–15 μm) of the electromagnetic spectrum.

- Geographical Information System (GIS): a powerful combination of instruments capable of receiving, recording, recalling, transforming, representing and processing georeferenced spatial data.
- Decision Support Systems (DSS): These are associated with and made up of sophisticated information systems, able to create a number of evolutionary scenarios by modeling of reality and then to provide the decision maker's choice from various possible solutions.
- Expert System (ES): these are tools that can mimic cognitive processes made by the experts and their ability to manage the complexity of a real situation by means of interdependent processes of abstraction, generalization and approximation.
- WebGIS: these are networked systems for the dissemination of geographic data stored on machines dedicated to the storage of databases, according to a complex network architecture.
- Ontology: this is simplified view of the world that consists of a set of types, properties, and relationship types.

The Geomatics techniques use sensors. In particular, the three-dimensional sensors are tools to generate a

3D model of the scene they are surveying [Russo et al., 2011]. Of particular importance are the sensors based on the use of light radiation, within which a further distinction can be made according to the nature of the light used to perform the measurement. Methods using natural light are called "passive" (photogrammetric technique, theodolites, etc.); but if the light is encoded so as to play a role in the measurement process, they are called "active sensors" (laser scanners, structured light projection instruments, radar, total stations, etc.).

Active optical sensors [Blais, 2004; Guidi et al. 2010] map directly to the spatial position of the surface or the point detected, sometimes coupled to information color. This type of active instruments has the main advantage of acquiring directly and in a short space of time large amounts of data relating to a very complex geometry with an accuracy boost. The combination of these features makes this kind of instrument ideal for many applications, both at long and close range, but not suitable for all environmental conditions and the material characteristics of the artifacts [El-Hakim et al., 1995].

1.1 Total Station

The first instrument for the measuring of angles was the optical transit. In the 1970's, the electronic theodolite began to replace the optical transit because it measured angles more accurately. By the early 1980’s there appeared a new instrument called “total station" an electronic/optical device that was able to perform all necessary measurements (total) by using different techniques in one single device (station). It is, therefore, an electronic theodolite (transit) to read angles integrated with an Electronic Distance Meter (EDM) to read slope and distances, allowing storage of the measurements performed, without having to transcribe these accounts manually.

The basic components of a total station are [Ghilani and Wolf, 2011]:

- The alidade: the upper mobile part of instrumentation that includes, the telescope and EDM, the angle meausurment system, the vertical circle, the microprocessor, the keyboard and the display, and the communication port. It is a shell, made of light aluminum alloy. Inside, on the

uprights and at the bottom, are allocated the circles to the angular readings, the various sensors and electronic devices, with the relative cabling, necessary to the overall management of the station, and also, in the robot stations, small electric motors implementing controlled rotations of the alidade and telescope. In the lower part, there are also provided one or two openings, diametrically opposite, used for mounting the panel reserved for the keyboard and the display.

The telescope is short, has reticles with crosshairs etched on glass, and is equipped with rifle sights or collimators for rough pointing (recent models are equipped with laser pointers). The telescopes, generally, have two focusing controls. The first, the objective control, is used to focus on the object being viewed; the second, the eyepiece, is used to focus on the reticle.

The EDM, electronic distance meter, is assembled so that its axis coincides with the line of sight of the telescope, so the telescope and the EDM are coaxial. The distance measurement can be carried out with the reflector prism (range of some kilometers), or reflectorless in which the reflection takes place directly on the collimated object (range of two kilometers). The EDM uses electromagnetic (EM) energy to determine the length

of a line. The light radiation emitted by EDM to the prism reflectors, or to the surfaces of objects in the non-prism mode, comes from that reflected by the prisms and redirected to the device, which is detected by a photosensitive sensor. The radiation, then, is converted into electrical signals that allow the measurement of distance by means of the technique of phase measurement, that is, evaluated in the phase difference between the beam sent and the return, or the technique of measuring pulses, in which the flight time of a light pulse returning to the device is rated.

- The base: this is a static part of instrument which has three pivots inserted in three corresponding holes of the tribrach, and here retained by the security device.
- The tribrach: consists of an upper plate having three holes where the three correspondents pivots of the base are insert, a clamping device to secure the base of the total station or accessories, and a circular level (bull's-eye bubble); three screws for leveling; a lower plate with thread to attach the tribrach to the head of a tripod.
- The optical plummet and laser plummet: built into tribrach or alidade and permits accurate centering over a point. In newer instruments, laser plummets have replaced the optical plummet.

Three classes of total station are available: Manual, semiautomatic and automatic [Gopi, 2007]. With the manual station, it is necessary to read the horizontal and verticals angles manually. The Semiautomatic Stations have mechanical motors allowing motorised angle movements both on the vertical and horizontal axes. When a servo station is able to recognise and track a reflector prism, it is called an Automatic Station. This characteristc is called Autolock by Trimble and Automatic Target Recognition (ATR) by Leica. The position of target is recognised from the station using either radio waves or imaging technologies. When the station can be controlled from a distance via remote control it is known as a Robotic total station. In the late 1990s, the swedish Dandryd introduced the first robotic total station called the Geodimeter.

The very latest total stations offer several functionalities that benefit standard surveying, like the systematic survey of the control points located on a monitored structure, grid scanning and atmospheric correction. With the grid scanning function the surveyor can programme the station to measure points by specifying a view window area and setting the horizontal and vertical intervals of the points to be measured. Rather than needing to aim at each individual

point, it is only necessary to decide the optimum point interval, the grid interval, in order to represent the object with sufficient accuracy. The distance measurement is based on the evaluation of a light signal that penetrates the atmosphere, which depending on the variability of its condition, influences the precision of measurement. The latest total stations, once inserted weather conditions, automatically apply to crude measure carried out a due correction.

The maximum accuracy of Total Stations is 1 mm/km for the distance and 0.5” for the angles.

In recent years, total stations coupled to an antenna system were produced with a GPS receiver mounted statically on the same station, or traveling on a telescopic pole. This allows us to integrate satellite measurements with those made by the station, determining the position of the instrument or points detected.

Total Stations are used today in many fields of application: engineering, topography, geology, architecture, Industrial modeling, Marine, Archaeology and Cultural Heritage, monitoring. In recent years they have been used to measure the movement of structures and natural processes with good results [Hill and Sippel 2002; Kuhlmann and Glaser 2002; Cosser et al., 2003; Gairns, 2008].

1.2 Global Navigation Satellite System (GNSS)

The Global Satellite Navigation Systems (GNSS) are systems for geo-radiolocation and terrestrial, maritime or air navigation, based on a constellation of satellites which emit radio signals, designed for positioning and navigation on any point of the earth or in its vicinity, characterized by global coverage [Biagi, 2009].

Each system can be thought of as comprising three modules, or segments:

- **The space segment**: is represented by the satellite constellation.
- **The control segment**: consists of a global network of ground facilities that monitor the status of satellites, determines the ephemerides and satellite clock offsets and uploads the navigation data to the satellites.

  The current GPS control segment includes a master control station, an alternate master control station, 12 command and control antennas, and 16

monitoring sites. The master control station in Colorado generates and uploads navigation messages and ensures the health and accuracy of the satellite constellation.

The GLONASS ground segment consists of: A System Control Centre located at Krasnoznamensk, a network of five Telemetry, Tracking and Command centers (TT&C), the Central Clock situated in Schelkovo (near Moscow), three Upload Stations, two Laser Ranging Stations (SLR), a network of four Monitoring and Measuring Stations, six additional Monitoring and Measuring Stations are to start operating on the territory of the Russian Federation and the Commonwealth of Independent States in the near future.

- **The user segment:** this consists of the GNSS receiver equipment, which receives the signals from the GPS satellites and uses the transmitted information to calculate the user's three-dimensional position and time.

The satellite positioning is realized through a spatial intersection, taking into account that the positions of the satellites are considered known in the WGS84 system. To estimate the unknown coordinates of the generic receiver located on the Earth's surface, one must know a sufficient number of ranges, i.e

satellite-receiver distances, at a given instant.

The satellite positioning can be effected in three ways:

- **Absolute positioning:** the coordinates of the vertex on which is placed the receiver are estimated only by processing the observations which it made with respect to the acquired satellites, the receiver then works individually and, given the low accuracy attainable with this technique, they run only code measurements.
- **Relative positioning:** two or more receivers are placed in the simultaneous acquisition of the observations of common satellites; the components of the vector joining the two receivers (baseline) are estimated. This technique makes it possible to achieve better accuracies, because it eliminates or reduces biases involved in the measurements.
- **Differential positioning:** a receiver, called rover, placed on the vertex to detect and estimate its coordinates in absolute positioning. These coordinates are corrected by a differential correction calculated from a base station, placed on a point of known coordinates, or by a network of permanent stations which is sent to the rover. In this case you can obtain good accuracies. This technique can be applied to measurements of code or phase.

The differential positioning can be performed for obtaining fixed positions (static) or for tracking (cinematic), both in post-processing and in real time (RTK).

The satellite-receiver distance can be derived in two ways: pseudo-distance measures (code measures), and phase measures [Biagi, 2009].

To define the coordinates of a point, with the **pseudo-distance measures or code measures**, the signals of four satellites are needed simultaneously, because the unknowns are the three coordinates of the receiver (X_R, Y_R, Z_R) and the synchronization error of the receiver clock with respect to the clocks of the satellites (δt_R-δt^S):

$$P_R^S = \tau_R^S c = c\,(\Delta T_R^S - (\delta t_R - \delta t^S)) = \sqrt{(X_R - X^S)^2 + (Y_R + Y^S)^2 + (Z_R + Z^S)^2} \quad (1.2.1)$$

Where:

τ_R^S is the travel time of the signal from the satellite to the receiver;

c is the speed of light;

ΔT^S_R is the delay observed by the receiver R to the satellite S;

δt^S synchronous error of the satellite clock with respect to the reference time GNSS;

δt_R synchronous error of the receiver clock with respect to the reference time GNSS.

The receiver, after synchronization of its clock, replies the code of the satellite and through the measured delay ΔT^S_R obtains the pseudo-distance P^S_R.

The **phase measure** is based on the calculation of the phase difference between the phase of the L1 and L2 sent from the satellite and its replica generated by the receiver, i.e. a sine wave of equal frequency f.

The equation of observation at time t is:

$$\Phi_R^S(t) = \Phi_R(t) - \Phi_S(t - \tau_R^S) \quad (1.2.2)$$

Where:

$\Phi_R(t)$ is the phase of the oscillator of the receiver at the time of observation;

$\Phi_S(t- \tau_R^S)$ is the phase generated by the oscillator of the satellite at the time of sending the signal.

Knowing that the phase of the oscillator of the clock at time t is:

$$\Phi_i(t) = f_0[t + \delta t_i(t)] + \Phi(t_0) = f_0 t + f_0 \delta t_i(t) + \Phi(t_0) \quad (1.2.3)$$

one obtains:

$$\Phi_R^S(t) = f_0 t - f_0(t - \tau_R^S) + f_0 \delta t_R(t) - f_0 \delta t^S(t - \tau_R^S) + \Phi_R - \Phi^S$$
$$= f_0 \tau_R^S + f_0\big(\delta t_R(t) - \delta t^S(t)\big) + \Phi_R - \Phi^S$$

(1.2.4)

The correlator of the receiver does not measure the number of integer cycles elapsed between the sending of a signal and its reception, so to the equation of observation must be added $N_R^S(t)$, integer ambiguity, which represents the number of carrier cycles including that between satellite and receiver, not directly observable:

$$\Phi_R^S(t) = f_0 \tau_R^S + f_0\big(\delta t_R(t) - \delta t^S(t)\big) + \Phi_R - \Phi^S + N_R^S(t) \quad (1.2.5)$$

To obtain the observation in metric units, the equation of observation in cycles is multiplied by the wavelength of the signal:

$$L_R^S(t) = \lambda \Phi_R^S(t) = c\tau_R^S(t) + c\big(\delta t_R(t) - \delta t^S(t)\big) + \lambda(N_R^S(t) + \Phi_R - \Phi^S)$$

(1.2.6)

The term of integer ambiguity of the phases is a multiple of 19 cm for L1 and a multiple of 24 cm for L2. To obtain the ranges, single, double and triple differences are computed. Single Difference is the difference between the phases received by two receivers

from the same satellite, Double Difference is the difference between two single differences computed for two stations and two satellites. Triple Difference is the difference between two double differences from measurements recorded at subsequent epochs. Assuming no cycle slips, or loss of lock has occurred, this eliminates the integer ambiguity, hence used to detect cycle slips and loss of lock.

Taking into account the tropospheric (T_R^S) and the ionospheric (I_R^S) effects, the single difference equation is:

$$L_{R1,R2}^{S}(\mathrm{t}) = c\tau_{R1}^{S}(t) - c\tau_{R2}^{S}(t) + c\left(\delta t_{R1}(t) - \delta t_{R2}(t)\right) + T_{R1}^{S}(\mathrm{t}) - T_{R2}^{S}(\mathrm{t}) - I_{R1}^{S}(\mathrm{t}) + I_{R2}^{S}(\mathrm{t}) + \lambda(N_{R1}^{S}(t) - N_{R2}^{S}(t) + \Phi_{R1} - \Phi_{R2}) \quad (1.2.7)$$

While the double difference is

$$L_{R1,R2}^{S1,S2}(\mathrm{t}) = c\tau_{R1}^{S1}(t) - c\tau_{R2}^{S1}(t) - c\tau_{R1}^{S2}(t) + c\tau_{R2}^{S2}(t) + T_{R1}^{S1}(\mathrm{t}) - T_{R2}^{S1}(\mathrm{t}) - T_{R1}^{S2}(\mathrm{t}) + T_{R2}^{S2}(\mathrm{t}) - I_{R1}^{S1}(\mathrm{t}) + I_{R2}^{S1}(\mathrm{t}) + I_{R1}^{S2}(\mathrm{t}) - I_{R2}^{S2}(\mathrm{t}) + \lambda(N_{R1}^{S1}(t) - N_{R2}^{S1}(t) - N_{R1}^{S2}(t) + N_{R2}^{S2}(t)) \quad (1.2.8)$$

The sources of error in the estimation of the actual position of a GNSS receiver are different, and each one has a different impact on the final calculation. Errors can be summarized as:

- **Selective Availability (SA):** is the introduction

of deliberate errors in the satellite signals in order to reduce the accuracy of the detection, allowing accuracies only in the order of 100-150 m. Such signal degradation was disabled on May 1, 2000.

- **Satellite Geometry:** this describes the relative position of the satellites from the point of view of the observer-receiver. If a receiver sees four satellites that are all arranged in the same area, such as the north-west, this leads to poor geometry. If the four satellites are well distributed throughout the firmament, the calculated position will be much more precise.
  To indicate the satellite geometry, the indices DOP (Dilution of Precision) are commonly used.
- **Orbit Satellite:** Although satellites are positioned carefully on extremely precise orbits, slight deviations of the same are possible because of gravitational forces. The data of the orbits are checked and adjusted regularly, and they are sent to the receivers in the data set containing the ephemerides.
- **Multipath (>10m):** this is due to the presence, in the vicinity of the receiver, of surfaces capable of reflecting the signal. To obviate this problem, the antennas are equipped with an appropriate screen, ground plane, which prevents, at least in

part, the reception of the reflected signals from the ground.

- **Atmospheric Effects:** the speed of propagation of the radio signals is reduced when the signals pass through the troposphere (delay from 2 to 10m) and the ionosphere (delay from 10-30m up to loss of lock), compared to the speed of propagation in the vacuum in which propagation is at the speed of 299,792,458 m/s.

  The ionospheric noise is due to the layers of atmosphere between 100 km and 1000 km altitude where there are ions and free electrons which interfere with the propagation of the GNSS. The local refractive index takes the following value:

$$n(r) = 1 \pm \frac{A \cdot N_E(r)}{f^2} \qquad (1.2.9)$$

Where:

$A=40.3\ m^3s^{-2}$

f is the signal frequency in Hz

$N_E(r)$ is the density of electrons, in number$\times m^3$, in a point.

By integrating along the path through the ionosphere one obtains, in metric units:

$$I_R^S = \int_{Iono_R^S} (n(r) - 1)dr$$

$$= \pm \int_{Iono_R^S} A\frac{N_E(r)}{f^2}dr = \pm\frac{A}{f^2}\int_{Iono_R^S} N_E(r)dr = \pm A\frac{TEC_R^S}{f^2}$$

(1.2.10)

Where TEC_R^S, Total Electron Content, i.e. the density of free electrons along the signal path per unit area. The content of electrons in the ionosphere varies significantly depending on the intensity of solar radiation incident in the atmosphere, which in turn depends on the intensity of solar activity and time of day; thus ionospheric disturbance presents great variability.

The GNSS receivers that use a single frequency partially eliminate the ionospheric effect by means of a model such as the Klobuchar model [Klobuchar, 1986] for the GPS and the NeQuick model [Arbesser and Rastburg, 2006] for the future Galileo, contained in the internal software of the receiver and whose parameters are contained in the navigation message transmitted from the satellite. Two frequency receivers allow the determination of TEC by using the different delays of the signals or by calculating the so-called iono-free combination.

The tropospheric noise is present from the ground to about 80-100 km altitude. Itis caused by the air and, in the layer of the first 10 km, by the presence of water vapor [Saastamoinen, 1972].
Given the local refractive index:

$$n(r) = 1 + k_1 \frac{P(r)}{T(r)} + k_2 \frac{e(r)}{T(r)} + k_3 \frac{e(r)}{T^2(r)} \qquad (1.2.11)$$

where *P(r)* is the pressure in mBar, *T(r)* is the temperature in °K, *e* is the partial pressure of water vapor in mBar and the constants are $k_1=77,624 \cdot 10^{-6} °K \cdot Bar^{-1}$, $k_2=-12,920 \cdot 10^{-6} °K \cdot Bar^{-1}$, $k_3=37,19 \cdot 10^{-2} °K^2 \cdot Bar^{-1}$,
by integrating, one obtains:

$$T_R^S = \int_{Tropo_R^S} \left(k_1 \frac{P(r)}{T(r)} + k_2 \frac{e(r)}{T(r)} + k_3 \frac{e(r)}{T^2(r)} \right) dr$$
$$= \pm \int_{Tropo_R^S} k_1 \frac{P(r)}{T(r)} dr + \int_{Tropo_R^S} N_E \left(k_2 \frac{e(r)}{T(r)} + k_3 \frac{e(r)}{T^2(r)} \right) dr \qquad (1.2.12)$$

The first integral is called dry or hydrostatic component of the noise and contributes to about 90% of the total noise, the second is called moist component and contributes to the remaining 10%.

- **Synchronization errors and rounding (>10m):** the

offsets of the clocks of board leads to a lack of synchronism between the incoming signal from the satellite and the duplicate from the receiver, introducing an error in the estimate of the distance of approximately 2 m. Rounding and calculating errors of the receiver add another meter.

- **Relativistic effects:** the relative speed of movement of a satellite with respect to the ground slows down the time on the satellite approximately by 7 microseconds per day, while the gravitational potential, lower on orbit of the satellite with respect to the ground, accelerates it by 45 microseconds. Therefore, the balance is that time on the satellite speeds approximately of 38 microseconds per day. To obviate the difference between clocks on board and ashore, the clocks on the satellite are corrected electronically. Without these corrections, the system generates GNSS position errors to the order of kilometers on a day of use.

Two GNSS systems are fully operative:

- **NAVSTAR GPS** (NAVigation System Timing And Ranging Global positioning System) or GPS: developed in 1973, with global and continued coverage, it is operated by the U.S. Department of Defense. The GPS

service was opened to the world for civilian use in 1991 by the USA under the name SPS (Standard Positioning System), with specifications different from the military system called PPS (Precision Positioning System). The main difference between the two systems was represented by the presence in the GPS system of Selective Availability (SA). It provides real-time position according to the WGS84 (World Global System 1984) geodetic reference system, valid for the whole Earth. In 1995, it its full operation was officially declared, i.e. the real-time navigation is guaranteed 24 hours a day.
The system presently consists of 31 operational satellites, but the United States is committed to maintaining the availability of at least 24 operational GPS satellites. The satellites are arranged in six orbital planes inclined at 55° with respect to the equatorial plane, so not covering the polar zones, in the shape of ellipses with a low eccentricity. Each orbital plane has 4 satellites, and the planes are disposed in such a way that every user on earth can receive signals from at least 5 satellites. The satellites altitude is 20.183 km and do two complete orbits in 11h 56m. Each satellite emits on the frequencies of 1575.42 and 1227.60 MHz, derived from a single oscillator with high stability clock equal to 10.23 MHz which

is multiplied, respectively, by 154 and 120 to obtain the frequency of the two carriers. The purpose of the double frequency is to eliminate error due to ionospheric refraction [Spaans, 1984; Wells, 1987; Achilli et al., 1993; Hoffmann-Wellenhof et al., 1994; AC01663170, 1995; Cina, 2000; Tsui, 2000; van der Marel, 2000; Alfred, 2004; Kaplan and Hegarty, 2005; Van Sickle, 2008].

- **GLONASS** (GLObal NAvigation Satellite System): this was designed and programmed in the mid-1970s, by the ex Soviet Union and is managed by Russia. The launch of the first satellite dates back to October 1982 and the constellation was completed, in the period of maximum efficiency with 24 satellites, in 1995. In the following years, due to the severe internal economic situation, Russia was not able to sustain the entire constellation. In 2002, with the improvement of the economic situation, the program of revitalization of GLONASS began.
  Currently the system is fully operational. It consists of 24 operational satellites distributed on three orbital planes, inclined at 64,8° with respect to the equatorial plane, that are 120° equidistant from one another, each containing eight satellites, uniformly distributed with a step of 45◦. The satellites altitude is 19.140 km and do

two complete orbits in 11h 15m. Each satellite emits on the frequencies of 1602 and 1246 MHz.

In 2003, the European Union approved the project of the European constellation called GALILEO. The full operation is planned for the end of 2019 and will count 30 satellites orbiting on three inclined planes with respect to the equatorial plane of about 56°, and at an altitude of 23,222 km. The orbits that will be followed by the satellites are MEO, Medium Earth Orbit.

There are, also, navigation satellite systems designed to cover specific areas of the globe. China has its own constellation, called Beidou Satellite Navigation and Positioning System, BDS, which currently operates on the h24 geographical rectangle between 70 ° East, 5 ° North and 140 ° East, 55 ° North. The development was announced of system coverage from local to global, with the COMPASS project, consisting of 27 satellites in MEO orbit, 5 geostationary and 3 in IGSO orbit, whose completion is expected before 2020. Japan has the QZSS constellation, Quasi-Zenith Satellite System, which currently offers interoperability to the GPS on Japan and neighboring regions. India has started the project of the IRNSS constellation, the Indian Regional Navigational Satellite System.

There are, lastly, the Satellite-based Augmentation

Systems, SBAS, consisting of a constellation of geostationary satellites with the task of sending differential corrections, calculated by a network of permanent stations on the ground, on the L1 frequency. In this way the accuracy of GNSS navigation and positioning is improved by up to 1-3 meters; each SBAS offers guaranteed accuracy through signal integrity and provides further useful signals to positioning. In Europe EGNOS is available (European Geostationary Navigation Overlay System), consisting of three geostationary satellites, equivalent to the US WAAS and the Japanese MSAS.

1.3 Laser Scanning

A **laser** is a device that converts energy from a primary form (electrical, optical, chemical, thermal or nuclear) to a beam of monochromatic, coherent electromagnetic radiation of high intensity: the laser light.

The fundamental discovery that allowed the emission of laser light is due to A. Einstein in 1917 [Einstein, 1917]. The term "L.A.S.E.R." is an acronym for "Light Amplification by Stimulated Emission of Radiation". It took several decades to achieve practical implementation of the instrument [Bertolotti, 1985; Trainer, 2010]. In 1954, H. Townes, J.P. Gordon and H.J. Zeiger (Columbia University, New York) [Gordon et al.,1955], and, independently, N.G. Basov and A.M. Prokhorov (Lebedev Institute, Moscow) [Basov, 1955], managed to realize the first microwave amplifiers based on the process of stimulated emission, the precursor to the laser, which were called MASER (Microwave Amplification by Stimulated Emission of Radiation). In 1958, Charles Townes and Arthur Schawlow theoretically developed the idea of an optical

amplifier enclosed within a pair of reflecting mirrors to form a resonant cavity intended to select and to amplify the light waves of a particular length [Schawlow and Townes, 1958]. Two years later, in 1960, Theodore Maiman created the first working laser. Maiman's laser was a "pink" ruby rod, with its ends silvered, placed inside a spring-shaped flashlamp [Maiman, 1960].

Just before the end of 1960, Ali Javan, William Bennet, and Donald Herriot made the first gas laser (a He-Ne laser) using helium and neon [Javan et al., 1961]. This laser is used in such applications as reading Universal Product Codes and surveying equipment. Charles Townes, in 1964, shared The Nobel Prize in Physics with Alexsandr M. Prokhorov and Nikolai G. Basov *"for fundamental work in the field of quantum electronics, which has led to the construction of oscillators and amplifiers based on the maser-laser principle"* [The Nobel Foundation].

The laser, from the physical point of view, is an electromagnetic radiation, or light wave, having this characteristics [Bornaz, 2006]:

- Monochromatic: must consist of a single frequency of light.
- Spatial coherence or unidirectionality: a laser beam doesn’t diverge (or rather, has a very low divergence) and this feature enables it not to lose

power and spread over a great distance.

- Temporal consistency: this must consist of waves of the same frequency and the same phase which are added to each other giving rise to a train of light which can be pushed with high intensity and high power output.

More simply, it is possible to define the laser as a focused monochromatic light radiation, formed by parallel waves in phase with each other.

At the present time, the condition of spatial coherence or unidirectionality is difficult to reach. The beams that make up a laser emission, in fact, are "virtually" parallel, or are suffering from a slight divergence that, within short distances, is absolutely negligible.

The phenomenon of divergence of the laser beam is linked to the limited size of the cavity in which it is produced as well as to the diffraction phenomenon due to the exit window of the beam.

In the absence of the phenomenon of divergence, a laser beam incident to any single surface, would have an almost punctiform section. The divergence of the beam is such that the actual footprint of impact, instead of a point, is an area (typically quite small).

Lasers are classified, depending on the nature of the active material used, substances that produces laser

radiation, into: solid state lasers, gas lasers, Semiconductor laser, Liquid Laser, Free electron laser.

Depending on their characteristics, lasers are grouped according to classes of hazard. The *IEC (EN) 60825-1:2001 "Safety of laser products part 1: equipment classification, requirements and user's guide"*, defines laser classes and measurement conditions, labelling, engineering controls etc, maximum permissible exposures (MPE) and accessible emission limits (AEL). The classes normally used are Class 1, 1M, 2, 2M, 3R, 3B. Class 4 lasers are not used for scanning instruments. Some recent terrestrial medium range instruments (e.g. Z+F IMAGER® 5010C) use a class 1 laser (*Lasers that are safe under reasonably foreseeable conditions of operation, including the use of optical instruments for intrabeam viewing).* The most powerful models can measure distances up to 6 km (Riegl VZ 6000) and use a Class 3B Laser *(Lasers that are normally hazardous when direct intrabeam exposure occurs – i.e. within the Nominal Ocular Hazard Distance. Viewing diffuse reflections is normally safe).*

Laser Scanning is a survey technique which allows us to obtain the shape, size and position (digital model) of objects by measuring, across short intervals of time, an extremely high number of points (in relation

to the amplitudes detected and the scanning step imposed) belonging to the surface of the same objects, using special instruments known as laser scanners.

3D laser scanning technology was developed during the last half of the 20th century in an attempt to recreate accurately the surfaces of various objects and places. The first 3D scanning technology was created in the 1960s. The early scanners used lights, cameras and projectors to perform this task. Due to limitations of the equipment, it often took a lot of time and effort to scan objects accurately. After 1985, they were replaced with scanners that could use white light, lasers and shadowing to capture a given surface [Abdel, 2011].

Since the appearance of the first Laser Scanners on the market, dramatic improvements in terms of measurement speed, accuracy and general usability can be observed over the last twenty years. The development of the Laser Scanner can be roughly categorized into four phases, or generations [Rudolf, 2011]:

- 1st generation (from 1997): The instruments are bulky, look like prototypes and the data storage and the power supply are external. The measurement frequency is between 1 and 5 kHz within a range of 50 to 200m. All systems are pulse based. Typical representatives are: CYRAX 2200, RIEGL LMS Z210.
- 2nd generation (from 2002): The data storage and

the power supply are still external to the instrument, but the systems become faster. The first phase based systems appear on the market. Typical representatives are: CALLIDUS, CYRAX 2500, ZOLLER + FRÖHLICH IMAGER 5003.

- 3rd generation (from 2007): The manufacturers start integrating the data storage and the power supply into the instrument. The range and the measurement speed are improved. Digital images are more and more combined with point clouds. Forced centering systems and reflectors or GNSS-antennas on top of the instruments allow a closer cooperation with traditional surveying methods. Typical representatives are: FARO PHOTON, ISITE 4400, LEICA SCAN STATION, RIEGL LMS Z-420i, ZOLLER + FRÖHLICH IMAGER 5006.
- 4th generation (from 2009): The data storage and the powering are fully integrated. The camera is also part of the acquisition and data treatment process. RIEGL introduces the Full-Wave-Form-Analysis, allowing the detection of multiple echoes in one measurement. In addition, the performance in terms of measurement speed and range is again improved. Typical representatives are: FARO FOCUS, RIEGL VZ 1000, ZOLLER + FRÖHLICH IMAGER 5010.

Laser scanning or Light Detection And Ranging (LiDAR)

systems use lasers to make measurements from a tripod or other stationary mount, a mobile terrestrial vehicle, or an aircraft [Pirotti et al., 2013].

The choice of instrument [Romsek, 2008; Boehler et al.,2003] must be carried out according to the specific use and taking into account multiple characteristics: accuracy; acquisition rate; measuring range; wavelength of the laser beam, taking into account the possible sources of exterior noise (sunlight, humidity) and the reflectivity of the scanned surfaces; field of view of the instrument; allocation of digital cameras inside or outside; ease of transport; type of power; capture software quality.

Laser Scanners can be classified [Blais, 2004], according to the technology used for the measuring distances, into three types:

- **Optical Triangulation:** The components of a triangulation laser scanner are, mainly, a laser source, a scanning mirror to direct the laser beam (generally a Mirror Galvanometer Scanner), a CCD and a lens (figure 1.3.1). The position of a point on the object is obtained by triangulation. In fact, it is solved a triangle in which the base and the adjacent angles are known. The angle of the light beam leaving the scanner is internally recorded, the angle of the laser beam incident on the CCD is also recorded and the base (the distance

between laser emitter and the center of the CCD receiver) is known from calibration. This type of scanner reaches 3D point standard deviations of less than 0.1 millimeter at very close range, less than 2 meters. The accuracy depends on both the length of the scanner base and the object distance.

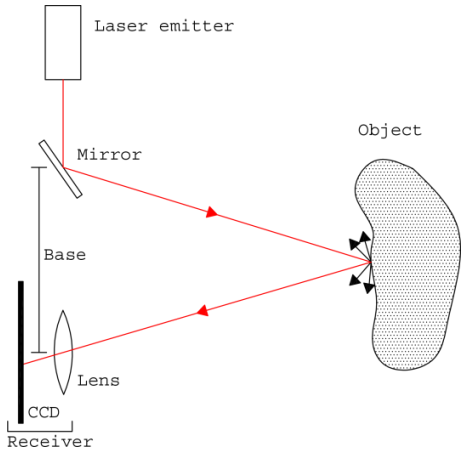

Figure 1.3.1: Principle of a triangulation laser scanner.

- **Time Of Flight (TOF):** is composed of a pulsed laser emitting the beam, a mirror reflecting the beam towards the scanned area (generally a Rotating Mirror Scanner), and an optical receiver subsystem, which detects the laser pulse reflected by the object (Figure 1.3.2). Since the speed of light is known, the travel time of the laser pulse can be converted to a precise range measurement. For short

and medium distances, the atmospheric characteristics do not affect the accuracy of range measurement. One can then write:

$$2D = v\Delta t \qquad (1.3.1)$$

Where:

D is the measure of distance.

v = c is the speed of propagation of the impulse in the medium considered (c_0 = 299,792,458 m/s).

Δt is the flight time.

To obtain a 5 mm accuracy, a time resolution of 33 ps in the electronics or an equivalent bandwidth of at least 30 GHz is required.

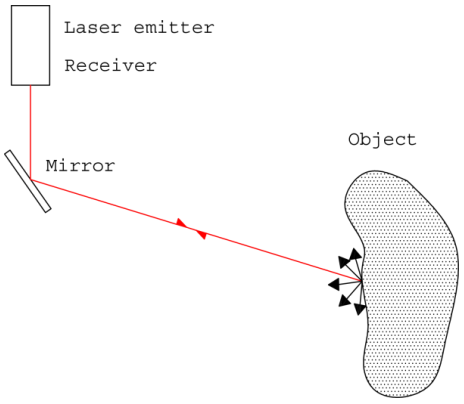

Figure 1.3.2: Principle of a Time Of Flight laser scanner.

Picosecond resolution implies very sensitive

electronics with high bandwidth, constant group delays, and excellent thermal stability [Blais, 2004]. Accuracy in the measurement is directly related to the signal-to-noise ratio. To reduce noise, multiple pulses are averaged, and resolution in the order of 1 to 10 mm is now standard; stability, especially thermal, and non constant group delays (drift and jitter) are major concerns that must be faced. Different methods have been proposed to create a reference signal used to auto calibrate the system. High-frequency bandwidth in the electronics is needed to amplify the large-frequency spectrum associated with pulses.

The maximum measurable range is, presently, of about six kilometers. The accuracy is between one millimeter and three centimeters, depending on the object distance.

A kind of TOF is a Waveform processing laser scanner [Mallet and Bretar, 2009], or echo digitization laser scanner, that uses pulsed time of flight technology and has real time waveform processing capabilities to identify multiple returns or reflections of the same signal pulse, resulting in multiple object detection.

- **Phase based:** the emitted laser light is modulated into multiple phases and the phase shifts of the

returned laser energy are compared. The scanner uses phase-shift algorithms to determine the distance based on the unique properties of each individual phase (figure 1.3.3).
The range is 25-350m.

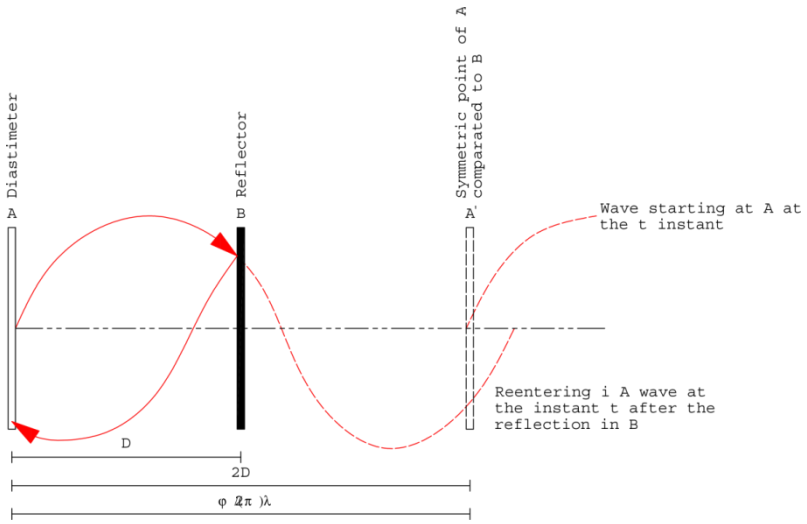

Figure 1.3.3: Principle of a Phase based laser scanner.

Let us consider, as an example the case of a wave with a wavelength (λ) and suppose we want to measure, using this wave, a distance of less than λ/2. The wave, after covering the distance D, is reflected on the opposite end and goes back to the starting point. The phase shift measured between the transmitted wave and the received one will be a function of the distance D. Let A be the emission point and B the point of reflection of the wave.

Let A' be the symmetric point of A with respect to B (which is then 2D distant from A). The distance D is:

$$D = \frac{\varphi}{2\pi} \cdot \frac{\lambda}{2} + n\frac{\lambda}{2} \quad \rightarrow \quad D = L + n\frac{\lambda}{2} \qquad (1.3.2)$$

where:

f = frequency

φ = phase shift

λ = wavelength = c/f

c = velocity of propagation

n = ambiguity

To measure a distance with a phase-based distance meter, it is therefore necessary to measure the phase shift φ and evaluate, without error, the integer number of half wavelengths.

Laser scanner measurements

The procedure for determining the coordinates of a point is distinct in two steps: data acquisition and calculation of the position.

Data acquisition involves three tasks (system calibration, georeferencing, measurement); the calculation of the position is obtained by data processing, which involves several steps: filtering and

deleting of features not belonging to the object; narrowing of the data; coordinate transformation and interpolation.

The greatest strengths of the laser scanner are: high speed and degree of automation; the survey is practically not affected by light conditions; very accurate three-dimensional geometric information; evaluation of the different reflectance values and, thus, possibility of evaluating the type of material constituting the detected object; possibility of integrating the survey with orthophotos or photos; possibility, through the analysis of the virtual model 3D, of visualizing and studying the object in terms of different aspects.

The accuracy of the laser scanner is directly affected by [Godin et al., 2001; Lichti et al., 2002; Voegtle et al., 2008; Beraldin et al., 2007]:

- the quality of the internal device that performs the measurement;
- the characteristics of the scanned material and scene, in terms of reflection, light diffusion and absorption (amplitude response);
- the orientation and the local shape of the surface struck by the laser;
- the characteristics of the working environment;
- the coherence of the backscattered light (phase randomization);

- the chromatic content of the scanned material (frequency response).

When radiation hits the surface of a real body, also called gray body, it is partially absorbed by the body, in part reflected by the surface and in part transmitted. The following dimensionless coefficients can be defined (varying between 0 and 1), which measure the interactions between energy and matter: Absorptivity (α): the ratio EA/EI between absorbed and incident energy; Reflectivity (ρ): the ratio ER/EI between the reflected energy and the incident energy; Transmissivity (τ): the ratio ET/EI between the transmitted and the incident energy.

Generally, the perfectly smooth surfaces reflect in a specular way, those wrinkled behave as perfect Lambertian reflectors, i.e. the direction of reflection is independent of that of incidence. Normally, the real surfaces do not behave as surfaces which are perfectly specular nor perfectly Lambertian surfaces but rather show an intermediate behavior (figure 1.3.4).

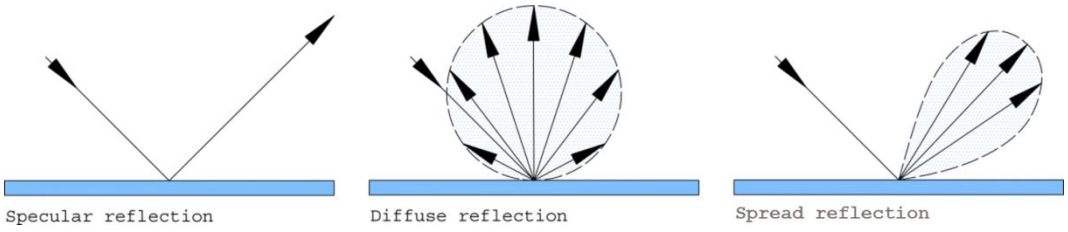

Figure 1.3.4: Specular, diffuse (Lambertian) and spread reflection from surface.

Data Acquisition

The laser scanner, once centered on a place and leveled, scans the desired object and returns its digital model in the form of a cloud of points. The design phase of the scan, a proper acquisition of the photographic images if a mapping of the photos on the 3D model is required, and the proper disposition of the eventual targets are essential steps for correct surveying [Sgrenzaroli and Vassena, 2007]. The project of a laser scan survey can be performed considering the model of the used laser (precision, maximum range, acquisition rate, field of view), the subject you want to detect (the geometry and the size of the object) and the environment in which you can find the subject.

To correctly perform a survey one must:

- scan in multiple locations: the choice of the number of scans depends on the field of view of the scanner.
- place targets inside the area detected or on the object to be detected, in order to ensure the geo-referencing of scans and allow their union. From every point of the scan at least 3 well positioned targets must be visible. The target can be of various types and vary in shape, size, and material; these features ensure that the target can be identified automatically by the acquisition software supplied with the instrument.

- if it is not possible to position artificial targets, one can use features recognizable on the scanned object [Gressin et al., 2012; Jaw and Chuang, 2008; Chillemi and Giacobbe, 2007]; features can be flat elements (stains, paintings, changes of the plaster) or spatial discontinuities (edges, holes). In other cases, it may be possible to replace the targets with a prism to be measured from a total station or with a GNSS receiver. Targets, prisms or antennas should be scanned at high resolution.
- reduce shadows and occlusions: the maximum visibility of the area to be detected must be guaranteed by reducing the phenomena of shadows due to the presence of objects, undercuts, etc.
- take into account the angle of acquisition: the quality of 3D points obtained by the laser scanner is also a function of the angle at which the laser beam is incident on the surface to scan.
- have a good overlap between the scans to ensure the completeness of the 3D model, avoiding shadows and occlusions, and a good union of the scans in the case of use of a targetless registration.
- try to have a homogeneous resolution scans in order to ensure the homogeneity of the geometric model both in terms of accuracy and of "density" of the point cloud.

Each laser scanner is equipped with a software designed specifically for the management of the acquisition phase. In general, these programs allow the definition of the general parameters of the acquisition (step scan, scan area), the real-time visualization of the results of the acquisition by a series of clouds of points, coloured in order to evidence the distances measured, and any RGB image recorded during the acquisition. After scanning, the operator can observe the acquired points in the monitor, change the point of view of the scan and move in the acquired point cloud in order to check its completeness.

Data Processing

The software for scans processing, as well as allowing the control and management of data acquisition, allows the pre-treatment of the acquired data (data cleaning, noise reduction, filtering and registration of point clouds), meshing (surface reconstruction, hole filling, smoothing), integration with other information (texturing), georeferencing and the extraction and export of geometric information [Karbacher et al., 2001; Bernardini and Rushmeier, 2002; Remondino, 2003; Rüther et al., 2014; Gomes et

al., 2014].

The data cleaning and filtering operation is necessary because of: the partial reflection of the laser on the edges; the errors in the calculation of the distance due to the presence of materials with different reflectivity; the presence of erroneous points caused by very bright objects; the atmospheric effects. To these errors should be added the points caused by the reflection of background objects, reflections originated in the space between scanner and the object (trees or objects in the foreground, people moving or traffic) and multiple reflections of the laser beam.

Registration

Each scan is carried out from a different point: thus, the point cloud coordinates are referred to a different local Cartesian reference system. Each reference system is centered in the instrument and arbitrarily oriented: it derives from this that the various point clouds related to the same object are independent, without any geometric links known *a priori*.

Registration is the set of all the operations needed to define the parameters of rotation and translation

that allow us to refer the various clouds to a single reference system.

The reference systems are the Intrinsic Reference System (IRS), an interior reference system, centered to the instrument, that gives relative coordinates, and the System Object Reference, usually materialized through a series of Ground Control Points GCP) with known coordinates. GCP are natural points or artificial targets identified individually in the scan.

The transformation from the intrinsic reference system in a given scan in the reference object system is made through a 3D rigid roto-translation, whose parameters can be calculated on the basis of control points, whose coordinates are known in both systems [Crosilla and Beinat et al., 2003].

The recording techniques based on the use of points, pre-signalized or not, assume that adjacent scans have a sufficient degree of overlap, not less than 30%, and that within this range there exist pre-signalized points, or directly detectable in the point clouds, of sufficient number to ensure the estimation of the parameters of the spatial transformation, which, as is known, is based on the following equations:

$$\begin{pmatrix} X_1 \\ Y_1 \\ Z_1 \end{pmatrix} = \begin{pmatrix} X_u \\ Y_u \\ Z_u \end{pmatrix} + \mathbf{R} \cdot \begin{pmatrix} X_2 \\ Y_2 \\ Z_2 \end{pmatrix} \qquad (1.3.3)$$

where X1, Y1, Z1 are the coordinates in the reference system of the first scan, X2, Y2, Z2 the coordinates in the reference system of the second scan, Xu, Yu, Zu the coordinates of the origin of the reference system of the second scan, and R the rotation matrix that rotates the axes of the reference system of the second scanning by making them parallel to those of the reference system of the first scan.

The relationship that links together the different scans can be defined in a direct way already during the acquisition of the measures, or it can be derived in an indirect way acting analytically on the 3D numerical models produced for each scan.

For the direct alignment, one must detect the position and the attitude of the instrument for each acquisition. If this is mounted on a mobile vehicle, the displacement and the variation of attitude between the different scanning positions must be continously derived by means of auxiliary mechanical devices, like odometers, or by GPS receivers, coupled with inertial systems.

With regard to the indirect alignment, two are the procedures mainly used for the alignment: by using targeted or natural points or by iterative calculations.

One of the most popular iterative methods, still implemented in most commercial software used for the

management and processing of 3D data, is the Iterative Closest Point (ICP) algorithm, developed by Besl and McKay [Besl and McKay, 1992].

The ICP algorithm is used to align two point clouds; it is pair-wise based, and applies, iteratively, a roto-rigid translation in space to one of the two clouds, considered the mobile one, so that it overlaps in the best possible way to another cloud, considered the fixed one. The method is called point-to-point, as opposed to the point-plan method developed by Chen and Medioni [Chen and Medioni, 1991]. In both methods, registration is made through the search for the minimum of an objective function.

In the first method, point to point (Figure 1.3.5), this function is the sum of the squares of the Euclidean distances of the corresponding points of the clouds. The corresponding points are defined as the couple formed by a point of a cloud and the nearest one belonging to the opposite cloud.

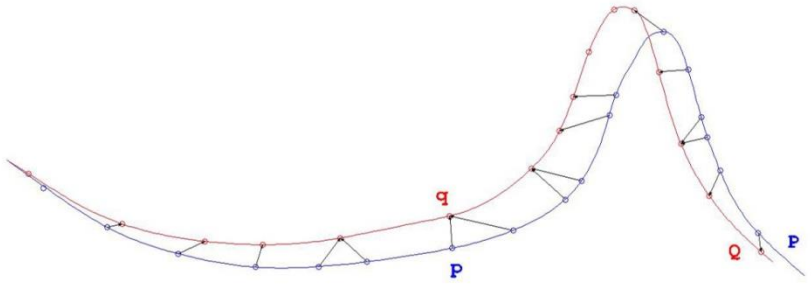

Figure 1.3.5: Point to point method [Bernardini and Rushmeier, 2002].

The algorithm proceeds in this way: given two surfaces, P and Q, to be aligned, a point belonging to P is considered, named p, and you search for a particular point of Q, said corresponding point q, which coincides with the closest point (point at minimum distance); in practice, for each point of the mobile cloud, the points within the fixed cloud are found, contained within a sphere of a given radius σ (multiple of a parameter entered by the user) and of these the closest one is considered, which will be the corresponding point. Such a parameter in the literature is conventionally estimated as twice the average distance of the points of a cloud; however, in the case of a severe misalignment, it will have to be increased accordingly.

The searched points are found by defining the Closest Point Operator C:

$$C: P \rightarrow Q \;/\; \forall p \in P \;\exists\, q \in Q \;:\; \min \|p-q\| < \sigma \qquad (1.3.4)$$

Once this operation has been performed for all points of the moving cloud, the rigid rototranslation of the cloud is found, that minimizes the sum of the squared distances. To this aim, after creating the couples, one can proceed to the minimization of the function:

$$e = \sum_1^N \|q_i - (Rp_i + T)\|^2 \qquad (1.3.5)$$

where N is the number of detected point couples, R and T are, respectively, the rotation matrix and the translation vector.

To obtain an optimal registration, more iterations of the search of corresponding points and distances minimization must be executed.

After finding the minimum, another iteration is performed to calculate the nearby points. At this point, however, the radius **σ** of the sphere within which you are searching is reduced by a given percentage (the criterion for this reduction varies according to the authors).

The convergence of the whole process will be reached when the variation of the roto-translation matrix between two successive iterations is less than a given percentage (generally when both translation difference and rotations dfference obtained in the last iteration are less than 1%).

When the point-to-plane error metric is used (Figure 1.3.6), the object of minimization is the sum of the squared distances between each source point and the tangent plane at its corresponding destination point. More specifically, if $s_i=(s_{ix}, s_{iy}, s_{iz}, 1)^T$ is a source point, $d_i=(d_{ix}, d_{iy}, d_{iz}, 1)^T$ is the corresponding destination point, and $n_i=(n_{ix}, n_{iy}, n_{iz}, 0)^T$ is the unit normal vector at d_i, then the goal of each ICP iteration is to find M_{opt} so that:

$$M_{opt} = \arg\min_M \sum_i ((M \cdot s_i - d_i) \cdot n_i)^2 \qquad (1.3.6)$$

where M and M_{opt} are 4x4 3D rigid-body transformation matrices [Low, 2004].

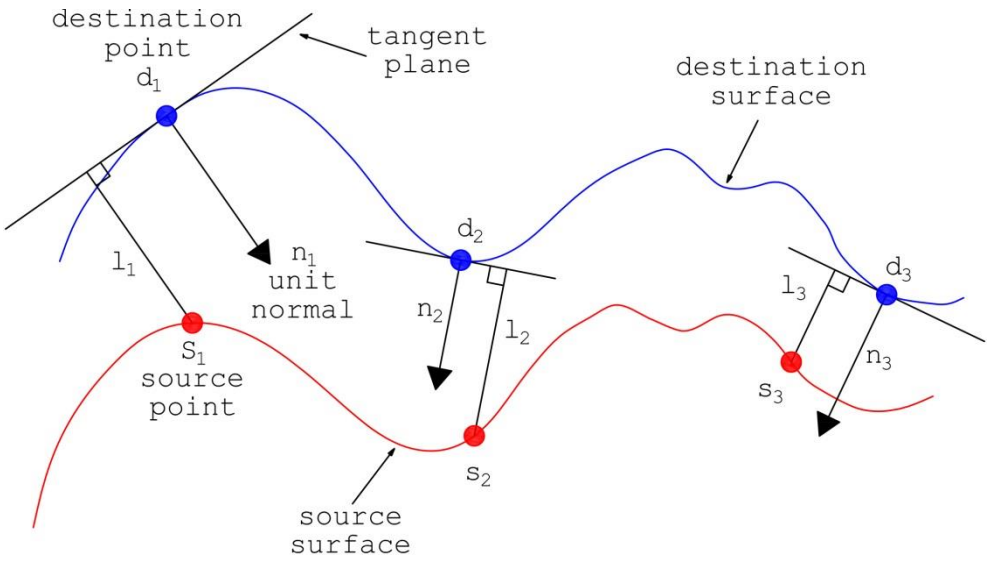

Figure 1.3.6: Point to plane error between two surfaces.

A 3D rigid-body transformation M is composed of a rotation matrix $R(\alpha, \beta, \gamma)$ and a translation matrix $T(t_x, t_y, t_z)$, i.e.

$$M = T(t_x, t_y, t_z) \cdot R(\alpha, \beta, \gamma) \qquad (1.3.7)$$

In both methods, the problem is to compute a rotation matrix R and translation vector T that can be solved in closed form by expressing the rotation as a quaternion

[Low, 2004], by linearizing the small rotations or by using the Singular Value Decomposition. More statistically robust approaches have been investigated to avoid having to preprocess the data to eliminate outliers [Haralick et al., 1989; Masuda et al., 1996].

Many variations of the algorithm have been proposed by other authors, in order to reduce these problems. Zhang [Zhang, 1994] introduces a maximum tolerable distance and an orientation consistency check to filter out spurious pairings. Dorai et al. [Dorai et al., 1997] model sensor noise and study the effect of measurement errors on the computation of surface normals.

The sequential use of pair-wise registration to align multiple views, leads to the accumulation of errors, so the global registration is not optimized (the residual error recording between all scans are not minimized). Turk and Levoy [Turk and Levoy, 1994] use a cylindrical scan as base; the other scans are registered to it. Other incremental approaches are proposed by Bergevin et al. and by Pulli [Bergevin et al., 1996; Pulli, 1999]. Blais and Levine [Blais and Levine, 1995] use a simulated annealing algorithm for a simultaneous solution of all the rigid motions. Neugebauer [Neugebauer, 1997] uses the Levenberg–Marquardt method to solve a linearized version of the least-squares problem.

Relaxation methods are proposed by Stoddart and Hilton and by Eggert et al. [Stoddart and Hilton, 1996; Eggert et al., 1998]: the problem is modeled by imagining a set of springs connecting to point pairs, and simulating the relaxation of the dynamic system.

Textures are also used to aid registration. They can be used for aiding a human operator for a first alignment [Gagnon et al., 1999], or for an automatic inizialization procedure [Roth, 1999]. The color can be considered as a fourth coordinate for each point in an ICP optimization Schutz et al. [Johnson and Kang, 1997; Schutz et al., 1998] propose an extended-coordinate ICP method, in which normal data (obtained from the range data) are used along with radiometric data. According to experiments conducted by Rusinkiewicz and Levoy (2001), the variants proposed did not produce significant benefits, with certain exceptions. At the conclusion of their analysis, they believe that the optimal ICP should: (a) search for the correspondence point-tangent plane; (b) carry out random sampling of points; (c) assign equal weight to all points; (d) exclude those points whose distance exceeds a threshold value; (e) eliminate the points at the edges of the areas of overlap between scans; (f) adopt an error metric based on the point-plan distance.

An alternative to the ICP method is represented by the 3D Least Square Matching, which represents the 3D

extension of the Least Square Image Matching method [Grün, 1985; Akca & Grün, 2004]. In general, this method estimates the parameters of the spatial transformation between two or more three-dimensional patches minimizing the Euclidean distance between the surfaces by means of least squares. This formulation allows us to seek the correspondence between surfaces oriented arbitrarily.

An observation equation is written for each element, e.g. for each point of the selected 3D patch. The geometrical relationship between the conjugate patches is given by a 7-parameter transformation; the unknown parameters of this transformation are considered as stochastic quantities, appropriately weighted.

Meshing

Once the registration step is completed, the point clouds are merged and a unique cloud is obtained. At this point, data processing is performed with the goal of obtaining a representation of the surface of the surveyed object: the mesh. A mesh is a collection of triangular (or quadrilateral) contiguous, non-overlapping faces joined together along their edges. A mesh therefore contains vertices, edges and faces and its easiest representation is a single face. Sometimes

it is also called TIN, Triangulated Irregular Network. Finite element methods are generally used to generate a surface mesh [Remondino, 2003].

The triangulation is the operation that converts the given set of points into a consistent polygonal model, i.e. in a mesh. Studies on triangulations date back to the age of Euclid (330-270 BC), but more recently we can refer to Peter Gustav Dirichlet (1805-1859), Georgy Voronoi (1868-1908) and Boris Nikolaevich Delaunay or Delone (1890-1980) as the fathers of the modern development of triangulation.

Bernardini and Rushmeier [Bernardini et Rushmeier, 2002] categorize the approaches for mesh integration methods in four classes: Delaunay-based methods, surface-based methods, parametric surfaces and volumetric methods, all of which present limitations.

An overview of the reconstruction techniques based on Delaunay triangulation has been published by Cazals and Giesen [Cazals and Giesen, 2006], paying particular attention to the assumptions and requirements of each geometric and algorithmic method.

The construction of a Delaunay triangulation can be done considering the dual of a Voronoi diagram.

Voronoi diagrams were considered as early at 1644 by René Descartes and were used by Dirichlet (1850) in the investigation of positive quadratic forms. They were studied by Voronoi (1907), who extended the

investigation to higher dimensions. The definition is [Voronoï, 1908]:

Let $S \subseteq \mathbb{R}2$ be a set of n points; we define the Voronoi region of $p \in S$ as the set of points $x \in \mathbb{R}2$, whose distance from p is less or equal to the distance from any other point in S, that is:

$$Vp=\{x \in \mathbb{R}2 \mid \|x-p\| \leq \|x-q\|, \forall q \in S\} \qquad (1.3.8)$$

The Voronoi diagram is formed by the Voronoi regions together with their shared edges and vertices.

The Delaunay triangulation for a set of points P in a plane, is a triangulation DT(P) such that no point in P is inside the circumcircle of any triangle in DT(P): Let $S \in \mathbb{R}2$ be finite and in general position, and let $a,b,c \in S$ be three points. Then abc is a Delaunay triangle if and only if the circumcircle of abc is empty.

For a set P of points in the (d-dimensional) Euclidean space, a Delaunay triangulation is a triangulation DT(P) such that no point in P is inside the circum-hypersphere of any simplex in DT(P). It is known [Delaunay, 1934] that there exists a unique Delaunay triangulation for P if P is a set of points in general position; that is, the affine hull of P is d-dimensional and no set of d + 2 points in P lies on the boundary of a ball whose interior does not intersect P.

Delaunay-based methods use the Delaunay complex D(S) associated to a set of points S in ℝ3 and impose a connectivity structure to the points.

A review of these methods was presented by Edelsbrunner in 1998 [Edelsbrunner, 1998]. Some techniques use the alpha-shapes [C et al., 1999]; other algorithms are the *power crusts* [Amenta et al., 2000]; the *cocones* [Dey et al., 2003] and the *eigencrusts* [Kolluri et al., 2004].

These algorithms are sensitive to noise and outliers because they interpolate the data points; to remedy this limitation, a preprocessing step is required, capable of "cleaning" input data. Another limitation is due to the limited size of the data set that can be processed, because these algorithms are extremely costly in performance.

Surface-based methods create or manipulate surfaces directly by connecting each point to its neighbor by local operations. Examples of such methods are zippered meshes [Turk and Levoy, 1994], ball-pivoting [Bernardini et al., 1999]; Soucy and Laurendeau [Soucy and Laurendeau, 1995] use canonical Venn diagrams to partition the data into regions that can be easily parameterized. Some of these algorithms can fail in regions of high curvature [Curless and Levoy, 1996]. Generally, these methods use fragments from the 3D models of each view and this generates noisy surfaces

because each view fragment is noisy. For this reason further post-processing is necessary.

Parametric, or deformable, surfaces methods use algorithms based on the idea of deforming an initial approximation of a shape, under the effect of external forces and internal reactions and constraints. Terzopoulos et al. use an algorithm based on application of intrinsic forces that induce a preference for symmetric shapes and it can infer a non-rigid motion, attainable also from a sequence of images [Terzopoulos et al., 1988]. Pentland and Sclaroff use an approach based on the finite element method and parametric surfaces [Pentland and Sclaroff, 1991]. Other approaches, that use one or more analytically generated surfaces to represent the integrated model, are: Radial Basis Functions [Carr et al., 2001], Partition of Unity [Ohtake et al., 2005], Poisson Surface Reconstruction [Kazhdan et al., 2006], statistical methods [Fleishman, 1978], parallel and out-of-core implementation [Bolitho et al., 2007, 2009], robust statistics to eliminate noise and outliers [Whitaker, 1998; Gomes and Faugeras, 2000].

Volumetric methods allow us to create an implicit volumetric representation, a 3D grid, of the final model. Each voxel, volumetric picture element, has a value corresponding to the signed distance between the voxel and the integrated surface. One of the most

popular methods is the Marching Cubes [Lorensen and Clein, 1987], which creates triangles within each uniform grid cell that intersects the iso-surface; this volumetric representation is also called a Signed Distance Field (SDF).

The various approaches differ in calculating the distance function from the available data: VRIP (Volumetric Range Image Processing) [Curless and Levoy, 1996]; Consensus Surfaces [Wheeler et al., 1998]; Marching Intersections [Rocchini et al., 2001]; and the method with unsigned distance fields of Hornung and Kobbelt [Hornung and Kobbelt, 2006].

A mesh is essentially a collection of vertices, edges and faces that define the shape of a three-dimensional object. A vertex is the representation of a position in space. An edge is the entity connecting two vertices. A face is a set of points in the space enclosed between edge and vertices. All these faces can determine polygons or much more complex structures. In a mesh, in order to be defined as such, one side is shared by the maximum two faces and is between two vertices; while a vertex is shared by at least two edges. A mesh is defined as closed if there are holes on its surface, otherwise it is said to be open. In these cases, all the elements that are on the edge are of finite boundary. The mesh can be represented in different ways, using different data structures suitable to store

vertices, edges and faces: Winged-edge, Half-winged-edge, Face-vertex, Quad-edge, Vertex-vertex.

Hole filling is the phase of closing non-digitized regions, i.e. holes. The closure of the holes can be: partial or complete, flat or in curvature, by means of a bridge between meshes. To face the diversity of topologies that holes can present in a model, several authors have proposed different methods [Davis et al., 2002]: for holes with simple topology, Delingette et al. [Delingette et al., 1991] and Chen and Medioni [Chen and Medioni, 1991], deform the surface until it adjusts to the model; Wheller et al. [Wheeler et al., 1998] and the variant Sagawa and Ikeuchi [Sagawa and Ikeuchi, 2008] propagate the surface in the hole border, but this way the propagation of distortions in borders can create erroneous reconstructions; Davis et al. [Davis et al.,2002] present a volumetric robust hole filling approach. There exist Integration methods that work with point clouds, i.e. power crusts [Amenta et al., 2000, 2001], cocones [Dey et al., 2001; Amenta et al., 2000] and ball pivoting [Bernardini et al., 1999].

There are other algorithms that operate a filtering of data by improving the readability and reliability of the obtained geometry: these are the so-called **smoothing algorithms** that perform a softening of the surfaces in order to better describe them. These

algorithms involve the introduction of changes, not always welcome, to the model; the software in use today allows us, however, to impose constraints and rules to avoid the unpleasant effects of the smoothing, such as the rounding of all sharp edges. Abrupt transitions and noises are thus eliminated. In this way, as well as a better representation of the model, the further advantage is obtained of reducing the overall dimensions of the requested computer memory, thanks to files of smaller size, and the consequent better manageability of the same patterns thus obtained. It is somewhat the result with the image compression algorithms such as JPEG or TIFF.

When there are a large number of unnecessary triangles in a mesh or the file size is too large, **decimation** is used which consists in lowering the number of triangles on a surface without distorting the detail or color of the mesh.

Laser scanners are used today in many fields of application: engineering, topography, geology, architecture, modeling Industrial, Marine, Archaeology and Cultural Heritage, Medicine, Criminal Investigation.

1.3.1 Full Waveform technology

The laser scanner with full waveform technology, enables a comprehensive analysis of the waveform of return laser signal that allows users to record a (theoretically) infinite number of echoes. Through the penetration of the laser beam along layers of vegetation and by digitizing the echoes returned, it is possible to make an automatic classification of the points and obtain parameters relating to the height and spatial configuration of the vegetation [Hug et al., 2004]. This allows us to obtain more accurate terrain models. This technology was introduced in the aircraft laser scanner as early as 2004, while the introduction of the first terrestrial full waveform laser scanner took place in 2008 with the Riegl LPM-321 model.

The operating mechanism of the full waveform technology is composed of two processing steps: the first concerns the echo-digitalization of laser signal, i.e. the decomposition of the return signal and the obtaining of parameters describing its complete waveform; the second step is concerned with classification of the wave in various echoes with an additional processing called full waveform analysis.

To illustrate the operation of these systems (Figure 1.3.1.1), the example is used of a laser scanner that must measure some well defined surfaces with an interposed tree that serves as a barrier [Pfennigbauer and Ullrich, 2008].

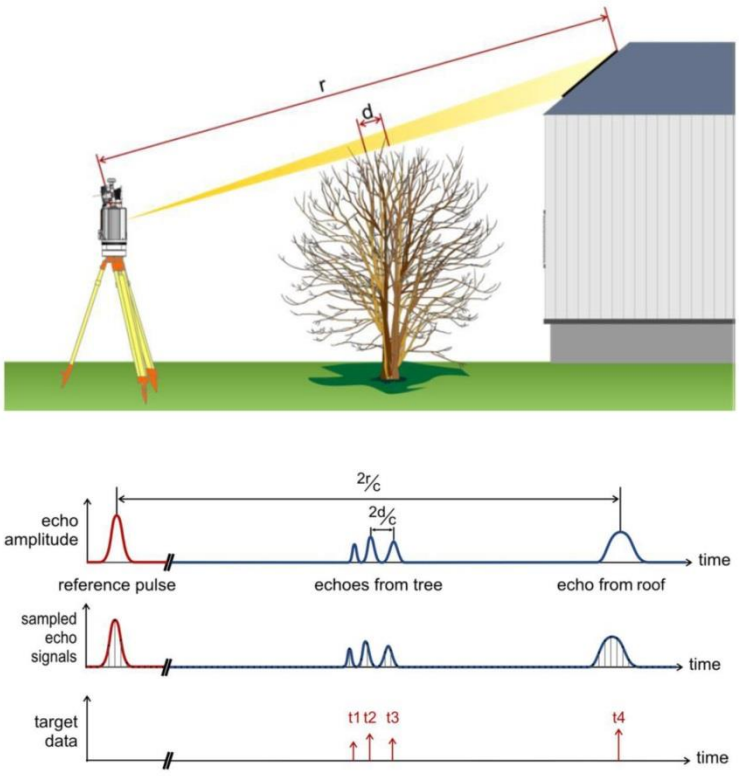

Figure 1.3.1.1 Illustration of interaction of the laser pulse with different target, the digitization process, and target extraction by FWA [Pfennigbauer e Ullrich, 2008].

In analogue systems it would only be possible to obtain information about the first object that the beam meets

along its path. Systems with full waveform, assuming that the beam footprint reaches all three elements, allows us to separate the various return echoes and to get more information about the properties of the hit targets. The only limitation of the system concerns the minimum distance between two neighboring objects actually distinguishable in a single return signal, said Multi-Target Resolution (MTR), which in the terrestrial laser scanner is usually of 0,80 meters.

From the parameters provided by the process of eco-digitizing of the signal, you can get a discrimination of the echoes by applying a Gaussian function [Ullrich et al., 2007]. A complex waveform caused by several backscattering targets can be modeled by the following formula:

$$P_r(t) = \sum_{i=1}^{N} P_i e^{\frac{(t-t_i)^2}{2s_{p,i}^2}} \qquad (1.3.1.1)$$

where $P_r(t)$ is the received power, t_i is the round trip-time of target *i*, P is the amplitude of target *i*, $s_{p,i}$ is the standard deviation of the echo pulse from target *i*, and *N* is the number of targets within the path of the emitted laser pulse. In some software, such as Pro Riscan of Riegl, the classification of the points is based exclusively on the sequence of the target that the laser beam meets along its path, for

which the object encountered for the first and the objects that follow each other linearly up to a last object found, the last discriminated echo, are distinguished. Usually all the points are grouped into four categories: *first and other*, that contain respectively the first and all intermediates echoes that are generated when the laser beam undergoes multiple reflections; *last*, containing those points that represent the last detected echo when in a same signal there are several return echoes; *single target*, containing the points that have provided a single return echo corresponding to continuous surfaces like blocks or rock walls and architectural artifacts [Riegl, 2012]. In some cases, the signal discriminator produces only two categories, first and last target, a condition which occurs when the distance between two successive targets is below the resolution threshold of the MTR.

The full waveform terrestrial systems are widely used for geological investigations, for the coverage of large areas, thanks to the considerable distance that can be reached (up to 6 km with the model Riegl VZ-6000), for purposes of security and monitoring.

1.4 Photogrammetry

"Photogrammetry is the art, science, and technology of obtaining reliable information about physical objects and the environment, through processes of recording, measuring, and interpreting images and patterns of electromagnetic radiant energy and other phenomena."
Society for Photogrammetry and Remote Sensing (ASPRS)

The photogrammetry is an image-based survey technique [Remondino and El-Hakim 2006], that enables us to obtain metric information, such as shape, size, and location of real objects by measurement and interpretation of photographic images.

The technique may be divided, depending on the method of acquisition, into three types: aerial photography, when the acquisition takes place from platforms or from satellites; aerial proximity photogrammetry, when the acquisition takes place from proximity platforms motorized or not; terrestrial photogrammetry, when the acquisition takes place from cameras positioned on the ground.

Inside the terrestrial photogrammetry, the

photogrammetry can be defined **close range** when objects are taken at a distance of less than 300 m from the camera. It is used mainly for archeological sites [Kersten and Lindstaedt, 2012] architectural and cultural heritage surveys [Yilmaz et al., 2007]. Often the technique's close range is complemented with laser scanner data [Beraldin, 2004; Remondino et al., 2005; Lerma et al., 2010].

The history of photogrammetry is related, in its theoretical principles, to the history of descriptive geometry and in particular to the formulation of the theory of perspective; while in its application it is linked to the history of optics, photography and related technological breakthroughs. In 1759, Johan Heinrich Lambert in his work "Perspectiva liber", defined the principles and mathematical laws on which photogrammetry would be based.

In the development of the technique of photogrammetric survey, it is possible to distinguish the following time steps:

- Pioneering phase (1850-1900). Photogrammetry was founded by Aimé Laussedat, who in 1851 outlined the procedures, based substantially on a forward intersection in which the measurements were obtained from the frames. Measuring quantities on the frame was, however, a significant source of error due to the distortion of the camera lens. In

1865, Ignazio Porro tried to remedy these errors, integrating this new technique with photogoniometer, an instrument which was used to measure the angles of the directions ranging from the lens center to the points of the photographed object.

- Analog and stereoscopic phase (1900-1960). The second age of photogrammetry began in the early twentieth century through stereoscopy (C. Pulfrich) and the principle of mobile mark (F. Stoltz), which allowed him to overcome the difficulties of the ambiguous recognition of the homologous points on two different frames. In 1909, then, E. Von Orel built the stereo-autograph, whereby the issue to pass by a couple of frames to the horizontal projection was resolved, not by calculating the coordinates of individual points, but in a continuous manner using physical elements of analogic type. Von Orel opened up the era of analog restitution; in this field progress was fast enough, especially through the work of scholars such as Wild, Nistri and Santoni. With the First World War there came the introduction of aerial photogrammetry.
- Analytical phase (from 1960 onwards). The dialogic setting in photogrammetry was linked to periods in which the limited means of calculation prevented

development of the analytical procedures necessary to pass from the perspective (photo) to the orthogonal projection (paper).

- Digital phase. From the '90s it was possible to produce and use digital images, structured in a matrix of small elements called pixels. This allows us to consider images as a matrix of numbers and, consequently, to perform the processing by computer in a fast, precise and semiautomatic way.

The photogrammetric cameras

Taking into account terrestrial photogrammetric surveys, the cameras may be classified into three types:

- **Metric cameras:** These produce frames very close to perfect central perspectives, thanks to complex optical mechanical devices and calibrated lenses of the highest quality. They have extremely stable internal geometry and are provided with a certificate of calibration; the older ones allowed calculatation of the interior orientation through fiducial marks. They are expensive, but very accurate.
- **Semimetrics cameras:** these are equipped with lenses

that produce sensitive distortions; the interior orientation can be reconstructed thanks to fiducial marks or a grid of reseau crosses. They are cheaper, but less accurate.

- **Amateur cameras:** these are equipped with lenses that produce significant distortions, there are not fiducial marks or reseau crosses. They are not expensive, but have low accuracy. In recent years, the possibility of easily performing calibration and, thus, obtaining all distortion parameters, allowed the widesprea diffusion of these cameras, currently adopted also for professional aims.

The lens of the photographic cameras introduces two types of deformations (Figure 1.4.1):

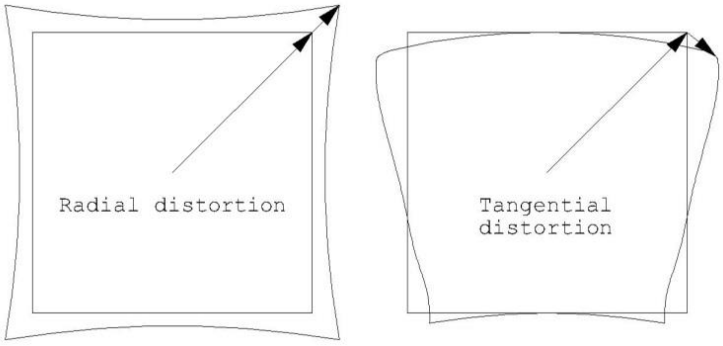

Figure 1.4.1: Radial and tangential distortion.

- **Radial:** it proceeds from the center of the frame to

the edges, i.e. the point on the image lies in the plane containing the camera axis and the object point.

- **Tangential**: The point on the image does not lie in the plane containing the camera axis and the object point. It has an effect which is generally less sensitive than the radial and for this reason, until the recent development of computers, it was not taken into account in normal photogrammetric applications. In each case, it can be modeled through appropriate polynomials (Figure 1.4.2).

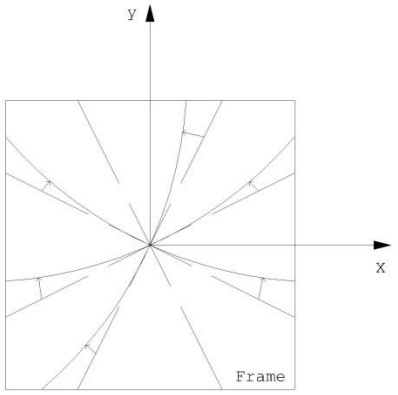

Figure 1.4.2: tangential distortion.

While in the metric cameras the problem is resolved upstream, in the amateur cameras, the problem is usually overcome through the elaboration of a mathematical model which approximates the corrections to be applied [Monti et al., 1999].

For the digital cameras, the skew coefficient has to be obtained, defining the angle between the x (columns) and y (rows) pixel axes.

Basic principle of photogrammetry

In order to determine the positions of the points of an object in the real environment, using the positions of the corresponding points on the photograph, you must define the geometric relationships between the positions of the three-dimensional points of the object and those of their images on the plan of photography (or sensor plane). At each three-dimensional point in the object space, there corresponds a point on the image plan (image space).

It is possible, with a sufficient approximation, to consider photography as a central perspective, according to which the segments connecting the points of the object with their corresponding image points (star projecting) all meet at a point O, called centre of projection.

Figure 1.4.3 illustrates the *image space* having reference system with origin in the Principal Point (PP) and ξ and η axes.

The **internal orientation parameters** are ξ_0 and η_0, coordinates of the Principal Point PP, and the focal

length c, that locate the position of the projection centre on the image plane. As well as these parameters the distortions must be considered. For the high-end cameras, the three internal orientation parameters, provided by the constructor, are assumed to be constant and specific.

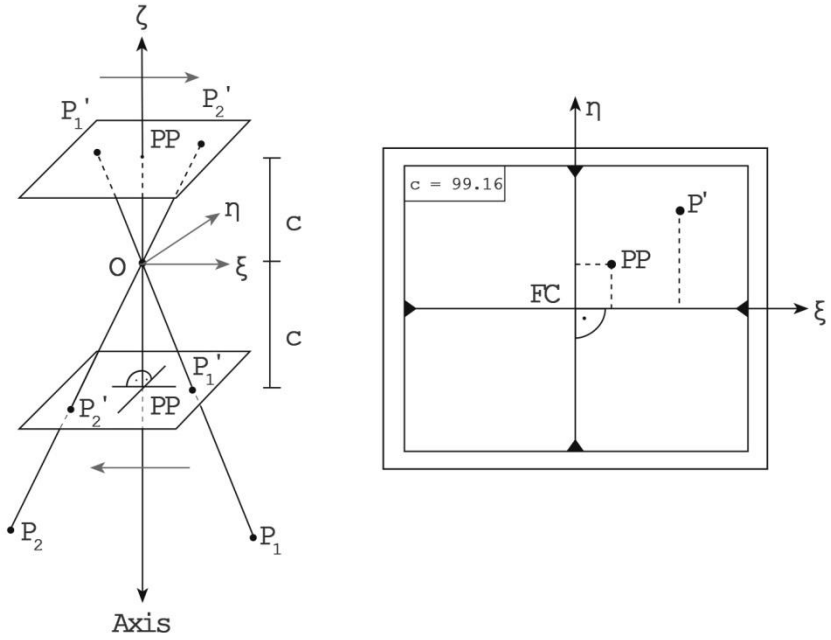

Figure 1.4.3: Internal orientation - characteristic points and adopted conventions. O: Centre of projection, or point of acquisition; PP: Principal point with coordinates ξ_0 η_0 ζ_0; c: focal length; FC: Fiducial Centre, intersection between the lines that connect the opposite Fiducial Marks [Gomarasca, 2009].

The **external orientation parameters** are six: the coordinates of the perspective centre X_0, Y_0, Z_0 (Figure 1.4.4), expressed with respect to the object reference system (generally the cartographic system) and the three rotation angles ω, φ, κ describing the photo camera attitude at the moment of acquisition. These can be derived by direct georeferencing, using position (GPS) and attitude (IMU, Inertial Measurement Unit) measurements, or through a Least Squares estimation process performed with respect to the Ground Control Points (GCPs).

Any photogrammetric problem is solved through the collinearity equations, knowing the interior and exterior parameters and the distortions.

Below, the relationships between the coordinates ξ, η of an image point P' on a frame and the X, Y, Z of the corresponding object point P, called collinearity equations, are shown:

$$\xi = \xi_0 - c\frac{r_{11}(X-X_0)+r_{21}(Y-Y_0)+r_{31}(Z-Z_0)}{r_{13}(X-X_0)+r_{23}(Y-Y_0)+r_{33}(Z-Z_0)} \qquad (1.4.1)$$

$$\eta = \eta_0 - c\frac{r_{12}(X-X_0)+r_{22}(Y-Y_0)+r_{32}(Z-Z_0)}{r_{13}(X-X_0)+r_{23}(Y-Y_0)+r_{33}(Z-Z_0)} \qquad (1.4.2)$$

where the coefficients r_{ij} are function of the exterior orientation parameters.

Collinearity equations express that, for each point

of a frame, the center of projection O, the image point and the object point are aligned on the same projecting radius.

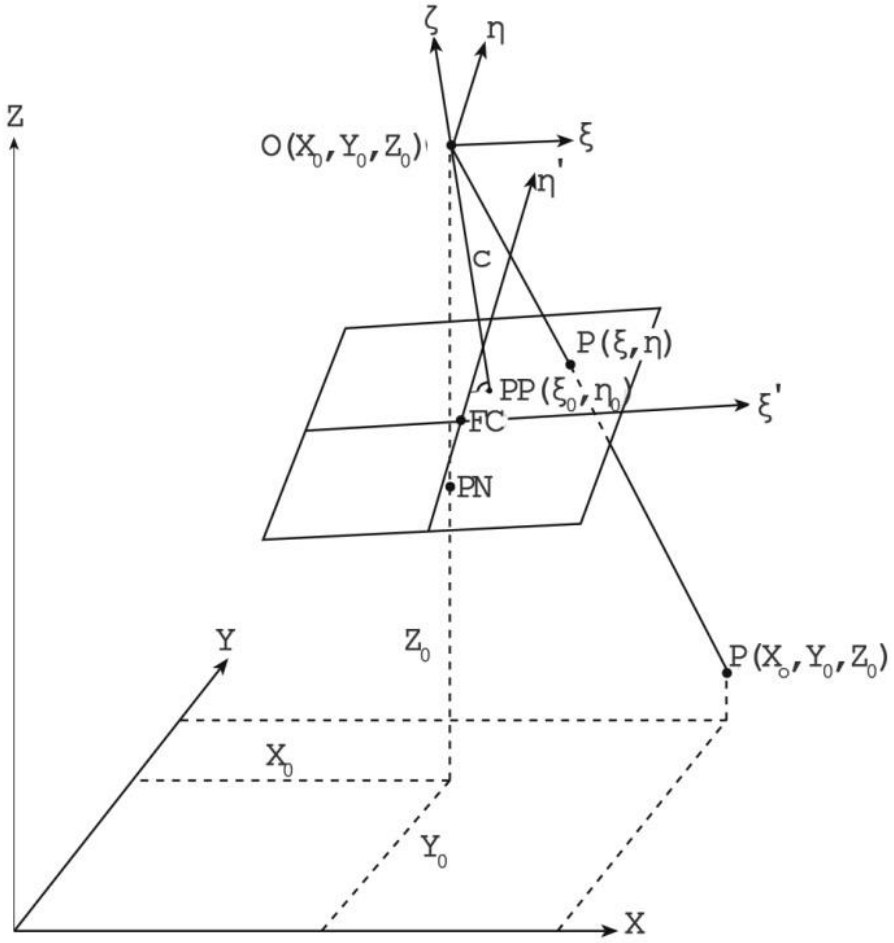

Figure 1.4.4: Relationship between the coordinates of image points and object-points [Kraus, 1994].

The inverse equations, for the transition from object

coordinates and image coordinates, are:

$$X = X_0 + (Z - Z_0)\frac{r_{11}(\xi-\xi_0)+r_{12}(\eta-\eta_0)-r_{13}c}{r_{31}(\xi-\xi_0)+r_{32}(\eta-\eta_0)-r_{33}c} \qquad (1.4.3)$$

$$Y = Y_0 + (Z - Z_0)\frac{r_{21}(\xi-\xi_0)+r_{22}(\eta-\eta_0)-r_{23}c}{r_{31}(\xi-\xi_0)+r_{32}(\eta-\eta_0)-r_{33}c} \qquad (1.4.4)$$

The attitude parameters (ω, ϕ, κ) are composed inside the r_{ij} coefficients, which represent the elements of the spatial rotation matrix R defined as follows:

$$R_{\omega\phi k} = \begin{pmatrix} cos\phi\ cosk & -cos\phi\ sink & sin\phi \\ cos\omega\ sink + sin\omega\ sin\phi\ cosk & cos\omega\ cosk + sin\omega\ sin\phi\ sink & -sin\omega\ cos\phi \\ sin\omega\ sink - cos\omega\ sin\phi\ cosk & sin\omega\ cosk + cos\omega\ sin\phi\ sink & -cos\omega\ cos\phi \end{pmatrix} \qquad (1.4.5)$$

Counterclockwise rotation ω, ϕ, κ respectively around the axes X, Y, Z are to be intended as sequential; they are defined as follows: primary or transversal rotation ω, secondary or longitudinal rotation ϕ; tertiary or skidding rotation κ.

Obviously, with just one photogram, it is impossible to model the 3D geometry of an object surface, so every zone of an object (or of land) must be represented at least in two photograms.

Image rectification

Image rectifying is a particular application of photogrammetry that can be performed on a single image.

It can be considered essentially as the transformation of a perspective image into an image of orthogonal type, like a photograph taken from infinity, with the projecting beams parallel to each other and orthogonal to the image plane.

This is possible today thanks to the use of appropriate software, that uses the coordinates of a few known points.

Digital photogrammetry

The digital or numerical image is represented by a matrix structure defined raster. The digital image is made up of a bidimensional matrix composed of rows and columns whose elements of finite size, the pixels (picture elements), describe the radiometric content of the image as a continuous function g(i,j) where i, j are spatial variables.

$$g(x,y) = \begin{bmatrix} g(0,0) & g(0,1) & \dots & g(0,C-1) \\ g(0,1) & g(1,1) & \dots & g(1,C-1) \\ \vdots & \vdots & \vdots & \vdots \\ g(R-1,0) & g(R-1,1) & \cdots & g(R-1,C-1) \end{bmatrix} \qquad (1.4.6)$$

Where:

i= 0,1,……R-1 row index;

j= 0,1,……C-1 column index;

R = maximum number of lines;

C = maximum number of columns;

g (x, y) = {0,1, ..., max} radiometric values.

For each pixel, two integer numbers are uniquely associated that indicate the position in row and column within the matrix. The number corresponding to the row varies from 1 to R with unitary step while the one corresponding to the column varies from 1 to C.

In particular, the formation of the digital image is a procedure which consists of two operations, quantization and sampling, the first of which is related to radiometric resolution and the second to the geometric one.

Radiometric resolution determines how finely a system can represent or distinguish differences of intensity, and is usually expressed as a number of levels or a number of bits, for example, 8 bits or 256 levels, that is typical of computer grey image files.

The geometric resolution indicates the number of pixels contained in a unit length and it is usually expressed in dpi (Dots Per Inch).

Usually, the pixels are square and geometric resolution influences the chance of seeing more details

of the scene.

A special feature of digital photogrammetry is the introduction of automated procedures, called Image Matching, to solve the problem of identification of homologous points. There are several methods of IM, classified into three major groups called Area Based Matching (ABM), Feature Based Matching (FBM), and relational matching.

1.4.1 Digital Image Correlation (DIC)

Digital Image Correlation (DIC) is a full-field image analysis method used for detecting and determining 2D and 3D displacements and the deformations of an object under load [Chu et al.,1985; Bruck et al., 1989; Pan et al.; 2009]. The method is based on grey value digital images and on correlation algorithms.

The success and the broad diffusion of this technique are due to the rapid developments in high resolution digital cameras and computer performances. Nowadays, DIC techniques are considered to be an effective and useful tool for deformation analysis.

DIC is used for Material Testing (Young's Modulus and Poisson's Ratio determination), Fracture Mechanics, Dynamic Measurements, and Study of advanced materials. The results of DIC measurements are surface contours, 3D displacements and strains. The accuracy is up to 1/100000 of the field of view.

Principles

Using a mono (for 2D) or stereoscopic (3D) sensor setup, each object point is focused on a specific pixel in the image plane of the relevant sensor. Once calibration has been executed, the intrinsic parameters for each sensor are known. The relative orientation of the sensors with respect to each other (extrinsic parameters), allow the calculation of the coordinates of each object point in two or three dimensions. To generate recognizable points on the object surface, a stochastic intensity pattern or a random coating are used, allowing the application of a correlation algorithm.

Correlation

The correlation algorithm is based on the tracking of the grey value pattern G(x,y) in small local neighborhood facets. It is generally performed by maximizing a correlation coefficient, that is determined by examining the intensity of pixels belonging to array subsets on two corresponding images. The cross correlation coefficient $r_{i,j}$ is defined as

$$r_{i,j}\left(u, v, \frac{\partial u}{\partial x}, \frac{\partial u}{\partial y}, \frac{\partial v}{\partial x}, \frac{\partial v}{\partial y}\right) = 1 - \frac{\sum_i \sum_j [F(x_i,y_i)-\bar{F}][G(x_i^*,y_i^*)-\bar{G}]}{\sqrt{\sum_i \sum_j [F(x_i,y_i)-\bar{F}]^2 \left[G(x_i^*,y_i^*)-\bar{G}\right]^2}} \qquad (1.4.1.1)$$

where $F(x_i, y_j)$ is the pixel intensity or the gray scale value at a point (x_i, y_j) in the non-deformed image. $G(x_i^*, y_j^*)$ is the gray scale value at a point (x_i^*, y_j^*) in the deformed image. $\bar{F}$ and $\bar{G}$ are mean values of the intensity matrices F and G, respectively. The coordinates or grid points (x_i, y_j) and (x_i^*, y_j^*) are related by the deformation that occurs between the two images. When the motion is perpendicular to the optical axis of the camera (this is the case with a monoscopic acquisition), the relation between (x_i, y_j) and (x_i^*, y_j^*)can be considered a 2D affine transformation, described by the following linear equations:

$$x^* = x + u + \frac{\partial u}{\partial x}\Delta x + \frac{\partial u}{\partial y}\Delta y \qquad (1.4.1.2)$$

$$y^* = y + v + \frac{\partial v}{\partial x}\Delta x + \frac{\partial v}{\partial y}\Delta y \qquad (1.4.1.3)$$

where u, v are the components of the translation of the center of the sub-image, Δx, Δy are the components of the distance from point x,y to the center of the sub-image. Thus, the correlation coefficient depends on

the displacements (u,v) and on their gradients $\frac{\partial u}{\partial x}$, $\frac{\partial u}{\partial y}$, $\frac{\partial v}{\partial x}$, $\frac{\partial v}{\partial y}$. With this technique, a matching accuracy of better than 0.01 pixel can be achieved.

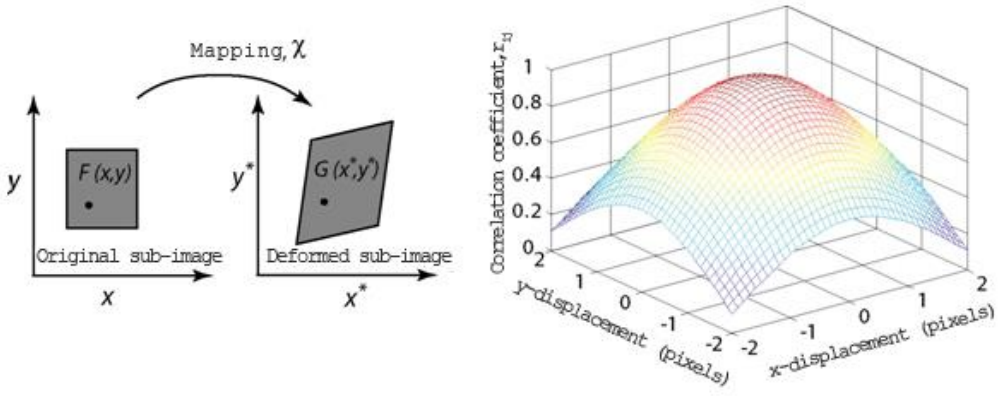

Figure 1.4.1.1: Basic concept of DIC (image extracted from https://en.wikipedia.org/wiki/Digital_image_correlation).

Propaedeutic to the measurements is the calibration of the camera, for which several methods are available [Zhang, 2000; Remondino and Fraser, 2006]; it is generally performed by taking images of a calibration panel under different perspective views. In our case, instead of the typical checkerboard printed on a cardboard, a metallic calibration board was used.

Results attainable

Calculating the transformation parameters for images under different loading conditions, both the displacement vector and deformation for each sub-image can be determined. Furthermore, taking into account the curvature of the object, the strain can be calculated by the parameter of the affine transformation and by the gradients of the deformation [Vendroux and Knauss, 1998; Hild and Roux, 2006; Detchevet al., 2011].

Advanced methods

The **Differential Digital Image Tracking** (DDIT) exploits the intensity peaks generated by the coating particles in the intensity domain, generally fitted by Gaussian distributions. These peaks can be tracked, thus allowing the determination of displacements, deformations and strains.

Digital Volume Correlation (DVC) is the extension of the above described technique to volumes. The DVC algorithm allows us to track full-field displacement information in the form of voxels instead of pixels.

2

The surveying of Cavalcanti palace

In the framework of the activities aimed at realizing a GIS for the protection of Cultural Heritage [Ansioso et al., 2015], paying peculiar attention to the historic town of Cosenza, a case study is represented by Cavalcanti's Palace, located in the ancient town of Cosenza, built in the 16th century and restored in 1772 [Altomare et al., 2013a, 2013b].

For the data acquisition phase, photogrammetric surveys, both in visible and infrared frequencies, integrated with total stations and a GNSS receiver are foreseen. All data acquisitions will converge in the

construction of a georeferenced 3D geometric model [Azhar et al 2008; Eastman et al., 2011; Smith and Tardif, 2012].

Starting from the existing DBT layers, in addition, an information system will be set up, that contains a set of layers related to structural aspects and to the territorial area with details regarding geotechnical characteristics, urban hydro-geological and seismic hazard data, vulnerability and exposure. The goal is the creation of the mapping of seismic risk, derived through algorithms that make use of all the data in the GIS [Chías et al., 2006; Saygi et al., 2013] and obtained through the survey. The GIS is intended, also, as a decision support system for Public Administrations and Civil Protection in case of emergency.

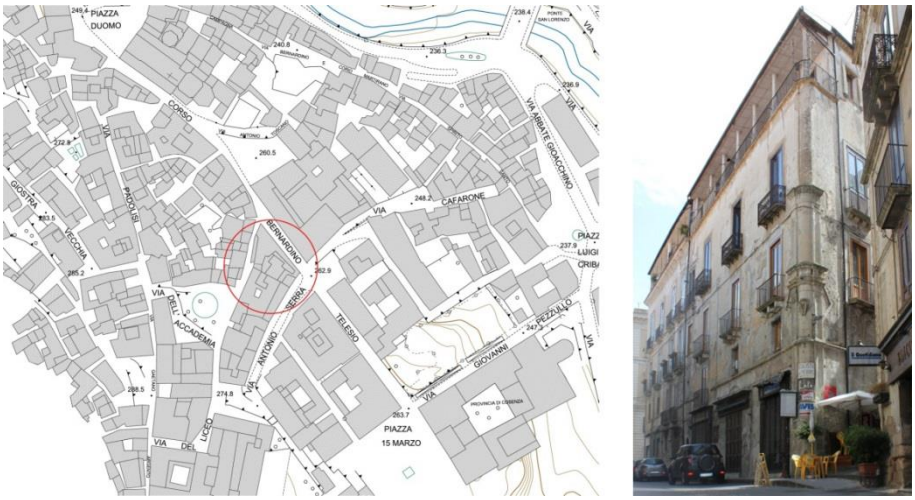

Figure 2.1: Location of Cavalcanti palace.

Palazzo Cavalcanti is situated in Corso Telesio (Figure 2.1). Its date of construction is uncertain. The first documentary sources date back to the sixteenth century, which coincide with the date assigned to the palace in the Charter of Camerota (1595), in which it is represented with the name of "Casa delli Parisi". The complexity of the building layout leads one to suppose that the aggregation of more constructions constituted the present building, which today is called **Palazzo Cavalcanti-Parisi**.

Figure 2.2: The degree of degradation and the crack pattern of the main façade.

To compile the record of the building, historical research was initially carried out, at the Superintendence for Architectural and Landscape Heritage of the Provinces of Cosenza, Catanzaro and

Crotone and the State Archive of Cosenza. Later surveys were carried out on the building in order to define the degree of degradation (Figure 2.2) and the crack pattern. Figure 2.3 shows the measures of a lesion.

Figure 2.3: Rectified image of a crack.

A peculiar survey was carried out to check the verticality of the main façade. For this purpose, a Leica 1200+ robotic total station was used by means of which an area of the facade was measured, characterized by a presumed swelling. The new robotic total stations allows one to obtain a scan of selected areas, by assigning horizontal and vertical steps. The result is a grid of points useful to obtain a Digital Surface Model. The speed of the acquisition is, of course, very low with respect to a laser scanner, but the main

positive aspect is the possibility to use a single instrument both for georeferencing and detail surveying, with less time and cost.

The area was selected in correspondence of a presumed swelling. The area size is 2.10 x 6.70 meters; to obtain a good point density, a square grid having an average step of 8 cm was chosen. About 2000 points from two station points were acquired, automatically, in order to cover the undercuts. The resulting point cloud was developed using the Rapidform® software.

To evaluate the entity of the swelling, the best fitting vertical plane was chosen as reference. In figure 2.4 the zone where the wall protrudes on the external side is represented in red, the blue zone has negative protrusion.

It is worth noting that the maximum value is about 8 centimeters. This value is greater than the irregularities in the facade realization and indicates a real swelling. This zone should be, thus, subjected to deeper structural analysis.

We must underline that the local measurements (by extensometers, calibers, etc..), unlike the total station surveys, allow only the detection of relative movements. In this way, it is impossible to establish which part of a structure is subject to a subsidence.

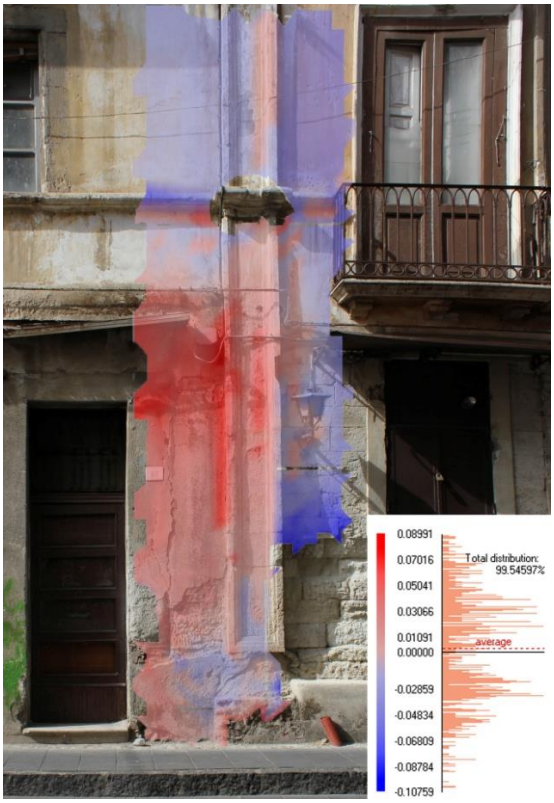

Figure 2.4: The deviations with respect to the average vertical plane are highlighted in colors: in red the positive protrusions.

The use of the total station allows also the georeferencing of the survey. This implies the possibility to assign to the measured points coordinates referred to a global reference system, external to the building. It is possible, this way, to know whether a variation in the dimension of a crack is due to the movement of one side, or to different movements of both sides.

3

Integration of 3D surveying techniques: the case of the Escuelas Pias Church in Valencia

The surveying of cultural heritage is carried out by using several techniques. In almost all cases, the integration of data collected by different instruments is needed. In the following example, the operations carried out for the 3D modeling of the Escuelas Pias Church and the results will be described.

The surveying was carried out in the framework of activities of the Universitat Politècnica De València (Upv), coordinated by prof. José Luis Lerma García.

After the description of the church and historical

notes, focus will be on the indirect registration results obtained with three different laser scanning software packages, highlighting similarities and differences, and the consequences while generating meshes. The 3D model carried out will then be described and the results of some investigations regarding the hypothesis about the design of the dome will be shown.

Escuelas Pías Church

The "Escuelas Pías" is a clerical religious order founded in the 17th century by St. José de Calasanz (1557-1648), dedicated to the apostolate and to the education of children and young people, especially the poor [Verdú, 1996]. It is the first free public school in Europe. To this order belongs the parish Church of St. Joaquin, also known as Escuelas Pías Church (Figure 3.1), located in the heart of the old town of Valencia (Spain).

Characterized by a central and decagonal plan, the Church was built between 1767 and 1772 under the patronage of the Archbishop of Valencia Andrés Mayoral Alonso de Mella (1738-1769). The project supervisor was the architect Antonio Gilabert (1716-1792). Joseph Puchol started to design the first level between 1767 and 1768. Antonio Gilabert modified the original plans

of Puchol, and the ornament turned from Gothic to Baroque style with neoclassical insertions.

Figure 3.1: Iglesia de las Escuelas Pías (Valencia, Calle Carniceros, 2).

The Church, with its imposing height of 48 m, is dominated by a large hemispherical dome of about 24 m in diameter surmounted by a lantern with fairing. The dome rests on ten large trapezoid section pillars and ten subsidiary spaces occupied by several radial chapels. This temple can be seen as a representative example of academic architecture of the late 18th century, due to the composition of the facade, the building itself and the architects involved in its construction. This Church represents a superb example where it is possible to appreciate the Classical turning point dictated by the creation in 1768 of the

Real Academia de Bellas Artes de San Carlos, which through its architecture, encouraged the flowering of the Classical Baroque style prevalent from the mid-18th century in the city of Valencia [Cruilles and Monserrat, 1876; Gómez, 1987].

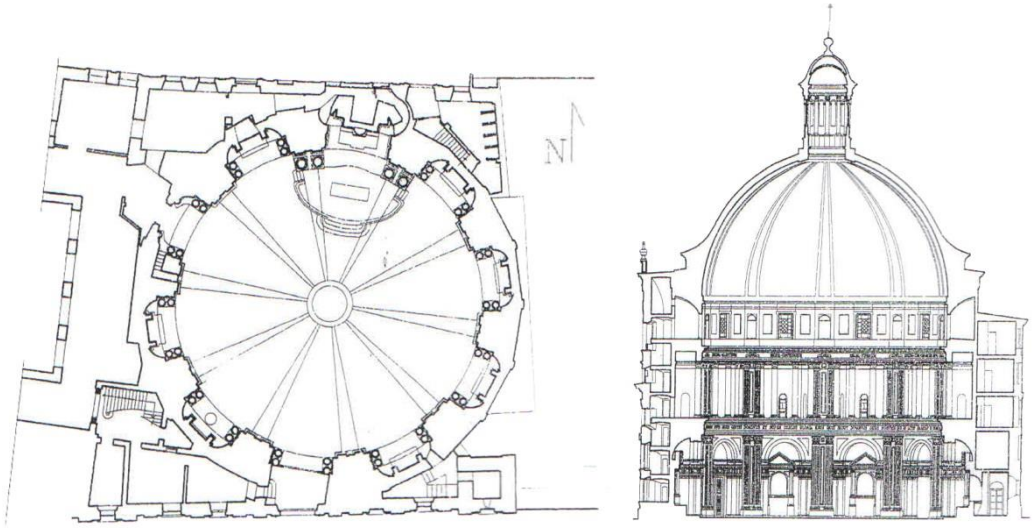

Figure 3.2: Plan and elevation of the Escuelas Pías Church [Verdú, 1996].

Surveying operations

For the survey of the Escuelas Pías Church, the FARO Focus3D S 120 was used, one of the present smallest and lightweight 3D laser scanners. The main characteristics of the instrument are (Table 3.1):

Ranging unit	Unambiguity interval: 153.49m (503.58ft)
	Range: 0,6m - 120m indoor or outdoor with low ambient light and normal incidence to a 90% reflective surface
	Measurement speed (Pts/Sec): 122,000 / 244,000 / 488,000 / 976,000
	Ranging error: □2mm at 10m and 25m, each at 90% and 10% reflectivity
Colour unit	Resolution: Up to 70 megapixel colour
	Dynamic colour feature: Automatic adaption of brightness
Deflection unit	Field of view (vertical/horizontal): 300° / 360°
	Step size (vertical/horizontal): 0,009° (40,960 3D-Pixel on 360°) / 0,009° (40,960 3D-Pixel on 360°)
	Max. vertical scan speed: 5,820rpm or 97Hz
	Laser (Optical transmitter)
	Laser power (cw O): 20mW (Laser class 3R)
	Wavelength: 905nm
	Beam divergence: Typical 0.19mrad (0.011°)
	Beam diameter at exit: Typical 3.0mm, circular
Multi-Sensor	Dual axis compensator: Levels each scan: Accuracy 0,015°; Range □5°
	Height sensor: Via an electronic barometer the height relative to a fixed point can be detected and added to a scan.
	Compass: The electronic compass gives the scan an orientation. A calibration feature is included.

Table 3.1: Main characteristics of FARO Focus3D S 120.

To measure accurately the Church, 40 scans were acquired, with a 0.07°/point resolution at a rate of 120,000 points/s. Spherical targets with a diameter of 14 cm were distributed across the church and at various heights in order to facilitate the alignment of scans in post processing.

In addition to the laser scanner acquisitions, several photos were acquired, in order to obtain a textured 3D model. External survey was carried out using a Leica Scan Station. A survey with a thermal camera was also carried out [Figure 3.3, 3.4].

The IR shots were used to detect hidden cracks, above all in the dome.

Figure 3.3: The survey with laser scanner and thermal camera.

Figure 3.4: A panoramic view of laser scanner acquisitions.

The Registration: comparison among different software

During the survey, each scan is completed from a different scan position and orientation, consequently with a different local Cartesian coordinate system. The various reference systems are centered in the instrument and oriented arbitrarily. Indirect registration is the set of operations necessary to define the exterior orientation parameters (rotation and translation) that allows each scan to reflect the clouds in a single reference system. For this aim, tie and control points, which are recognizable in the

overlapping point clouds, are generally used. These points may just be features of the object (e. g. corners, edges) or special targets (e.g. spheres, cones or flat targets with high reflectivity).

If global coordinates are needed, the control points have to be surveyed by geodetic methods (total station, GNSS); bundle adjustment can also be implemented. In any case, three or (better) four known points in a point cloud will yield better results than just using tie points.

Theoretically speaking, a large scanning overlap allows users to obtain many surface points and to apply a solution using surface conditions only (such as ICP). The drawback of such a methodology is twofold: (1) the error propagation for a large number of scans may cause unacceptable residuals; (2) objects characterized by regular surfaces do not have enough geometrical strength to fix a solution (planes yield two degrees of freedom for translation and one for rotation; spheres three rotation ones; cylinders one translational and one rotational, etc.). In our case, control points obtained through spherical targets were used inside the church. Global coordinates were not requested. Therefore, no geodetic survey was performed.

Spherical targets have the advantage, compared to other types of target, of being multidirectional and can be *a priori* automatically recognized by the

scanning software from any direction, in our case, the FARO Scene®. FARO Scene software is able to recognize the spherical shape and extract its center as the point of binding [Figure 3.5].

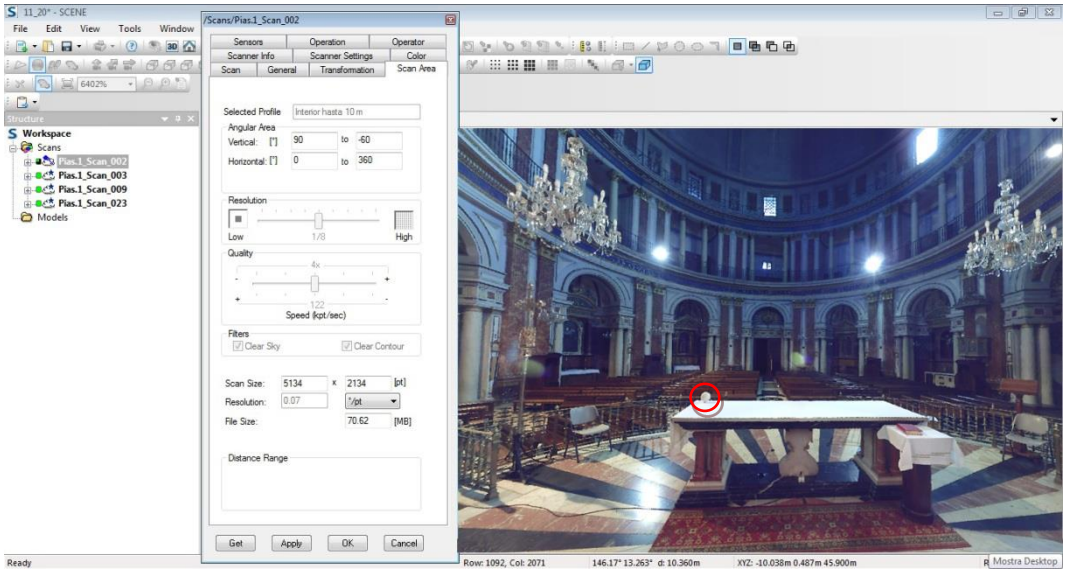

Figure 3.5: Screenshot of FARO Scene®; a spherical target is circled.

The procedure to register can be summarized in the following steps [Figure 3.6]: (1) identification of the position of the targets in the various scans; (2) identification of at least 3 common targets between 2 scans; (3) assignment to targets of the same nomenclature for each scan; (4) union of scans that have at least 3 common target with the same nomenclature; (5) creation of a group of aligned scans.

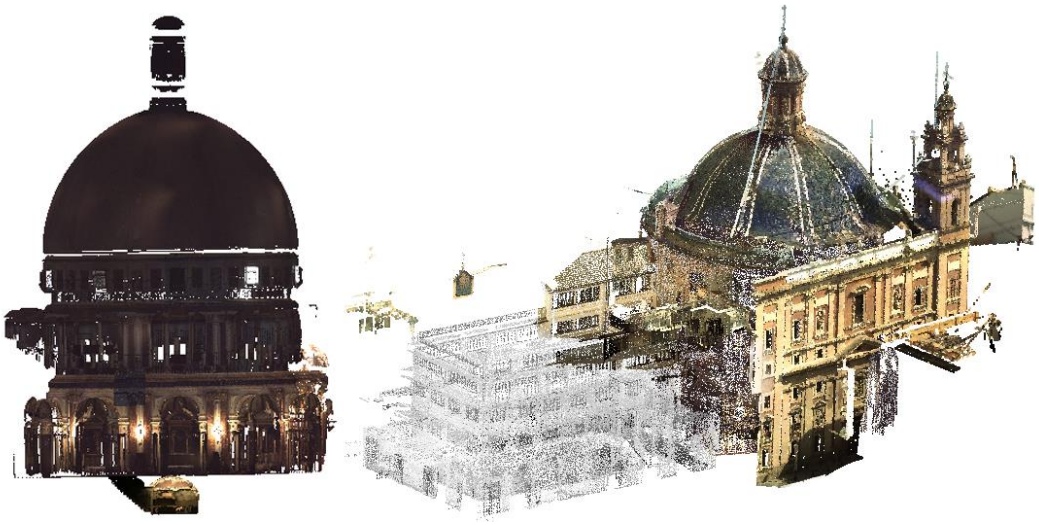

Figure 3.6: Aligned scans.

In this case study, four scans were aligned using the four visible spherical targets. The same coordinates were used in three different software packages in order to compare the results. The coordinates of the targets were obtained with FARO Scene.

FARO Scene®

In FARO Scene it is possible to use different types of reference objects to register. Spherical targets were extracted manually by selecting the points corresponding to each target scan and performing an optimization. In this way the coordinates of the targets in different scans were found.

Registration was undertaken taking into account that: (1) all the spheres must be completely visible inside the scan; (2) the radius of the sphere used in the scan must be set in the command Match Sphere Setting, in our case 7 cm; (3) the optimal detection of the spherical surfaces requires at least 60 points.

One scan was also marked as reference, enabling the attribute Scan Reference in the dialog box of the properties of the Scan tab. It is necessary to run Pre-process on all scans in FARO Scene to mark targets/spheres.

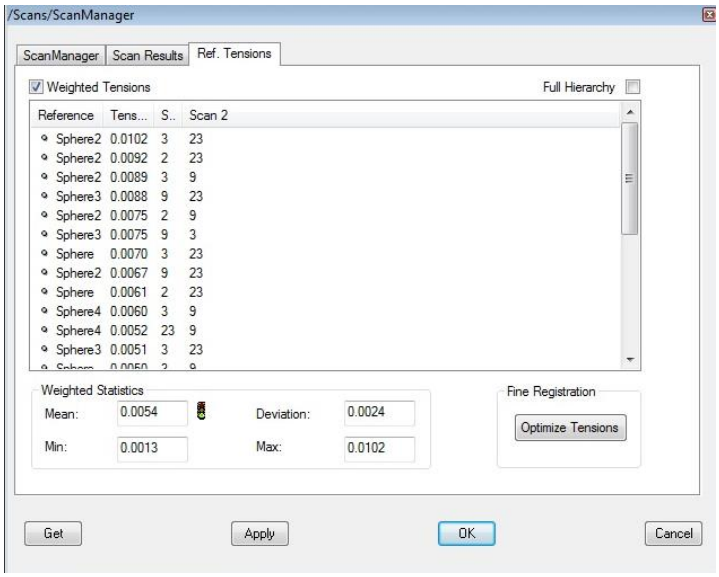

Figure 3.7: Summary of registration with FARO Scene®.

The registration started using the option Place Scans

(Force by manual target names) having previously numbered all the targets. A group of aligned scans with a standard deviation of 0.002 m was achieved. Figure 3.7 shows the screen with the statistics after registration. In the column Tensions below, the Euclidean distances are shown between the different scan positions per Reference (Sphere).

Leica Cyclone®

Leica Cyclone Register is based on the transformation of a rigid body, in which the estimation of parameters is performed by least squares, following closed form. The calculation of the matrix is carried out through quaternions and their multiplication to define axis and rotation angles as proposed by Horn [Horn, 1987]. To align the scans with Leica Cyclone software, several scans were imported in .pts format. For each scan, some points, named vertices by the software, were created and transformed into targets using the command Tools - Registration - Add / Edit record label. These vertices have the coordinates of the centers of the spherical targets.

Once the targets are labelled in all scans, using the command Auto-Add Constraints the targets are displayed in the list of constraints. After selecting the same scan as reference (Home ScanWorld), the alignment of scans was launched. A standard deviation of 0.0022 m

was achieved for the aligned scans.

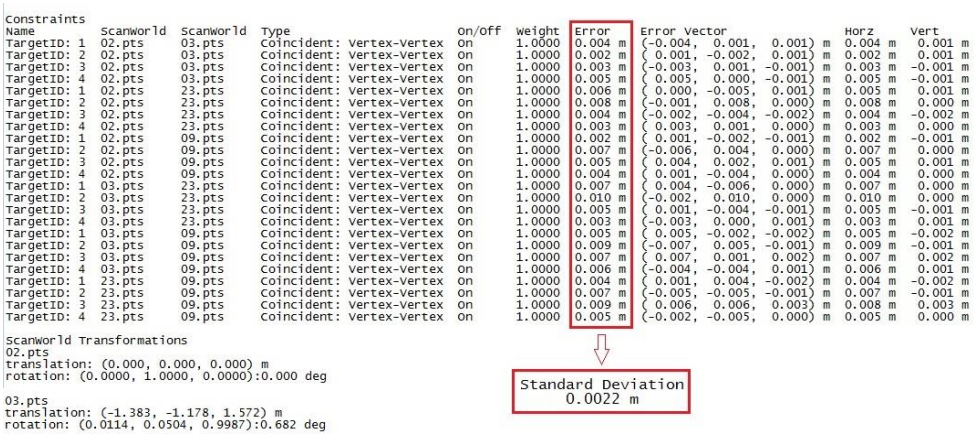

Constraints

Name	ScanWorld	ScanWorld	Type	On/Off	Weight	Error	Error Vector	Horz	Vert
TargetID: 1	02.pts	03.pts	Coincident: Vertex-Vertex	On	1.0000	0.004 m	(-0.004, 0.001, 0.001) m	0.004 m	0.001 m
TargetID: 2	02.pts	03.pts	Coincident: Vertex-Vertex	On	1.0000	0.002 m	(0.001, -0.002, 0.001) m	0.002 m	0.001 m
TargetID: 3	02.pts	03.pts	Coincident: Vertex-Vertex	On	1.0000	0.003 m	(-0.003, 0.001, -0.001) m	0.003 m	-0.001 m
TargetID: 4	02.pts	03.pts	Coincident: Vertex-Vertex	On	1.0000	0.005 m	(0.005, 0.000, -0.001) m	0.005 m	-0.001 m
TargetID: 1	02.pts	23.pts	Coincident: Vertex-Vertex	On	1.0000	0.006 m	(0.000, -0.005, 0.001) m	0.005 m	0.001 m
TargetID: 2	02.pts	23.pts	Coincident: Vertex-Vertex	On	1.0000	0.008 m	(-0.001, 0.008, 0.000) m	0.008 m	0.000 m
TargetID: 3	02.pts	23.pts	Coincident: Vertex-Vertex	On	1.0000	0.004 m	(-0.002, -0.004, -0.002) m	0.004 m	-0.002 m
TargetID: 4	02.pts	23.pts	Coincident: Vertex-Vertex	On	1.0000	0.003 m	(0.003, 0.001, 0.000) m	0.003 m	0.000 m
TargetID: 1	02.pts	09.pts	Coincident: Vertex-Vertex	On	1.0000	0.002 m	(0.001, -0.002, -0.001) m	0.002 m	-0.001 m
TargetID: 2	02.pts	09.pts	Coincident: Vertex-Vertex	On	1.0000	0.007 m	(-0.006, 0.004, 0.000) m	0.007 m	0.000 m
TargetID: 3	02.pts	09.pts	Coincident: Vertex-Vertex	On	1.0000	0.005 m	(0.004, 0.002, 0.001) m	0.005 m	0.001 m
TargetID: 4	02.pts	09.pts	Coincident: Vertex-Vertex	On	1.0000	0.004 m	(0.001, -0.004, 0.000) m	0.004 m	0.000 m
TargetID: 1	03.pts	23.pts	Coincident: Vertex-Vertex	On	1.0000	0.007 m	(0.004, -0.006, 0.000) m	0.007 m	0.000 m
TargetID: 2	03.pts	23.pts	Coincident: Vertex-Vertex	On	1.0000	0.010 m	(-0.002, 0.010, 0.000) m	0.010 m	0.000 m
TargetID: 3	03.pts	23.pts	Coincident: Vertex-Vertex	On	1.0000	0.005 m	(0.001, -0.004, -0.001) m	0.005 m	-0.001 m
TargetID: 4	03.pts	23.pts	Coincident: Vertex-Vertex	On	1.0000	0.003 m	(-0.003, 0.000, 0.001) m	0.003 m	0.001 m
TargetID: 1	03.pts	09.pts	Coincident: Vertex-Vertex	On	1.0000	0.005 m	(0.005, -0.002, -0.002) m	0.005 m	-0.002 m
TargetID: 2	03.pts	09.pts	Coincident: Vertex-Vertex	On	1.0000	0.009 m	(-0.007, 0.005, -0.001) m	0.009 m	-0.001 m
TargetID: 3	03.pts	09.pts	Coincident: Vertex-Vertex	On	1.0000	0.007 m	(0.007, 0.001, 0.002) m	0.007 m	0.002 m
TargetID: 4	03.pts	09.pts	Coincident: Vertex-Vertex	On	1.0000	0.006 m	(-0.004, -0.004, 0.001) m	0.006 m	0.001 m
TargetID: 1	23.pts	09.pts	Coincident: Vertex-Vertex	On	1.0000	0.004 m	(0.001, 0.004, -0.002) m	0.004 m	-0.002 m
TargetID: 2	23.pts	09.pts	Coincident: Vertex-Vertex	On	1.0000	0.007 m	(-0.005, -0.005, -0.001) m	0.007 m	-0.001 m
TargetID: 3	23.pts	09.pts	Coincident: Vertex-Vertex	On	1.0000	0.009 m	(0.006, 0.006, 0.003) m	0.008 m	0.003 m
TargetID: 4	23.pts	09.pts	Coincident: Vertex-Vertex	On	1.0000	0.005 m	(-0.002, -0.005, 0.000) m	0.005 m	0.000 m

ScanWorld Transformations
02.pts
translation: (0.000, 0.000, 0.000) m
rotation: (0.0000, 1.0000, 0.0000):0.000 deg

03.pts
translation: (-1.383, -1.178, 1.572) m
rotation: (0.0114, 0.0504, 0.9987):0.682 deg

Figure 3.8: Leica Cyclone Register 7.1 diagnostics report.

3DVEM – Register®

3DVEM – Register is a low-cost and user-friendly software developed for registration of LiDAR datasets by GIFLE at the Polytechnic University of Valencia. The indirect registration method among point clouds and/or 3D models is based on a 3D rigid transformation that is adjusted globally through a virtual reference network. The registration can be solved either by least-squares adjustment or by robust estimators (both Danish Method and Minimum Sum). To register you need to know the coordinates of the centers of the targets. From the drop-down menu Data/Import Files, the scans were imported in .pts format. For each scan, the target coordinates were

imported in txt format through the Targets/Spheres/Points Panel. For the registration, the 3DVEM – Register selects the best reference system [Fabado et al., 2013]. After alignment, the same scan was selected as reference. A standard deviation of 0.0023 m was obtained for the aligned scans. It is worth noticing that 3DVEM – Register reports on the precision estimates of the exterior orientation parameters for each scan. Therefore, it is very easy to confirm the quality of the final registration.

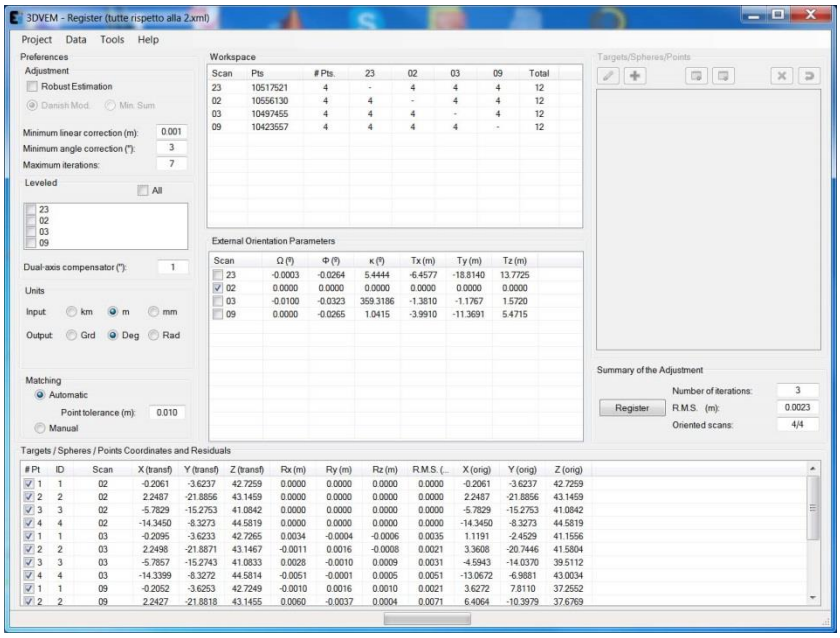

Figure 3.9: Summary of the registration with 3DVEM–Register v. 1.0.010.

Registration evaluation on the dome

To evaluate the registration performance, meshes were obtained from the registered point clouds. 3DReshaper® software was used for meshing. For each mesh, only the point cloud obtained from the union of registered scans was used, without filling holes and without noise reduction. All this was done in order to have a reference reflecting the point cloud, without arbitrary filters.

The comparison between the model and the point cloud, for all three clouds aligned with the three different software packages was made in Geomagic Studio® software [Figure 3.10]. The regular intrados dome of the church was used as testing area. The different points-deviations model results are presented below.

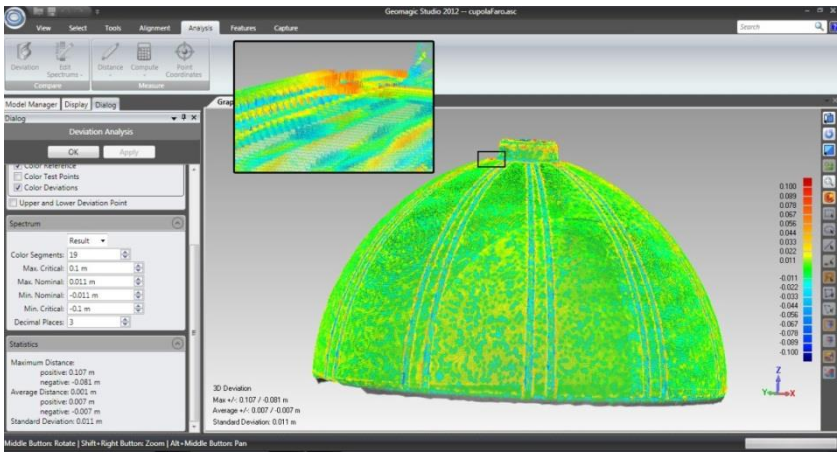

Figure 3.10: comparison between model and point cloud after FARO Scene.

The overall comparison can be summarized in the following Table 3.2. Quite similar distance differences are obtained with the three registration software. Only the maximum positive distance achieved with FARO Scene deviates more than both Leica Cyclone and 3DVEM – Register. It is worth noticing that the values are quite comparable, with slightly better results for the 3DVEM – Register software.

	$+ d_{Mean}$	$- d_{Mean}$	d_{Mean}	$+ d_{Max.}$	$- d_{Max.}$	σ_d
Faro Scene	0.007	-0.007	0.001	0.107	-0.081	0.011
Leica Cyclone	0.006	-0.007	0.001	0.092	-0.075	0.011
3DVEM – Register	0.006	-0.007	0.001	0.089	-0.079	0.010

Table 3.2: Distance deviations between point clouds and meshes (in m).

Table 3.3 reports on the differences achieved among meshes. The closeness in the output meshes after registration with Leica Cyclone and 3DVEM – Register is evident. In fact, the values are very similar. However, mesh obtained after registration with FARO Scene shows a greater deviation, not only with Leica Cyclone but also with 3DVEM – Register. The values are, in any case, thoroughly acceptable, given the accuracy of the instrument used and the size of the Church.

	+ dMean	- dMean	dMean	+ dMax.	- dMax.	σd
Scene - Cyclone	0.005	- 0.004	0.000	0.085	- 0.100	0.007
3DVEM – Register - Scene	0.004	- 0.005	0.000	0.072	- 0.086	0.007
3DVEM – Register - Cyclone	0.001	- 0.001	0.000	0.048	- 0.053	0.002

Table 3.3: Comparison between the different results of the deviations mesh-mesh.

In conclusion of the registration step, obtained indirectly by using only spherical targets, we can make the following remarks [Artese et al., 2014]:

- The registration results achieved with the different software packages yield equivalent residuals when comparing point clouds and 3D models coming from the same software;
- The comparison between the meshes extracted from different point clouds confirms that the results have the same order of magnitude. However, it is due to the derived exterior orientation parameters that the differences among registered output datasets coming from different registration implementations yield deviations higher than expected with FARO Scene, while almost identical results are achieved with Leica Cyclone and 3DVEM®-

Register;

- There are substantial differences while handling targets. It is possible to import directly the targets in 3DVEM®-Register in different ASCII formats while the user needs to create either vertices in Leica Cyclone or objects in FARO Scene. Furthermore, there is no need to know point/surface normal vectors. After the datasets are imported, all three registration packages run quickly the registration, 3DVEM®-Register being the fastest. This fact is relevant when dealing with large registration datasets where not only targets but coordinated points can be used to quickly solve out the registration with maximum reliability through the virtual reference network.
- The results show a substantial agreement between the three solutions. Noteworthy is the fact that the software 3DVEM®-Register gives the error estimates for each station;
- To have more meaningful results, additional studies should be undertaken with larger datasets regarding both scan positions and different numbers of targets.

3D model and detection of structural problems

The survey executed by laser scanner highlights some aspects, not yet solved, regarding the form and the building history of the church: first of all, the shape of the dome.

The masonry dome, built by using bricks, is often described erroneously as a hemisphere, similar to the Pantheon. Actually, the dome presents a radial symmetry, but the vertical section is obtained through two circular arches, with a radius of 28.50 m. The building of the dome was very troublesome, due to its large dimensions. In correspondence to several dome slices, some cracks can be observed. Furthermore, the floor presents a slope: it is not clear if the slope is the same as in the original project, or if other problems occurred during construction.

Comparison between actual and ideal shape of the dome – Thermal camera surveying – Cracks on the dome

The results of the laser scanner survey allowed us to obtain the deviations of the dome surface with respect to a likely design surface. As reported above, the surface of the dome is quite different compared to a semi-sphere, so the diffused hypothesis about a "copy"

of the Pantheon scheme is wrong.

It is highly interesting that the deviation between the real surface (best fitting ideal surface) and a bohemian vault (slice of dome), that is the more likely design surface, is at a maximum near the cracks, where these are present.

In the following figures, we can observe:

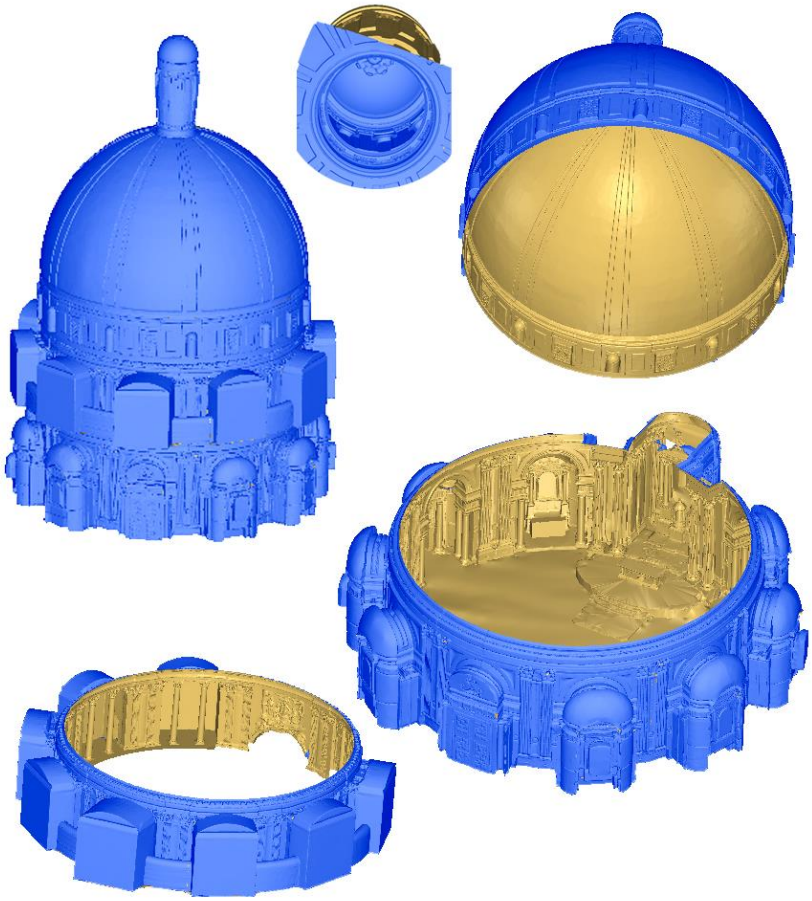

Figure 3.11: The 3D mesh of the Escuelas Pías Church.

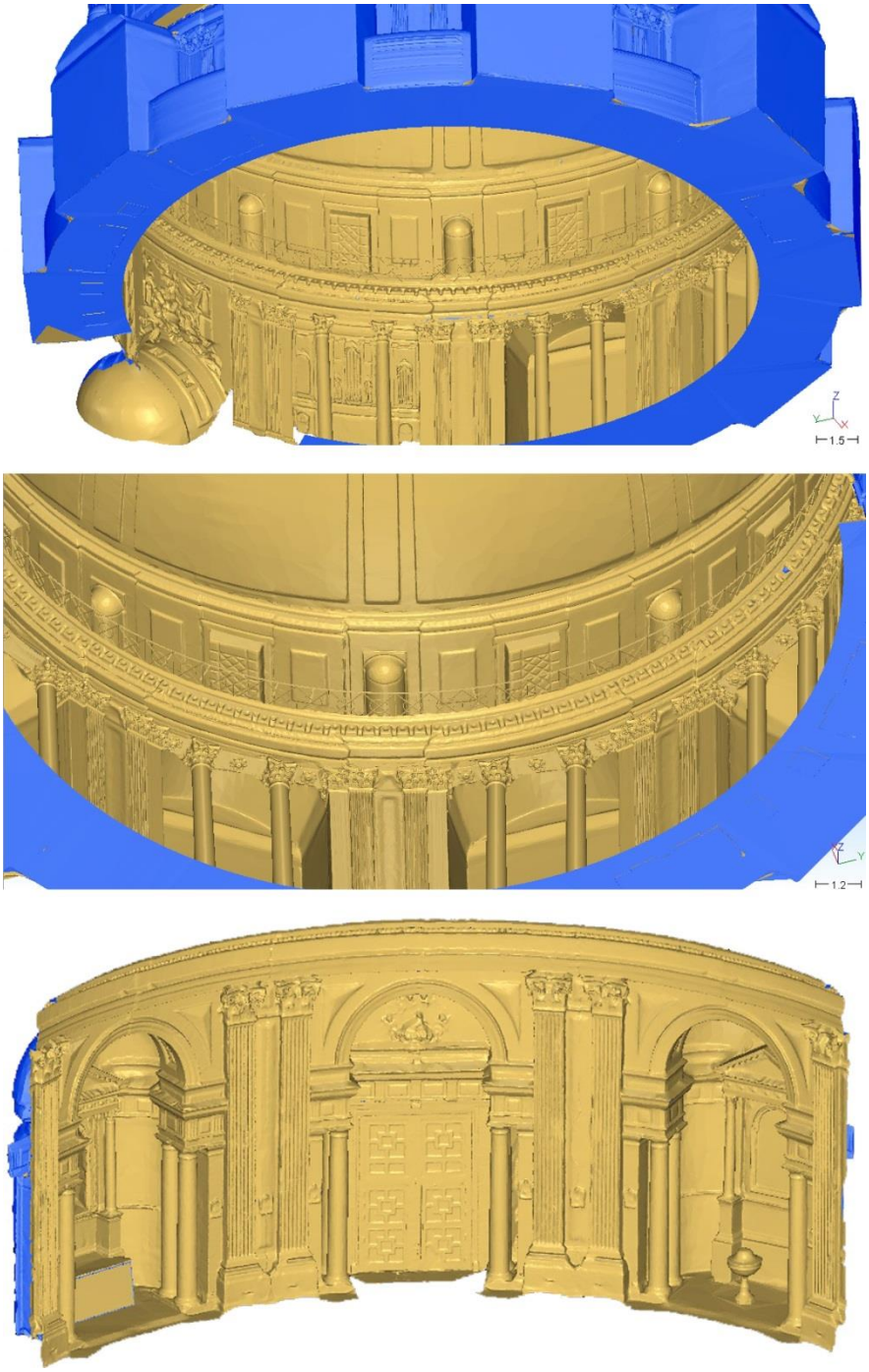

Figure 3.12: Level of detail of the mesh.

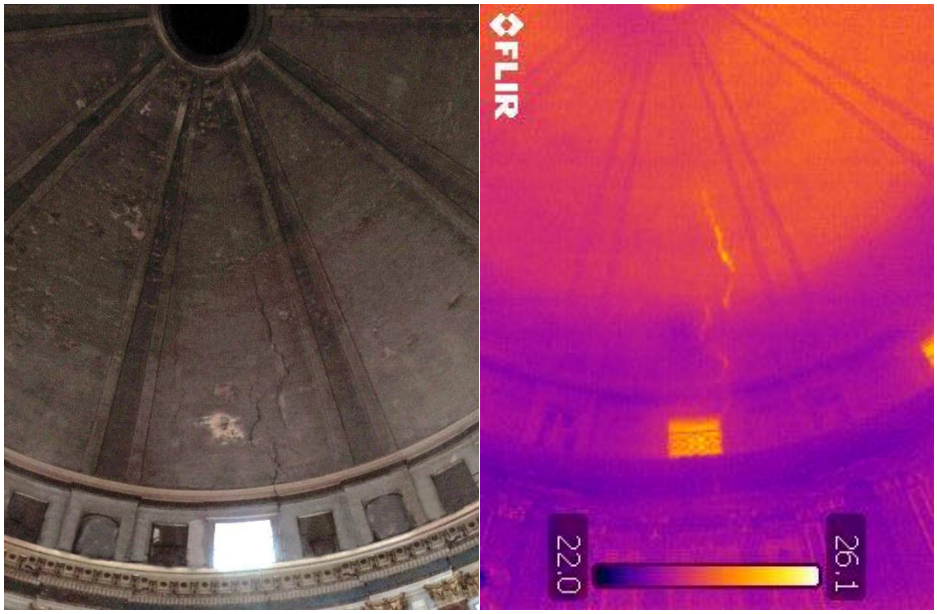

Figure 3.13: The crack on a dome slice and the corresponding thermal image.

Figure 3.14: A view of the 3D model textured with the thermal image.

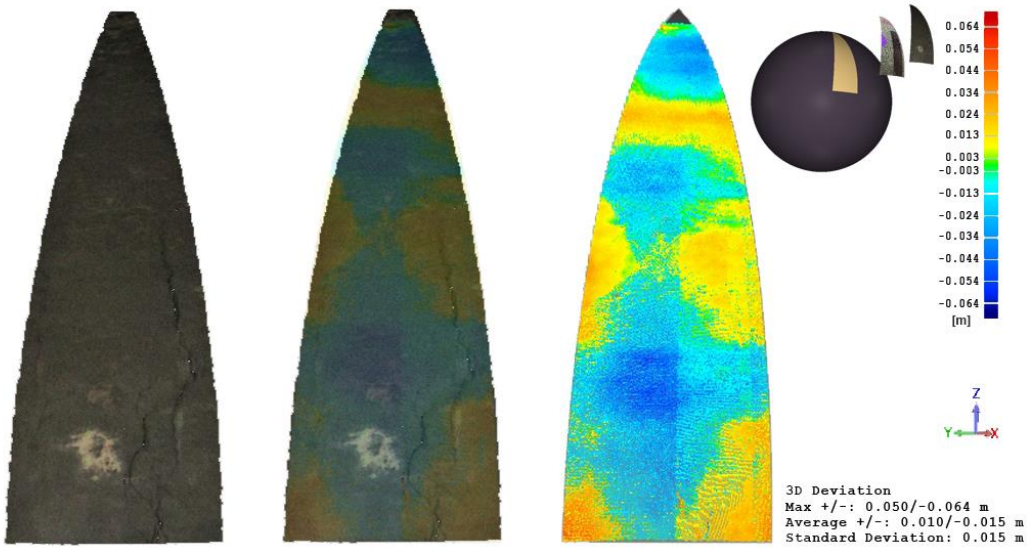

Figure 3.15: The deviations between ideal and actual surface.

The deviations of the symmetry axis

Another question regards the floor and the axis of drum, dome and lantern.

The low slope, present in the floor, is not directed towards the main altar, but has an orthogonal direction, so it is unlikely that it was foreseen in the original project. The axis of the church should give some information useful for hypothesizing the causes of the floor slope.

To find the axis of the church, horizontal sections were obtained on the 3D model every meter; the

centroids of the sections, were then found. The most likely axis should be the line that interpolates all centroids. The axis found with the above described procedure shows a deviation of about 0.44 degrees with respect to the vertical (from the floor to the top of the dome). The centroids move in the direction of the transept to the left for an observer looking at the principal altar. The floor of the church has a slope of about 0.137 degrees in the same direction. Since the biaxial compensator of both laser scanners used for the survey has a precision of 0.015 degrees, the slope of the floor is real. Given that the deviation of the axis is to some degree greater than the slope of the floor we could make the following hypotheses: (a) the whole church suffered a subsidence after its realization, (b) due to small errors during the building, the central axis was not vertical also at the end of its realization.

In the following, we can see some views of the 3D model. Figure 3.16 shows a nadiral view with the bottom and upper fitting circles (the translation of the center is evident) and a zoom of the nadiral view, in which the envelope of the horizontal sections centroids is highlighted (Cyan: lower church and drum - Pink: Dome - Yellow: lantern). Figures 3.17 show two axonometries (the thin black line is the vertical in the bottom center).

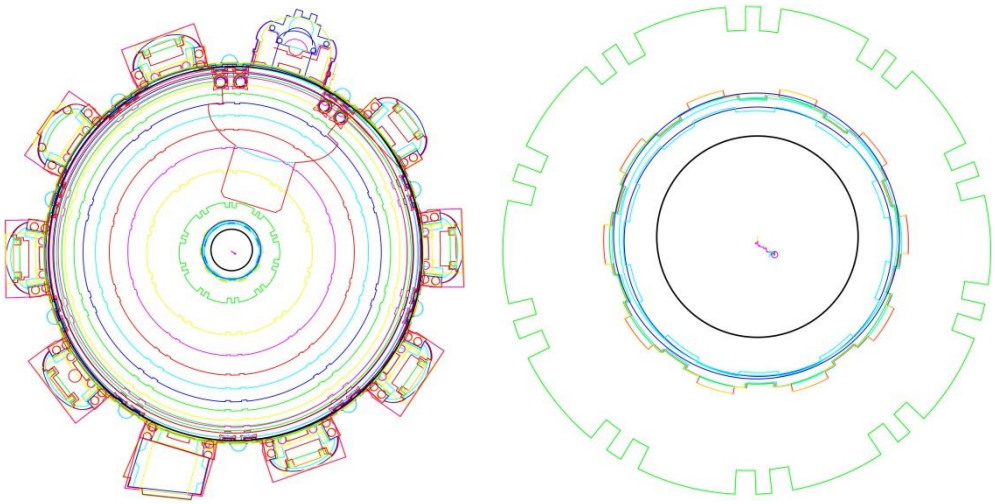

Figure 3.16: Nadiral view and zoom.

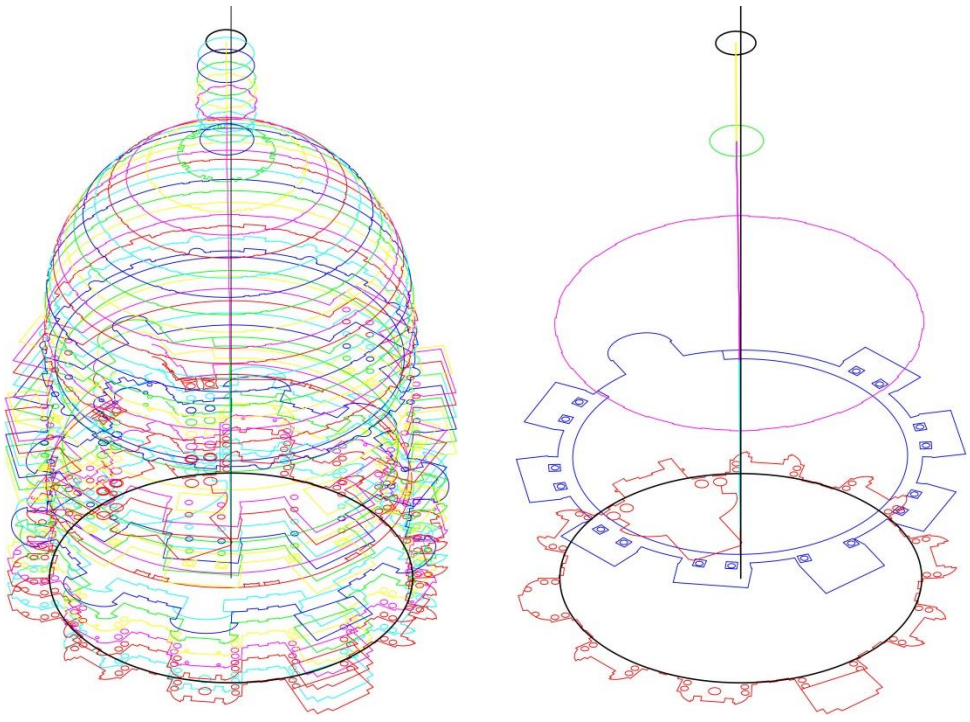

Figure 3.17: Axonometric views.

It should be noted that the direction of the axis of the lantern is quite different form the one of the church. This is evidenced by the position of the projection of the centroids on a horizontal plane. At this point we can consider as valid both hypotheses about subsidence and small aligning errors. In any event, the data collected and the results of the processing offer useful information to historians of art and to structural engineers for reconstructing the building history and better understanding the origin of the structural problems of the church.

4

The investigations carried out on the church of Santa Maria dei Longobardi in San Marco Argentano.

The thermographic analysis was aimed at understanding the structure of the church façade (Figure 4.1). It started from the previous collection of historical information about the construction and reconstruction of the building. Over the centuries, in fact, the church has undergone many alterations that have distorted its original architectural characteristics. Historical information is, therefore, crucial to formulating realistic assumptions on the original

system and to comparing the results of imaging studies performed.

Figure 4.1: Present elevation of the Santa Maria dei Longobardi church, in San Marco Argentano.

There is, therefore, a synergistic effect between the two types of investigation by means of which information is carried out on the stratification of the building phases and on elements concealed and incorporated due to successive restorations and curtain walls. The original can be reconstructed from a series of graphics and photographic documentation, as well as from archival records [Archivio Storico Diocesi San Marco Argentano-Scalea; Archivio di Stato di Cosenza; Pacichelli, 1703; Amirante, 2005; Antologia dell'Archivio Selvaggi; Cristofaro, 1932;

Soprintendenza B.A.P. delle Province di Cosenza, Catanzaro e Crotone].

It is characterized by the presence of two symmetrical openings in the upper part of the facade. The first graphic documentation (a drawing of the abbot Pacichelli, Figure 4.2) shows, in addition to the two openings at the top, a central portal. The subsequent documentations highlight the presence, in correspondence of the two windows, of two portals (Figure 4.3).

Figure 4.2: G.B. Pacichelli, Il Regno di Napoli in prospettiva, view of di San Marco.

The façade has two portals but there is no trace of windows. We wanted to investigate the presence of such windows.

Figure 4.3: A photo of a religious procession in 1936 (archive of Parrocchia Sacro Cuore di Gesù, San Marco Argentano).

In order to avoid invasive techniques, we used a thermal imaging camera [Hum-Hartley, 1978; Fidler, 1980; Voltolini et al., 2007; Grinzato, 2012] along with a total station. The camera used is a FLIR E40bx. It is equipped with a double sensor for inspection controls in the buildings. The measuring range, between -20 and + 120°C, optimizes the performance of the IR detector to provide quality images. The 3.1 megapixels CCD camera for the visible assures detail to better document the object in view.

Through the use of the camera using a passive technique, the presence of the two windows is highlighted, currently walled, in correspondence of which the heat flow is evidently changed compared to the rest of the wall.

A Leica robotic 1201+ total station was used. By using it simultaneously to the camera, we evaluated the exact positioning of the windows in the facade and with respect to the entire church-bell tower complex. During the investigation with the thermal camera it was possible, thanks to the laser pointer, to highlight the top of the openings. The 3D model of the entire church was obtained. The positioning of the hidden windows evidenced the displacement of the portal adjacent to the bell. The Thermographic investigation showed that the current portal is moved toward the center of the façade (Figure 4.4).

Figure 4.4: Thermal shots: the hidden openings and the different position of the gate adjacent to the bell tower.

In conclusion, it is evident that the use of infrared techniques, appropriately integrated with Geomatics techniques, allows us to effect not only the detection of hidden elements but also their geometric characteristics and location with extreme precision. This can be of great help if restoration work is foreseen: actually, it is possible to minimize any invasive procedures. The interventions can be accurately programmed and they may be limited to minimum actions; this is very important for prestigious plasters and coatings.

5

The survey, the representation and the structural modeling of ancient and modern bridges

In the last few years, at the SmartLab laboratory at the University of Calabria, activities were developed in the field of surveying, monitoring and representation of structures. In the framework of these activities, Geomatics techniques have been used widely for the surveying of bridges since 2014.

The authorities in charge of maintenance of the road structures (ANAS, Regions, Provinces) have to face different problems for both new and dated

structures. In the first case, you have the working plans and the design drawings, so the goal of the surveys is to get the *as built*, to be compared with the project, for testing activities and accounting of work performed, as well as for documentation purposes [Fuchs et al., 2004, Zogg and Ingensand, 2008]. In the case of dated structures, very often it is very often not possible to obtain the design documents, so then the survey is also used to reconstruct the manner of execution and disassemble the organism into the structural elements that were considered and dimensioned during the design phase [Lubowiecka et al., 2009]. The results of the measurements are used for documentation and representation purposes, as well as for the reconstruction of the constructive procedures. The finite element modeling of the structures was obtained to simulate their behavior in case of earthquake. The analysis of the calculation results allows us to identify the critical parts of the structures, possibly to be reinforced, and which present the maximum stress. The surveys and representations are used also for the identification of degraded areas or which have detachments of bar coverage, on which we must intervene with actions of recovery and restoration.

An accurate finite element model is used, finally, for the identification of the vibration modes of the

structure independently from external stresses, necessary for predicting its behavior under dynamic loads.

The following describes the operations performed for surveying and modeling of two bridges located on two roads managed by the Province of Cosenza.

The first bridge has been recently built, and it is characterized by a superstructure realized with precast pre-stressed concrete girders and provided with seismic isolators. In this case, the activity is mainly aimed at getting an *as built*, useful for control and documentation. The second bridge dates back to the 50s of the last century: it is an arch bridge made of reinforced concrete. The survey in this case is aimed at the exact reconstruction of its geometry, the identification of foundation settlement and finite element modeling, to simulate the behavior of the structure under seismic conditions.

Instruments and methodology

It was decided to use laser scanner technology, with an integrated camera, and a GPS for the georeferencing, in order to acquire large amounts of geometric and photographic data in a short period (Figure 5.1).

Figure 5.1 The instruments used: Laser Scanner Riegl VZ 1000 and GNSS receiver Leica Viva.

The choice of the laser scanner to perform a survey in a satisfactory manner, with adequate precision and completeness of representation, must take into account, in addition to the mandatory considerations about the accuracy and the flow rate, some other practical-operational features.

Fundamental to this is the evaluation of the number of scans necessary for the complete visibility of all parts of the object to be surveyed, and the conditions in which it must operate to perform the survey. The laser scanner RIEGL VZ 1000 was used, with the following characteristics:

- Accuracy of single point: ± 8mm.
- Range: from 1m to 1400 m.
- Sampling frequency: until 122.000 points/sec.
- Field of view: 100°(Vertical) - 360° (Horizontal).
- Leveler and magnetometer.
- GPS receiver.
- Nikon D610 Camera with a 20 mm calibrated lens.
- Acquisition of pulse waveform return.

This last characteristic allows us to discriminate the terrain or a object from the vegetation that covers it. The processing of data from the laser scanner was performed with the RiscanPro® and Geomagic® software.

It must be noted that the laser scanner is equipped with a GNSS receiver which allows just an approximate positioning of the station (single point positioning) with the use of the code and the method of pseudoranges, whereby, to obtain an accurate geo-referencing, we used a Leica Viva dual-frequency receiver, capable of receiving the signals from GPS and GLONASS constellation. For the data processing of satellite measurements in differential mode, we made use of data acquired by the permanent station GNSS positioned at the Laboratory of Geomatics, Department of Civil Engineering - University of Calabria, which captures data at a frequency of one second. The

processing of the acquired data, performed with the Leica Geo Office® software, provided the coordinates of the station points with centimeter accuracy.

The Arenazza bridge

The Arenazza bridge, in the locality of Ceramide near the town of Cetraro (CS), is located at km 0+250 on the Provincial Road number 270 (Figure 5.2).

Figure 5.2 The Arenazza bridge.

It is a bridge with two spans, with a deck consisting of pre-stressed concrete beams laid side by side and an

overlying reinforced concrete slab; the beams are resting on the abutments and on the central pier, equipped with seismic isolators. The main aim of the survey was to verify the conformity of the realized construction with respect to the project. For this reason, it was not necessary to carry out scans on the two sides of the road, it was sufficient to get the dimensioning of construction elements (abutment, pier, beams, bearing).

Figure 5.3 Scans before and after filtering.

The presence of a metal fence that prevented access to the area north of the road did not constitute, therefore, a problem. It was sufficient, besides, to have only one station point, chosen so as to be able to scan the maximum part of the bridge (Figure 5.3).

The instrument, used with the compensator, equipped with the external Nikon D610 camera and the GNSS receiver, was configured with a resolution of 0.08°/pt and a scan rate of 120,000 points per second. Some details of the bridge (seismic isolators) were scanned with a resolution of 0.007°/pt in order to reconstruct their geometry in a more accurate way. For georeferencing, the station coordinates obtained by GPS were used, combined with indications of the magnetometer which is fitted to the laser scanner.

After reducing the point cloud through the operations of noise filtering, decimation and filtering of the redundancy, we faced the phase of surface reconstruction, through the mesh.

By imposing the existence of known geometric primitives (plans), the simplified geometry of the construction was obtained, to be compared with the project drawings.

From the three-dimensional model vertical and horizontal sections were produced. The detailed scans were used for modeling the bearings (Figure 5.4).

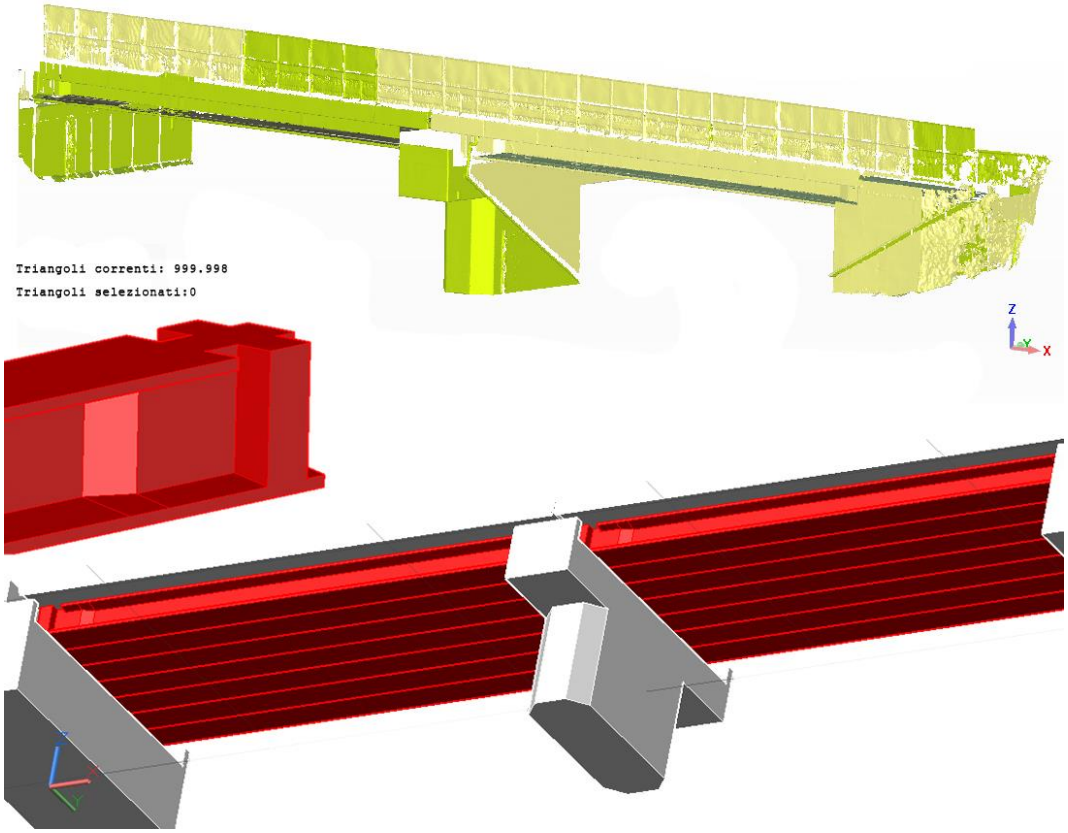

Figure 5.4 Mesh of Arenazza bridge.

The Caprovidi bridge

The Caprovidi bridge, in place at S. Angelo, at the town of Cetraro (CS), is located at km 1+900 of Provincial Road number 26. Is a reinforced concrete arch bridge, cast in place, with two frame piers convergent with the plinths of the supporting arch (Figure 5.5).

Figure 5.5 The Caprovidi bridge.

Three scans were used (Figure 5.6). Due to the topographic situation, in fact, it was not possible to obtain access to the area on the hydraulic right side of the river, for which some parts were not visible; the thick vegetation was also an obstacle which prevented scanning of some parts of the bridge abutments. Lastly, the support bases of the arch and of the Y piers are covered by backfill terrain. For each scan a partial spatial overlap with the adjacent ones was planned.

Figure 5.6 Union of scans and detail of a colored point cloud.

Two scans were performed from the two sides of the bridge; for the third acquisition, performed under the

deck, the instrument was positioned with an inclination of 90°. Also in this case, some details of the bridge were scanned with more definition. Cylindrical targets were positioned, having a diameter of 14 cm, to facilitate the alignment of the scans in the data processing. The reference system of the first station was used also for the subsequent ones. The targets, having reflecting surface, were positioned in such a way as to be easily and clearly visible in the scans. For accurate georeferencing, acquisitions were used performed by the dual-frequency GNSS receiver, post-processed along with the data collected from the fixed permanent station. The filtering and the reduction of the point clouds was particularly delicate. While having the possibility of discriminating the return pulses, a thorough job on the part of the operator was necessary, since the automatic procedures were influenced by the vegetation and the geometry of the work. In the absence of the project drawings, the survey was aimed at the reconstruction of the structure, but also at obtaining the initial design (reverse engineering). For this reason, two 3D models were created: the first was obtained directly from the mesh generated after the steps of registration, filtering and decimation; the second one is the geometrically regular model, which should constitute the project work. The first model can be used for

documentation, while the second is used as a basis for structural modeling. Recent applications aim at obtaining the finite element model directly from the point cloud [Castellazzi et al., 2015; Vosselman et al., 2004]. In figure 5.7, the mesh obtained after the elimination of the vegetation is observed. There is an evident lack of information, especially in the areas of the foundations.

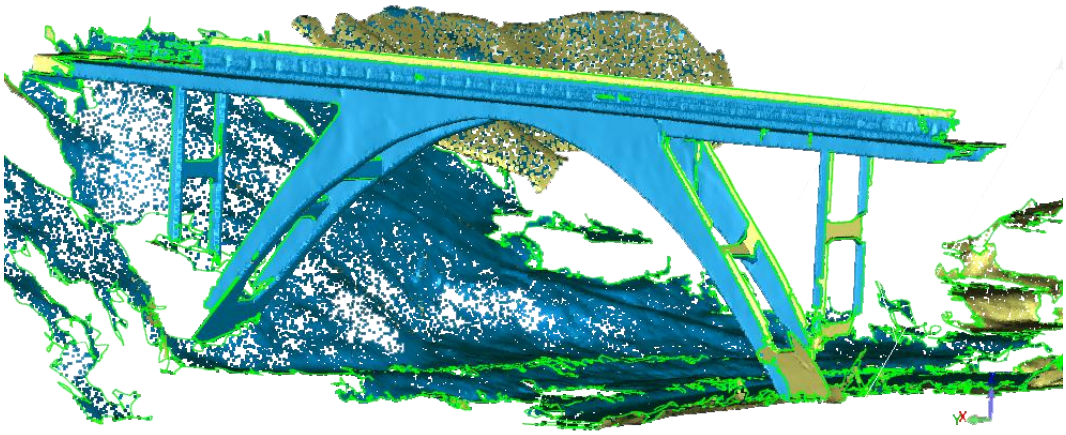

Figure 5.7 Mesh without vegetation.

The on-site investigation and detailed measurements allowed us to integrate the results of the laser scanner survey and to develop the likely geometric model of the project, shown in Figure 5.8 with the main structural elements highlighted in different colors.

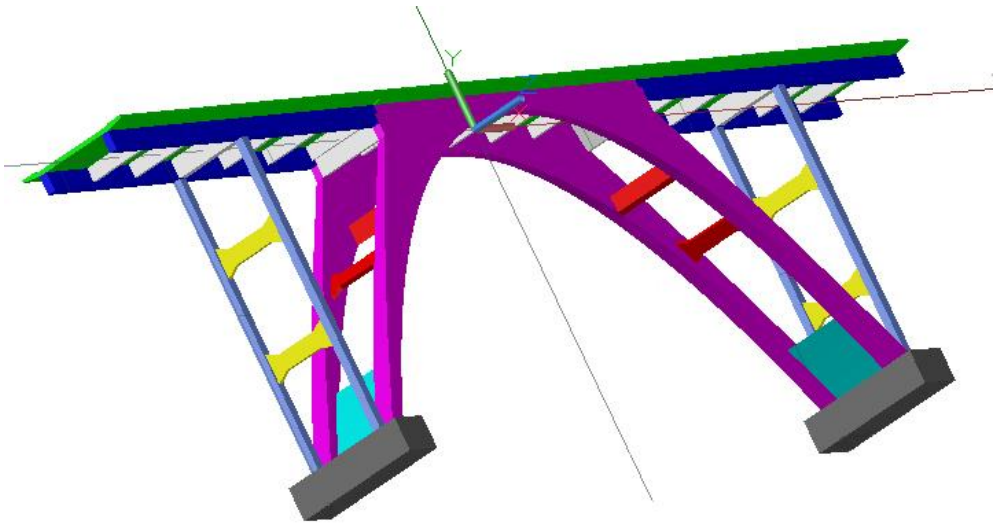

Figure 5.8 The geometric model.

Figures 5.9 and 5.10 show the deviations between the ideal geometric model and the point cloud.

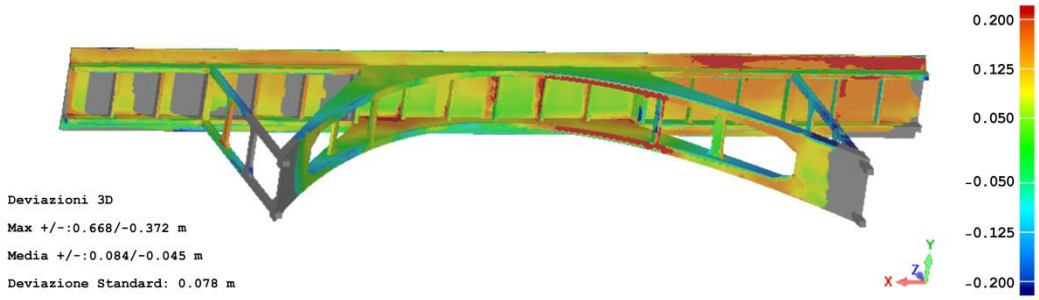

Figure 5.9 Deviations points-model.

It can be observed that the deviations are typically of centimetric order, within the manufacturing tolerances for this kind of structure (cast on site).

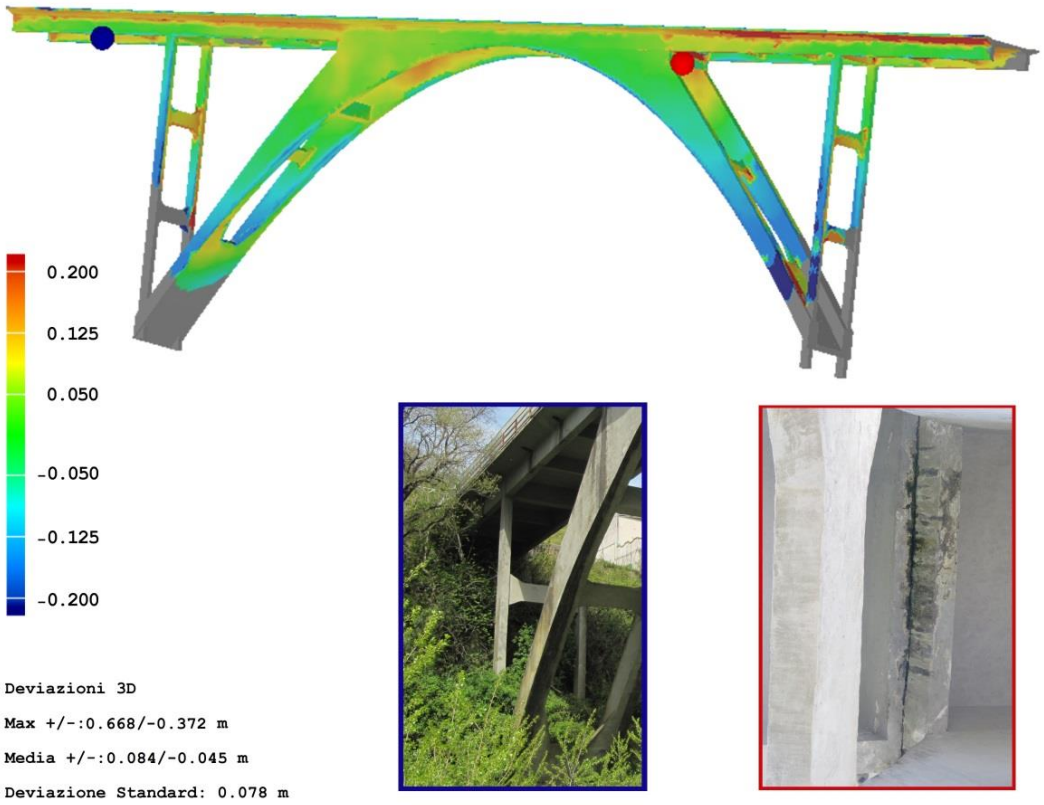

Figure 5.10 Deviations points-model in correspondence to deteriorated areas and vegetation.

The red and blue areas identify irregularities generally due to detachment of material. The very high values of the maximum and minimum deviations are due to the presence of some unfiltered points, automatically assigned by the software to a wrong surface.

During vectorization, we proceeded to eliminate eventual interference between the various simple solids that form the overall volume. The model so obtained, in

this case, was used for the dynamic identification, a very useful procedure also for detecting possible damage to the structure. The initial model was transformed into the finite element model (FEM) and analyzed using the Abaqus® [ABAQUS, 2014], structural analysis software which through automatic procedures imports the vectorized graphic model and converts it into a finite element mesh, in this case 4-node tetrahedral elements with only 3 degrees of freedom per node (Ux, Uy, Uz). This type of element was used to generate the mainly structured and anyway quite regular mesh, without losing accuracy, even in zones with variable thickness (Figures 5.11 and 5.12).

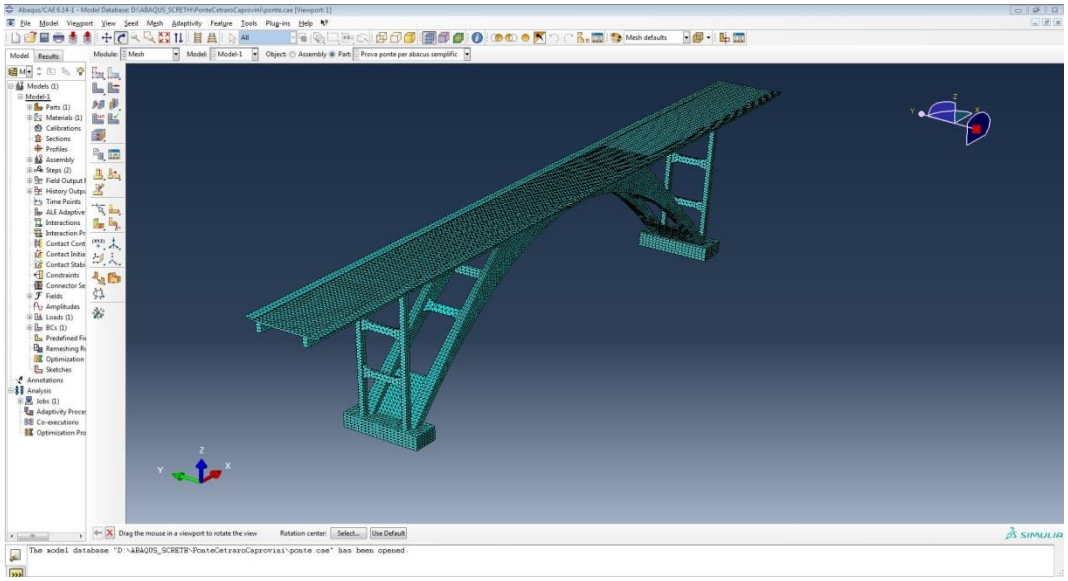

Figure 5.11 FEM model generated automatically from the CAD model.

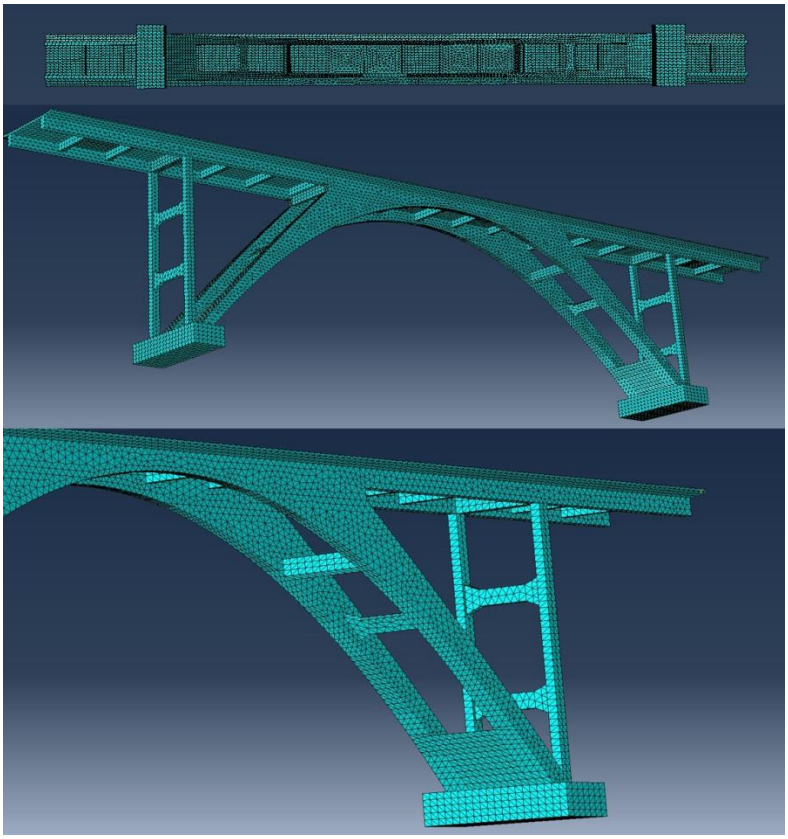

Figure 5.12 Views of the FEM model.

The outputs of the structural calculations performed on the finite element model, were compared with those obtained through *in situ* measurements obtained by positioning some unidirectional acceleration transducers on the bridge, arranged in an appropriate manner, of piezo-electric type, with a sensitivity equal to 10 V/g. These sensors identified the real vibration modes of the structure subjected to ambient noise and uncontrolled stress, FDD (Figure 5.13).

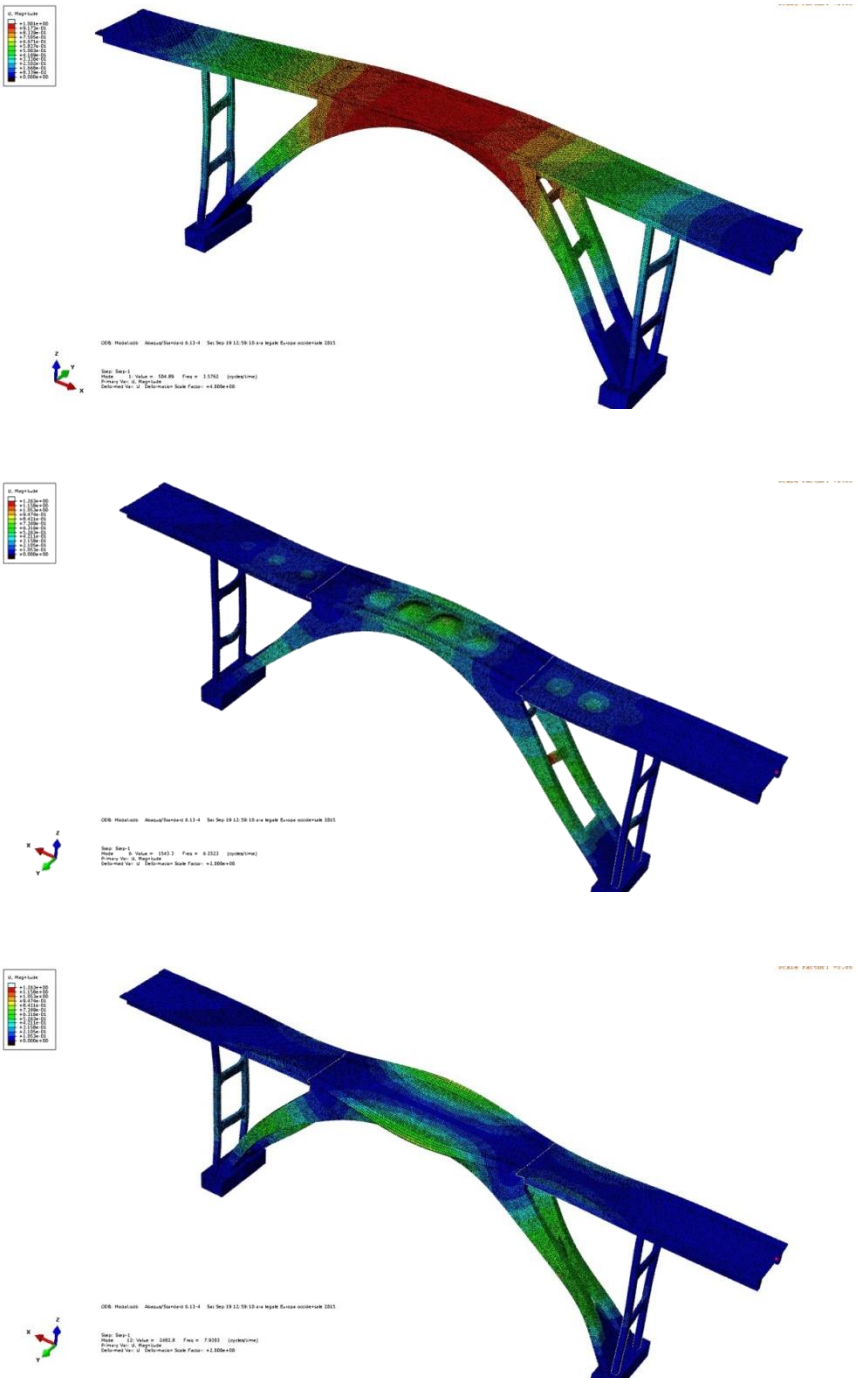

Figure 5.13 vibration modes.

The analysis results are in perfect agreement with the measurements *in situ* and specific procedures were not necessary for updating the identification of the mechanical characteristics of the structure, which were in agreement with the design values or measured on site [Artese et al., 2015].

Future activities: the S.Angelo bridge

The results obtained in the first cases showed the usefulness of Geomatics techniques both for the documentation and for structural modeling of modern bridges. Another activity regards the ancient constructions in brick masonry and stones, which present special problems, and several examples of which are present and still used along the roads.

A very interesting construction is the Sant'Angelo Bridge, also known as the Hannibal Bridge. It is a Roman bridge dating from the II sec. B.C., located between the towns of Altilia and Scigliano, in the Province of Cosenza (Figure 5.14). The scans of the construction were performed, while the building of the model is still in progress.

Figure 5.14 The Hannibal Bridge.

Like in the previous cases, the activities of survey (Figure 5.15) were carried out through the use of two techniques: terrestrial Time of Flight laser scanner Riegl VZ 1000 to acquire the geometric characteristics, and GNSS receiver for georeferencing.

Figure 5.15 Survey of the Hannibal Bridge with Laser Scanners and GNSS receiver.

To scan the bridge in its entirety, five station points were chosen. The scans carried out have provided very high density point clouds (Figure 5.16), which describe the surface of the object with extreme detail. For the connection of individual scans it have been used cylindrical target, and common points (tie points).

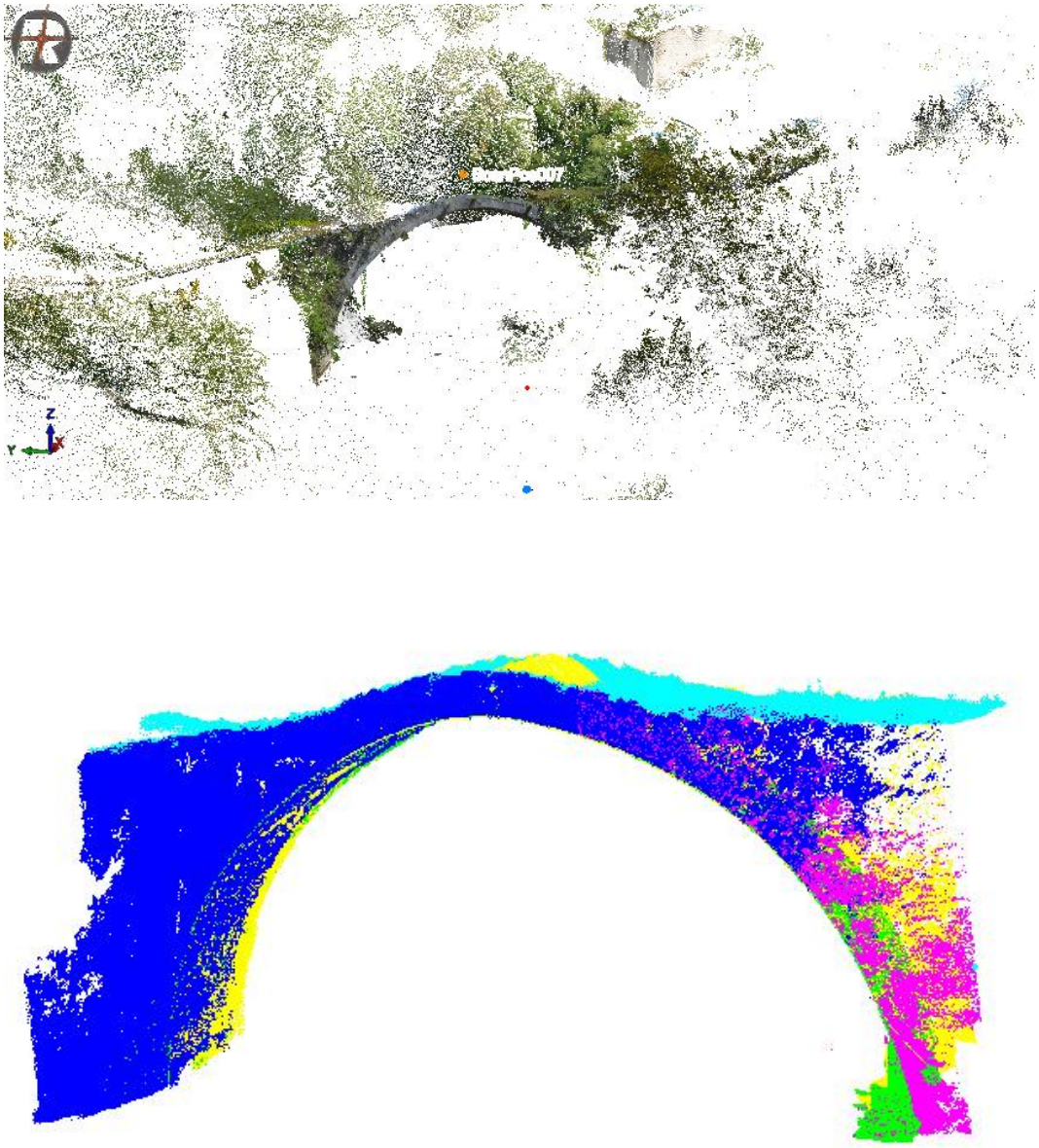

Figure 5.16 The union of the scans.

6

The DIC method used for the test of some composite material specimens

The DIC method was used for the test of some composite material specimens, carried out in the framework of the activities of the Smart-Lab. The test was integrated with an IR survey.

To carry out the test, several activities were involved: (a) calibration of camera lens, (b) determination of the scale of the frames, (c) synchronization of testing machines and digital camera, (d) calibration of the DIC software by using specimens with known geometric and mechanical characteristics,

(e) testing on fiber reinforced concrete specimen, (f) comparison of the results obtained by DIC and test machine.

Calibration of camera lens

A full frame Nikon 610 camera (35.9 x 24.0 mm CMOS sensor FX format) was used, with a resolution of 24.3 Mpixels (6016 x 4016). The pixel size is 5.97 μm.

To calibrate the 55 mm Nikkor lens used for the tests, the Camera Calibration Toolbox for Matlab® was used, with the added possibility to exclude points or to modify their position in the photo. The results of the calibration are reported in figure 6.1.

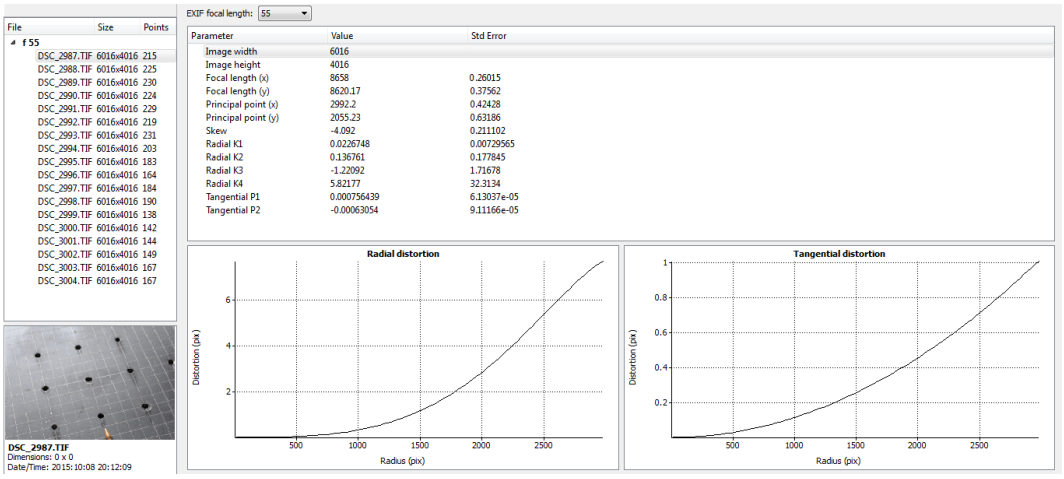

Figure 6.1: Results of the lens calibration.

Determination of the scale of the frames

For each test, the camera was positioned on a very robust stative, in front of the specimen. The distance between the grips, easily detectable in the frames, was measured by a digital caliper; in addition, the known dimensions of the specimen could allow us to rectify the frames. In this case, the rectification was not necessary, thanks to the very accurate orthogonal nature of the line of sight of the camera with respect to the plane of the specimen. Thus, the scale of the frames has been easily obtained from the ratio of the distance in mm between the grips, and the same distance in pixels.

Synchronization of testing machines and digital camera

To synchronize the acquisitions of the test machine, the photo-camera and the IR camera, two chronometers were used (Figure 6.2). After the time start-up, a photo of their displays, close to each other, was acquired. The first chronometer was positioned near the monitor of the computer used to drive the test machine, the second one was positioned close to the specimen. In this way it was possible to synchronize the frames of the video of the specimen with the ones of the test machine computer.

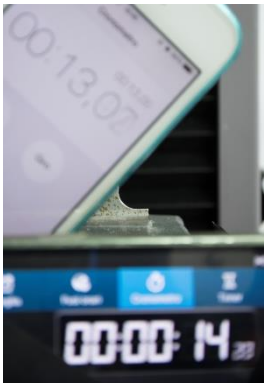

Figure 6.2: The chronometers used for the synchronization of testing machines and digital camera.

Calibration of the DIC software by using specimens with known geometric and mechanical characteristics

The test was carried out by using three aluminium "dog bone" specimens. The dimensions are shown in figure 6.3, the thickness is 1 mm, while the characteristics of the alloy are reported in table 6.1.

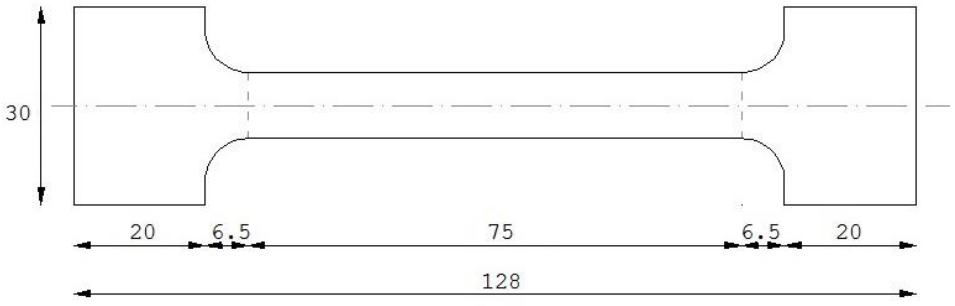

Figure 6.3: Dimensions of the aluminium specimen.

PHYSICAL AND MECHANICAL PROPERTIES

(BS EN 485-2:2008)

Density	2.70 g/cm3
Melting Point	555 °C
Thermal Expansion	24 x10-6 /K
Modulus of Elasticity	70 GPa
Thermal Conductivity	180 W/m.K
Electrical Resistivity	0.038 x10-6 Ω .m
Proof Stress	255 Min MPa
Tensile Strength	300 Min MPa
Elongation A50	mm 9 Min %
Hardness Brinnell	91 HB

Table 6.1. Properties of the specimen aluminium alloy.

Two tests were carried out following the technical rules UNI EN 10002-1. The test machine is an INSTRON MTS model Criterion series 40.

The lens aperture was set to 5.6: this value allows a good lens resolution; the limited field depth was not a problem, because of the plane and flat surface of the specimen.

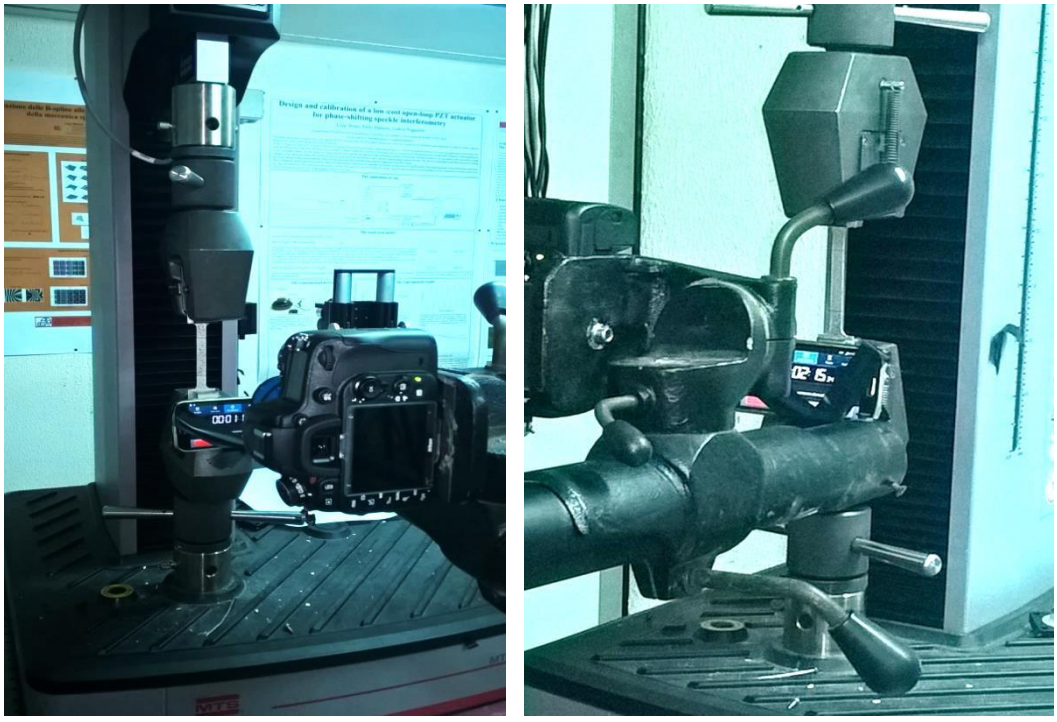

Figure 6.4: The apparatus for the shooting of the test on the aluminium specimen.

In figure 6.4 we can observe the camera mounted on the stative, the specimen and the chronometer. The distance between camera and specimen was 26 cm; the distance between the grips, measured by a digital caliper, is 98.0 mm. In the first frame, the distance is 570 pixels, so the frame scale is 1 pixel = 0.172 mm. Theoretically, the DIC should be able to perform the matching with a precision of .01 pixel, so a theoretical resolution of about 2 μm could be obtained.

Digital Image Correlation is performed using several software programs. The most diffused code is implemented in the Image Processing Toolbox™ MATLAB®. The best results are obtained by commercial software; in our case, the frames were processed using the program VIC-2D™ of Correlated Solutions, that guarantees very high performances. The displacements measured by the test machine are in agreement with the ones computed by the program: the maximum difference is about .06 mm for a final displacement of 4.00 mm. This difference of 1.5% is practically constant during the tests. Taking into account of an approximation of about 0.1 mm for the measurements carried out with the caliper and the length of 98 mm, the relative error is about 0.1%, quite lower than the difference detected; furthermore, 0.06 mm is about 0.33 pixels, rather greater than the DIC resolution. Thus the difference of 1.5% can be considered as a systematic deviation between the measurement systems.

In the following, we will comment on some results.

In figure 6.5 one can see the distribution of the Von Mises strain at the end of the test 1. Note the direction of the principal strain, not perfectly aligned with the vertical direction. Higher points do not belong to the specimen, but to the grip, so the corresponding values are not meaningful.

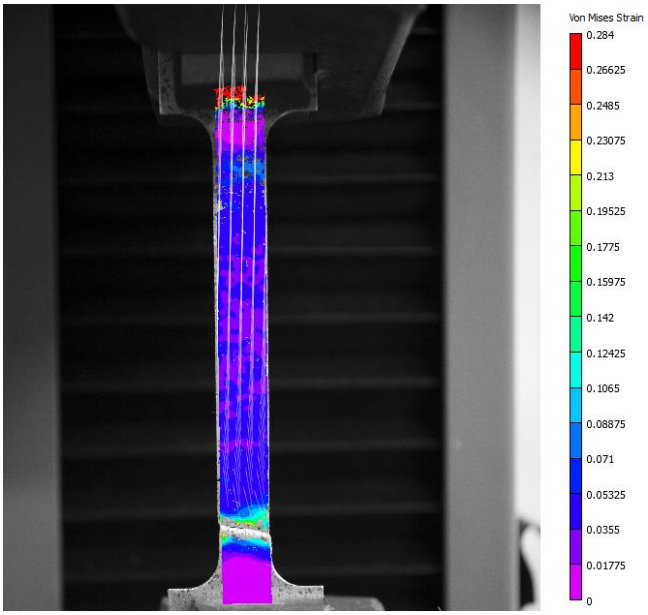

Figure 6.5: Von Mises strain at the end of the test 1.

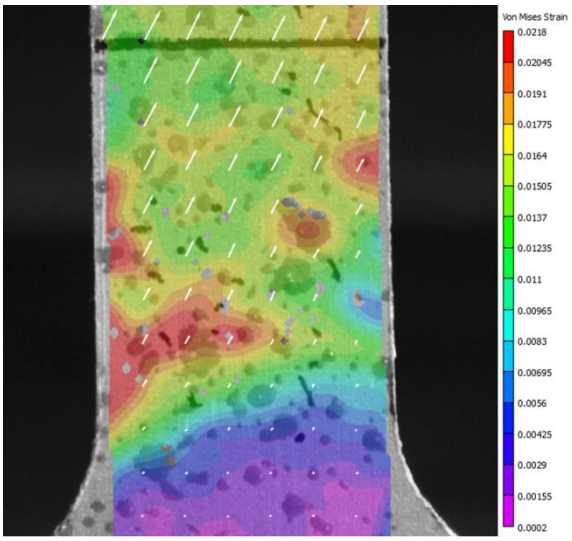

Figure 6.6: Zoom of Von Mises strain in the first phase of the test 1.

Figure 6.6 shows a zoom of the distribution of the Von Mises strain in the first phase of the test 1: maxima values are in the zone of the final crack.

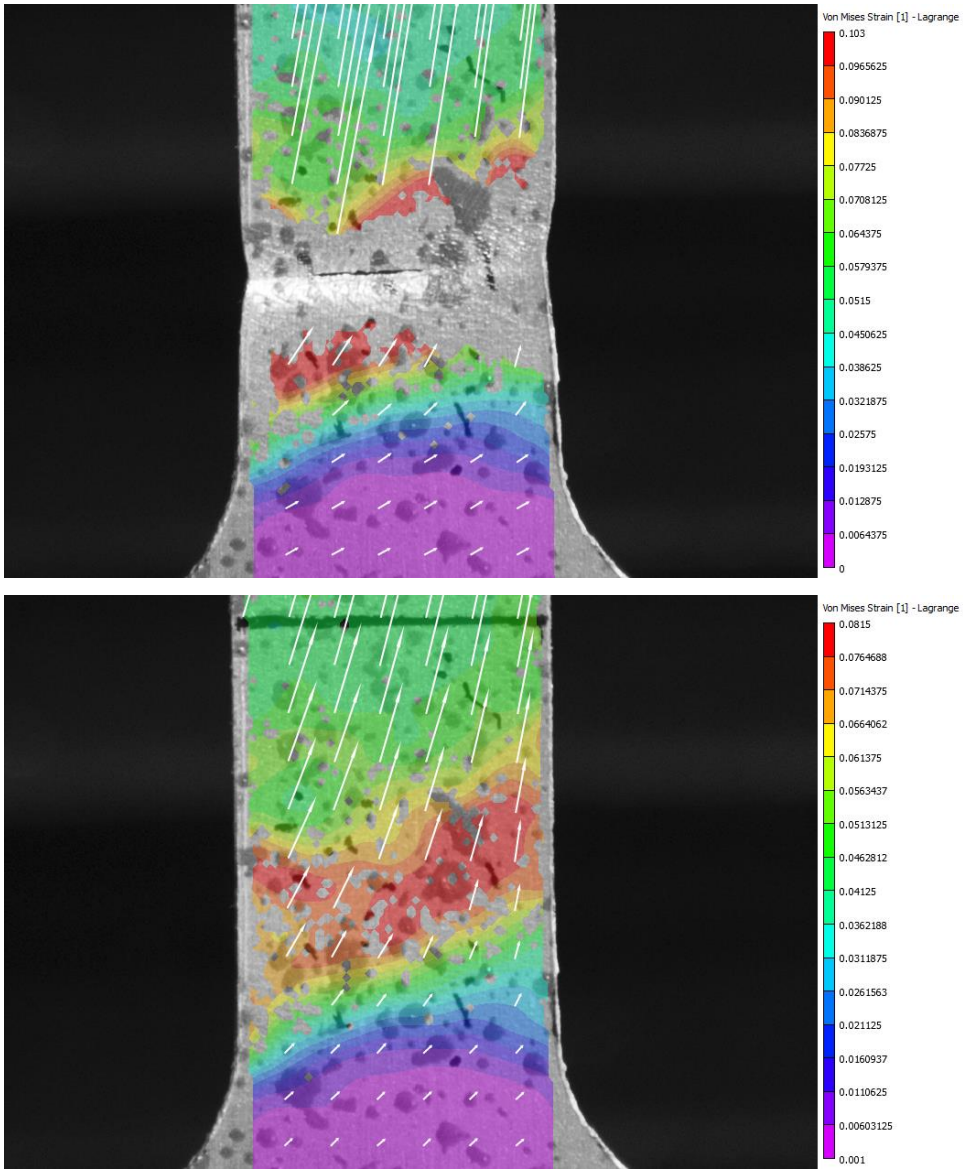

Figure 6.7a, 6.7b: Zoom of Von Mises strain.

The different directions of the strain are clearly visible in figures 6.7a, 6.7b where the situation at the beginning of cracking and at the end of the test is represented.

This agrees with the displacements represented in figure 6.8 that are greater in the right zone of the specimen.

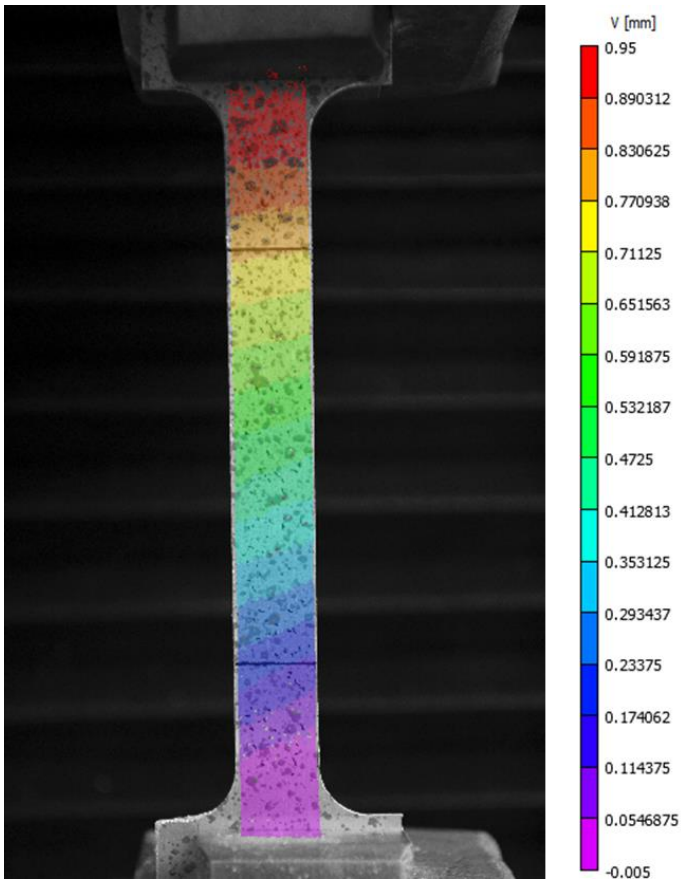

Figure 6.8: Vertical displacements at the time of figure 6.7a.

Depending on the irregularities of the displacements, the interval of confidence **σ** of the DIC method changes.

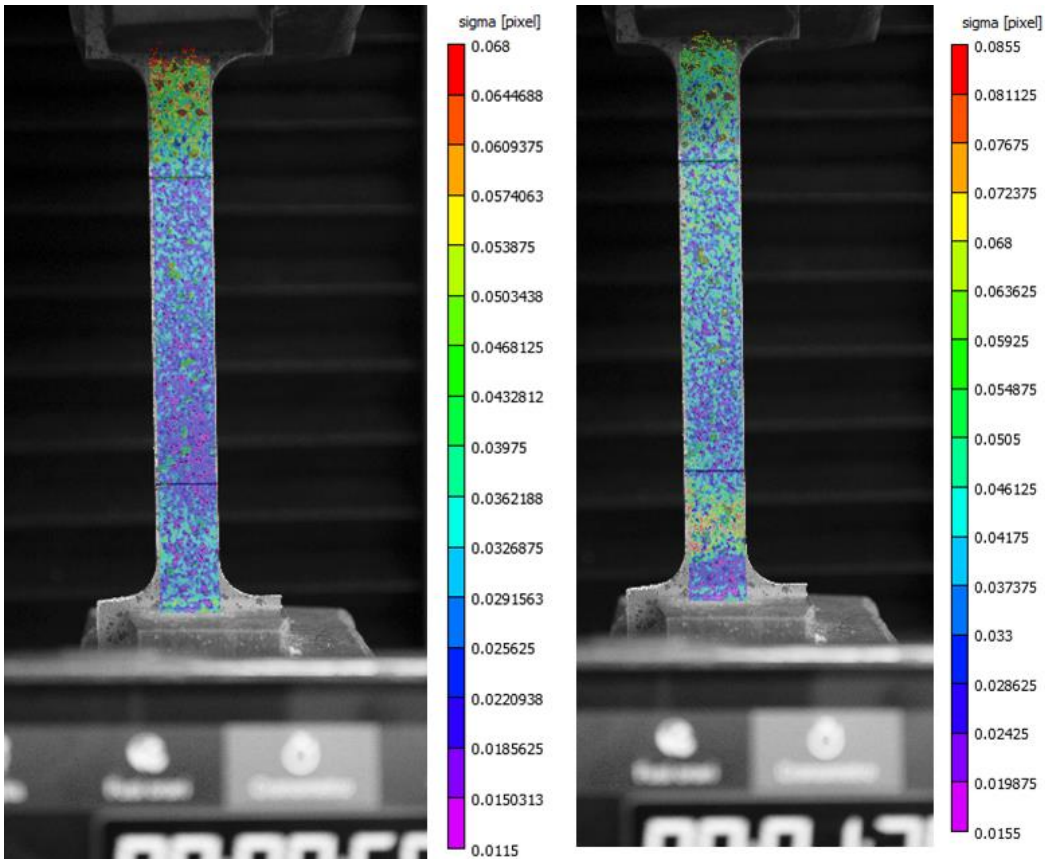

Figure 6.9: Interval of confidence during the test 1.

In figure 6.9, we can observe that **σ** is greater in the higher part of the image, due to lighting problems, and it increases in the zone of the future crack. Once the crack is formed, it will be impossible to perform the correlation in its neighborhood. This is confirmed

by figure 6.10, where minimum and maximum strain are highlighted and the zone of the crack is without information.

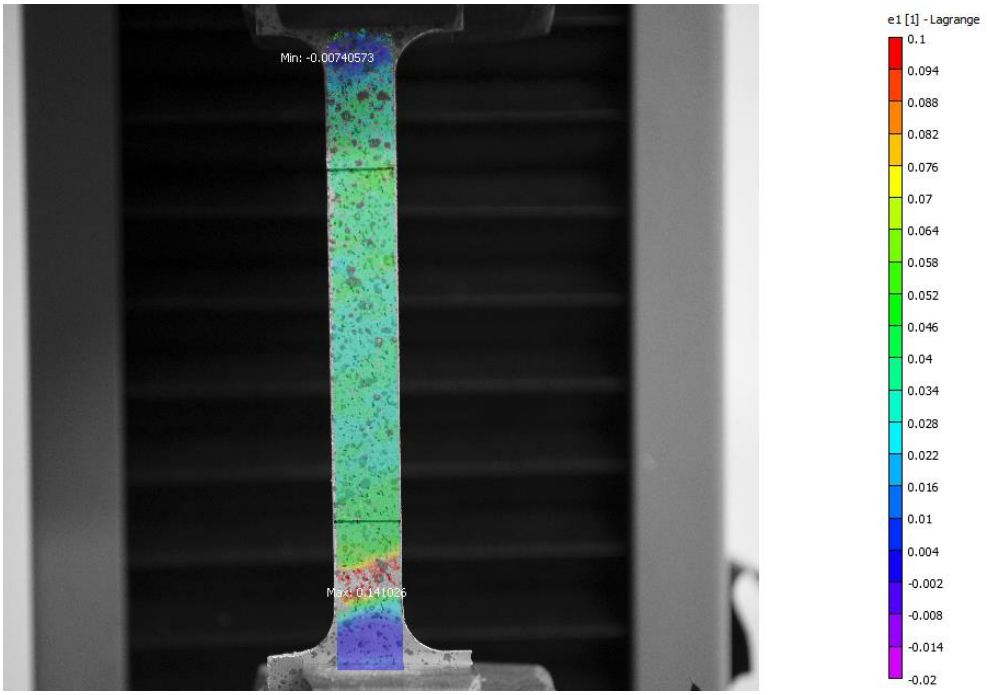

Figure 6.10: Principal strain at the end of the test 1.

Tests on fiber reinforced concrete specimen

Some tests were carried out on fiber reinforced concrete specimens. Both monotonic and cyclic bending tests were performed.

The test machine INSTRON 8501 with a maximum load of 100 kN was used. The machine is equipped with a computerized controller and with a climatic cell MTS, not used for the tests.

During the tests, the images were acquired by the camera NIKON D610 and by the thermal camera FLIR E50, with a thermal resolution of 0.05°C, a frame rate of 60 Hz and a 25° x 19° Field Of View (FOV).

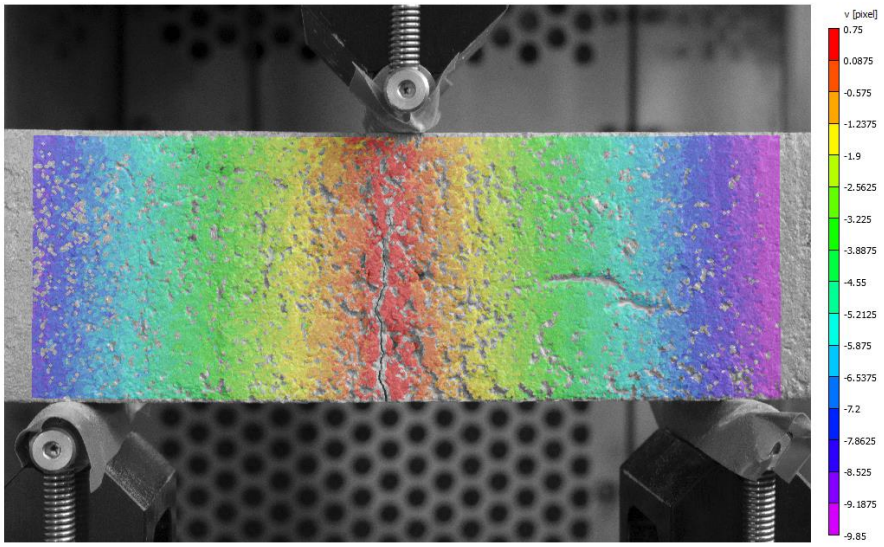

Figure 6.11: Final vertical displacements for monotonic test.

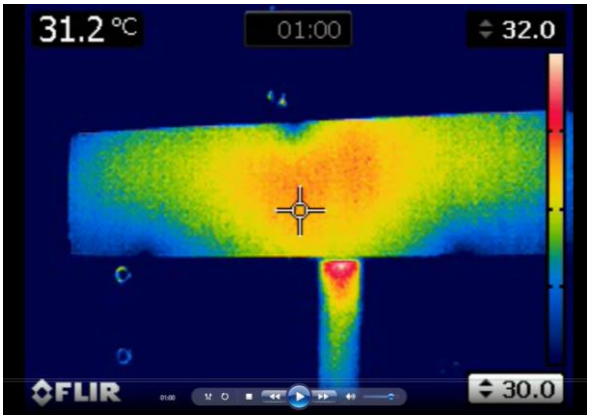

Figure 6.12: Thermal frame acquired during monotonic test.

Figure 6.12 is a thermal frame of the monotonic test: the temperature in the upper-left refers to the central point, highlighted by the cross. The zones close to the bearers and the loading roller are colder. During the test, the temperature remained constant.

In figure 6.13, the distribution of the vertical displacements during the cyclic test, obtained using DIC method, is shown. The white frame is the zone taken into account for obtaining the graphics reported in the following.

In figure 6.14 the strain in the X direction during the cyclic test is shown; the values are averages obtained for the region inside the white frame of figure 6.13.

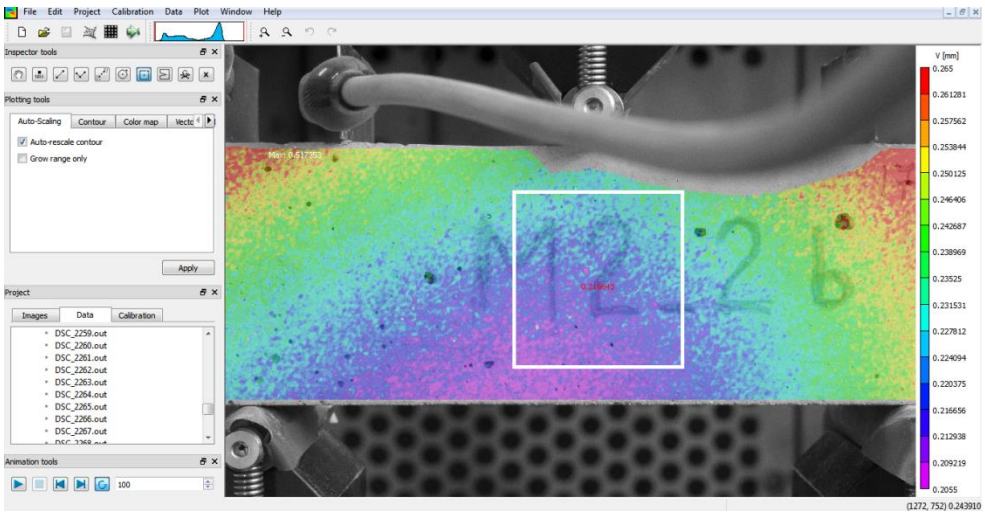

Figure 6.13: Vertical displacements during the cyclic test.

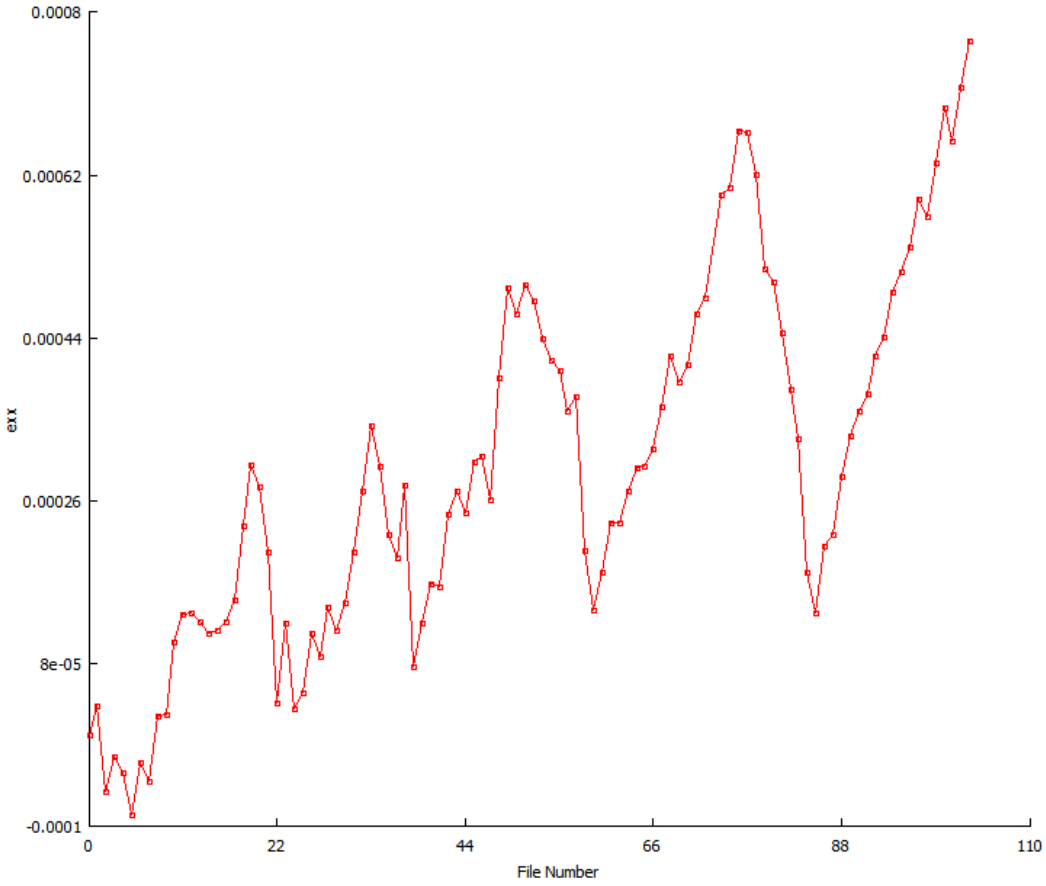

Figure 6.14: Strain in the X direction during the cyclic test (average values for the white frame of figure 6.13).

Comparison between the results obtained by DIC and test machine

Figure 6.15 shows the vertical displacements during the cyclic test; the values obtained using the DIC method (in pixels) are averages for the region inside the white frame of figure 6.13.

Figure 6.16 shows the displacements of the loading beam of the test machine during the cyclic test. Given the scale of the frames used for DIC analysis, the results of the two methods are in agreement, with a difference of about 2%.

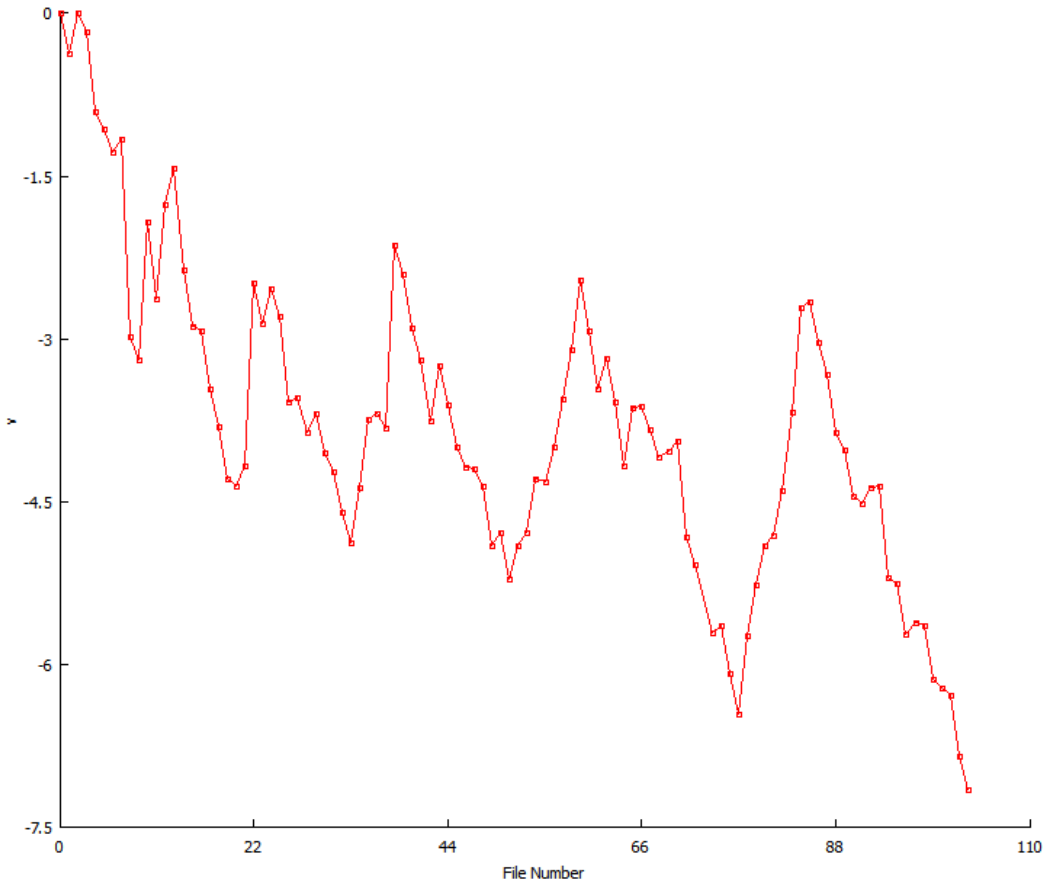

Figure 6.15: Vertical displacements during the cyclic test (average values for the white frame of figure 6.13).

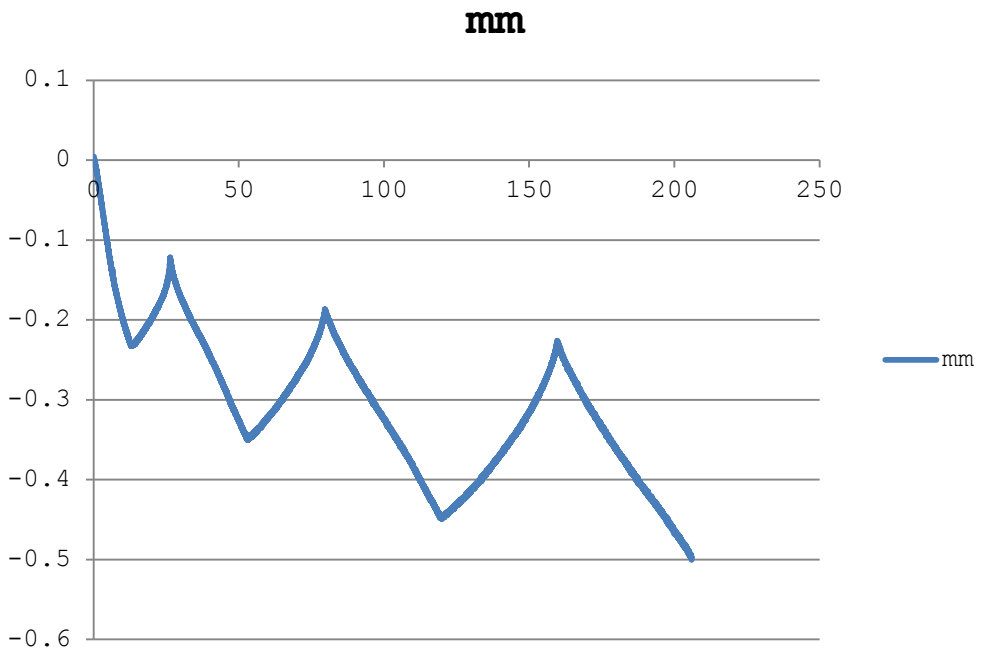

Figure 6.16: Traverse displacements of the loading beam of the test machine during the cyclic test.

Remarks on the reported results

A good agreement between test machine and DIC results was found: the differences are less than 2%. This permits us to explain the growing diffusion of this method for laboratory tests. The DIC method overcomes some limits of the techniques using single point acquisitions (extensometers, strain - gauges, etc..).

E.g., there are no problems connected to the possibility of slippage between the extensometer and the specimen.

DIC methods allow us to obtain Deformation and Strain Fields, so the values of the searched characteristics can be found for each point of the specimen surface visible in the frames.

This allows, *inter alia*, the opportunity to detect alignment errors of the test machine and/or machining errors in the manufacture of the specimens.

IR frames allows us to detect irregular temperature distributions and are useful for control aims, when a climatic cell is used.

7

Landslide monitoring

The survey and the representation of the land have been part of the main objectives of Geomatics disciplines since their origins. The methods of modern geomatics, composed of a combination of different sensors and devices for the storage, transmission and processing of data of environmental type, allow us to obtain extremely detailed representations of the earth's surface, from which it is possible to derive much information useful to geological investigation [Fabris et al., 2011; Achilli et al., 2015].

It is possible to distinguish two main fields of geological investigation: (a) the **geomorphological characterization**, i.e. the study of the developmental

aspects of a territory and the group of transformations due to the effect of various physical agents through their morphological representation; and (b) the continuous and/or discontinuous **monitoring**, covering the systematic control of changes in the spatial configuration of an area with respect to a predetermined time interval.

The monitoring is generally extended to the structures sited near the crown and the ridges of the landslide. In the case of great phenomena, a large number of activities (geological, geotechnical, etc) are performed, and the need to coordinate all of the studies is felt. For monitoring landslides, the measurements are performed by using total stations [Stiros and al. 2004], photogrammetry [Scaioni and al. 2014], conventional laser scanner [Kasperski and al. 2010; Sui and al. 2008; De Agostino and al. 2012; Artese and al., 2013], and recent models capable of giving full waveform [Mallet and Bretar 2009; Pirotti and al. 2013; Di Salvo and al., 2014]. Global Navigation Satellite System (GNSS) receivers are used since several years, and recent applications use also low-cost instruments [Glabsch and al. 2009]. SAR interferometry is used both from satellite [Kimura and Yamaguchi 2000; Bratus, 2015] and ground based [Tarchia and al. 2003; Lingua and al. 2008].

The tools and methods of Geomatics allow us to

identify and classify the main structural components of an area, and to interpret their spatial correlations and dynamics, with a quantitative description of the earth's surface [Pike and al., 2009]. It is possible to derive, from the Digital Terrain Model, deterministic and probabilistic models, used to evaluate the dynamic and evolutionary mechanisms present in an area, to predict possible scenarios of transformation and for risk assessment. The typologies of information can be only metric, or concern quality aspects related to specific geological features [Pavlopoulos and to. 2009]. The extraction of this information is usually done at the end of a process of processing data that allows us to obtain 3D models endowed with a high level of detail. The representation of an area, through modeling of the natural elements that compose it, is a fundamental tool for analyzing and controlling the mechanisms of instability that often characterize terrain slopes and rock faces [Scaioni and Alba, 2010], to assess the levels of risk [Ferrero and al, 2011], and to simulate the possible paths of falling rocks and stone material according to analytical models of investigation [Slob et al, 2004].

All geomatics activities should be integrated with geotechnical surveys, in order to better understand the collapse mechanism of the landslide and to set up a model, also useful for early warning [Artese and al.,

2015]. The parameters to be measured, during monitoring, can be: **direct parameters** i.e. quantities that describe directly the behavior of the landslide (vertical and horizontal movements, deformations, rotations); **indirect parameters** i.e. data representing the boundary conditions of the landslide (pore pressure, groundwater levels, meteorological parameters, hydrology, seismicity). The frequency of surveys, during monitoring, depends on: the scope of the monitoring; the evolution of the phenomena; the observation periods. The type of data collection can be manual (executed by operators), automatic (managed by remote centers) and mixed. Generally monitoring is activated for safety purposes to population centers, infrastructure and engineering installations, or for study aims.

The Vermicelli Landslide

In March 2010, after a winter animated by prolonged heavy rains, preceded by a long rainy period, on the north-west of the University of Calabria, on the slope of Contrada Vermicelli, some landslides were activated, two of which, the most significant, are next to each other but clearly distinguished (Figure 7.1). These have caused concern in anticipation of a possible

retrogressive evolution toward upstream, which could endanger some buildings placed on the summit of Vermicelli hill and the road, as well as some properties of the University.

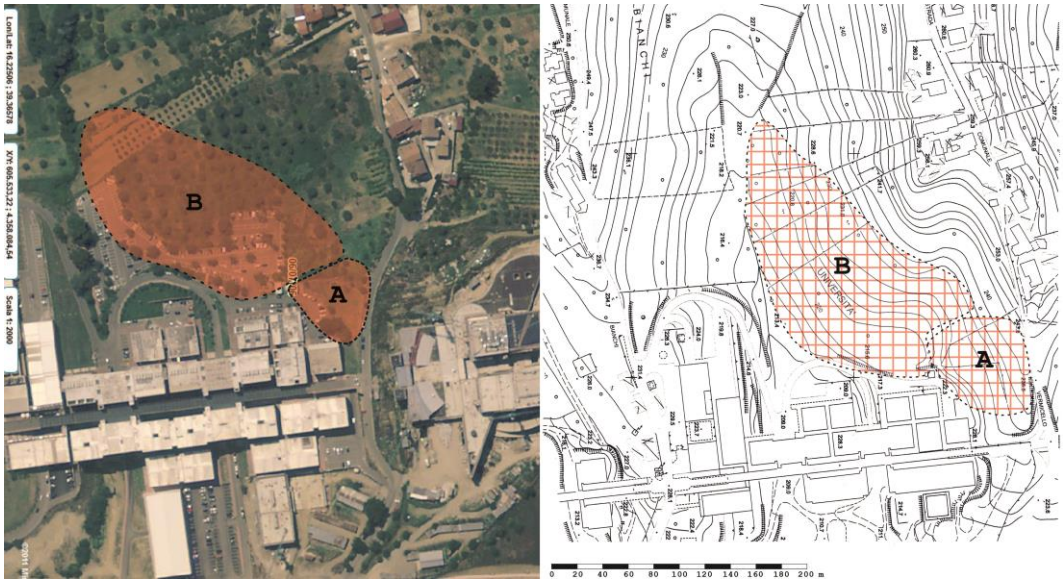

Figure 7.1: The University of Calabria Landslide. Ortophoto and Cartography.

The landslide system in question was classified on the basis of direct observations and consists of two major landslides [Magarò et al., 2012] (Figure 7.2):

- Slide A is a *Rotational slide*, i.e. *a slide in which the surface of rupture is curved concavely upward and the slide movement is roughly rotational about an axis that is parallel to the*

ground surface and transverse across the slide [Highland, 2004]. The lateral scarps are clearly detectable; in the zone at the foot, all of the parking area seems to be involved. The rotation of the landslide body causes the formation of a landslide scarp, the more trend to the vertical direction as lower as is the center of rotation, a lowering of the upper part of the landslide body and a lifting, accompanied by a forward displacement: the foot of the landslide.

- Slide B is a *Translational slide*, with probable sliding surface arranged in correspondence with a level clay. *In this type of slide, the landslide mass moves along a roughly planar surface with little rotation or backward tilting* [Highland, 2004]. It is clearly detectable in the area of the head, while the foot is observable only in the high part of the parking lot, where it skims the landslide A and for the remaining part coincides with the bed of the *Bianchi* channel. Probably, the slide occurs along the surface of contact between a layer of sandy silt-clay and a layer of silty clay. The landslide is bounded by a deep traction fracture of a width of between 20 and 40 cm and a depth of 40-60 cm. It is possible that the original depth was increased and that the fracture has been partially filled with material from the

collapsed walls. The lowering of the side of the valley is modest, 10-20 cm, and this leads to suppose a slip of translational type.

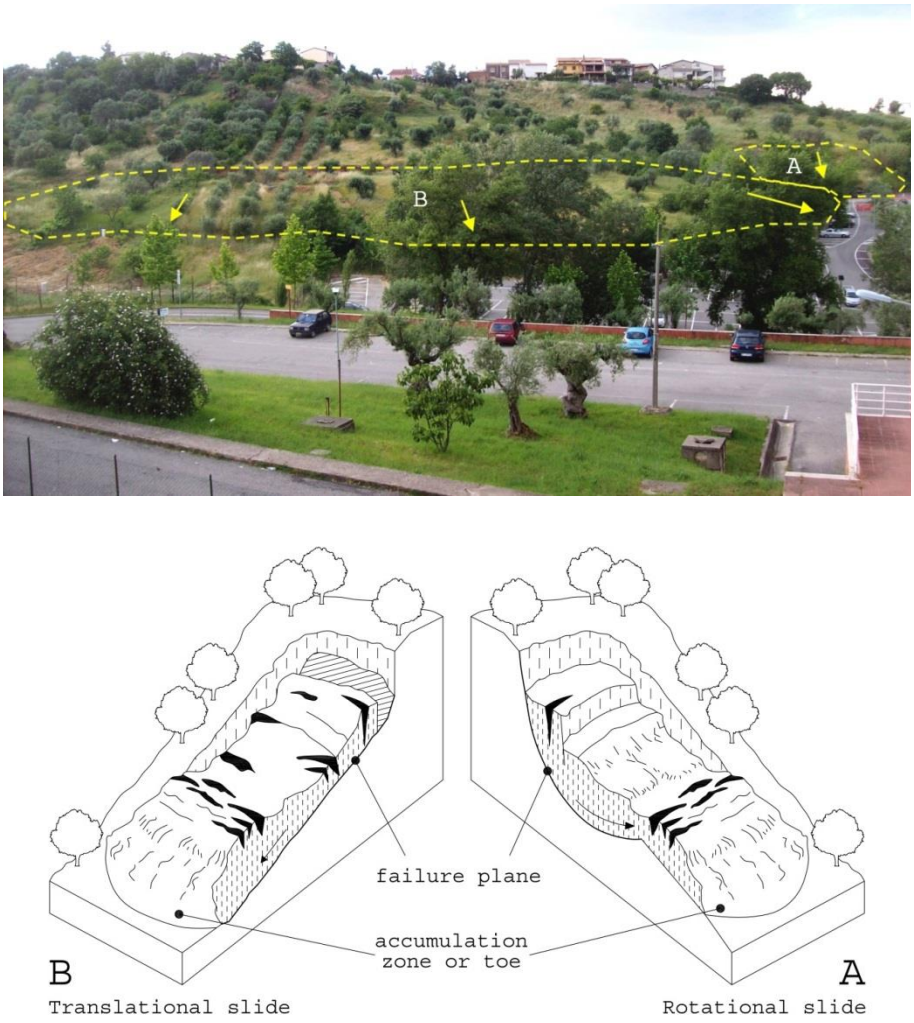

Figure 7.2: The two landslides and the classification of slope movements [Varnes, 1978].

The survey was executed using the terrestrial laser

scanner RIEGL VZ-1000 with full waveform technology, and involved the whole landslide. The instrument provides a measurement range greater than 1.400 m, a 5 mm repeatability, an efficient measurement rate up to 122.000 measurements/sec, a wide field of view of 100° vertical and 360° horizontal, and uses an invisible laser beam for eye safe operations.

The survey was aimed at creating a 3D model (Figure 7.3) with high resolution, usable for geomorphological investigations and geotechnical analysis.

At the same time a 3D model (Figure 7.4) was made starting from the 1K map of the area of the University of Calabria (flight 2006).

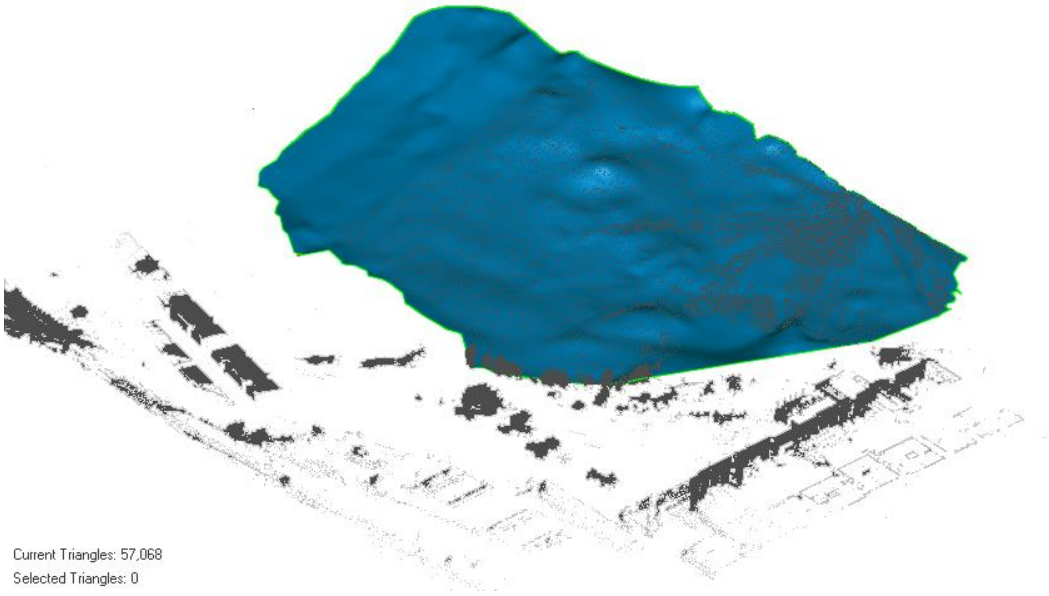

Figure 7.3: Model from the survey.

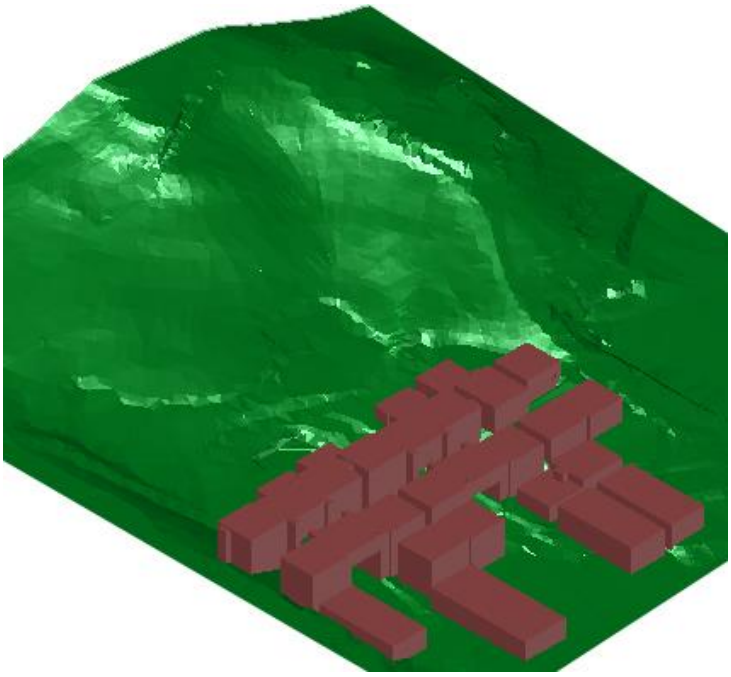

Figure 7.4 Model from 1K map.

The survey was carried out in one day, performing two scans from two stations, with a resolution of 10 cm at a distance of 100 m. Georeferencing of the survey, in the UTM-ETRF2000 system, was performed using the GNSS receiver and the magnetometer the laser scanner is equipped with, high precison not being necessary.

For the processing of point clouds the software Riegl Riscan Pro® was used; for modeling and analyzing the difference between the surfaces of the two models the Geomagic Studio® Software was used.

The stored scans are aligned through tie-points, i.e.

the vertices of the university “cubes” and the dormitories. At first, all scans, each with its own reference system, were referred to a coordinate system of the project corresponding to the one internal to the instrument in the first scanning position. The interactive tool multi-station adjustment was then applied to minimize the alignment errors by calculating the best geometry of overlap between the two scans. The optimized alignment allowed us to obtain a standard deviation less than 2 cm.

After the alignment, we proceeded with the filtering and the consequent removal of those points that cannot be used for the reconstruction. Initially the points not lying in the study area were simply removed manually; after that a selection was conducted and the automatic deletion of the irrelevant points by the multi-target classification from the full waveform analysis. The mere differentiation of echoes was not enough to correctly identify land points. It was decided, therefore, to resort to a procedure called terrain filter, by means of which it is possible, in an entirely automatic manner, to extract and eliminate, with high accuracy, the additional points belonging to the vegetation and to extraneous elements. The tool is based on an iterative procedure capable of generating a series of surfaces, equidistant from the surface of interest, with respect to which an automatic selection

is made of the points too external or excessively far away from the surface to reconstruct. Although much of the points belonging to the vegetation and to foreign elements were removed automatically, we encountered some problems in those areas with the presence of compact vegetation. For the filtering of these areas, we resorted to additional localized operations of filtering and to manual removal. Finally the clouds were resampled using a octree procedure. From resampled data a mesh was created with a resolution of 2 cm using the Geomagic Studio software, in order to preserve as much detail as possible.

The most obvious problem during the reconstruction was the impossibility of obtaining closed and perfectly continuous surfaces, especially in the part where the vegetation was too dense. Due to the lack of information about the real shape of the land in these areas, it was decided to close the holes with approximate planes or geometric surfaces, respecting the morphology of the visible parts.

Once the model is created, it is overlapped to the one obtained from maps, using as tie points the vertices of the university “cubes” and the dormitories.

From the comparison of the two models, it was possible to make some observations. In figure 7.5, the two landslides are recognizable, their real limits and the depletion and accumulation zones.

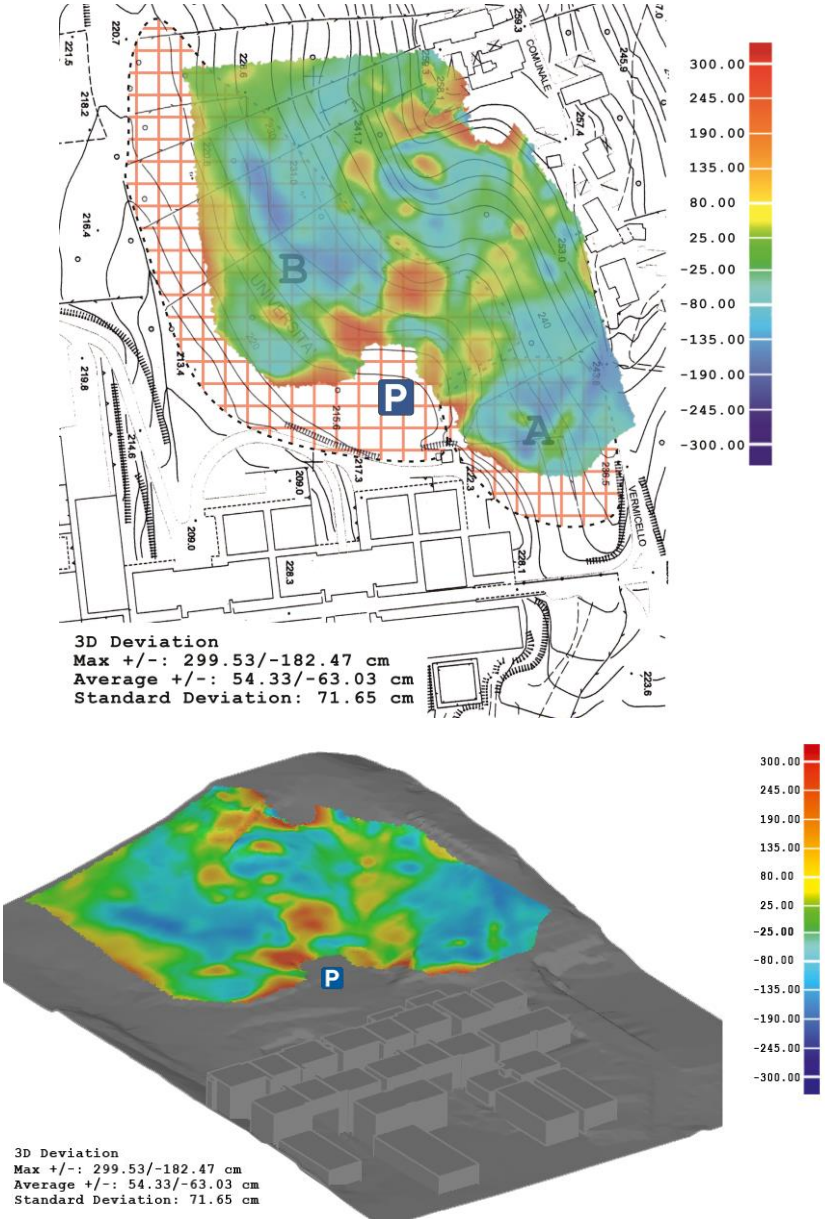

Figure 7.5: Comparison of the two models.

The precision of the results depends fundamentally on that of Cartography. We can evaluate an accuracy of the

final result of about 25 cm.

The survey can also be used for studies and analysis of the evolution of the area or to monitor additional collapse events: through the data acquired at different times it is possible to examine the evolution of the phenomenon.

From the 3D model derived from the scans, it is possible to derive a set of geometric entities such as polylines and contour lines, which can be exported and reused in a CAD program and allow the evaluation of distances, volumes, trajectories and the interaction between various elements [Hoffmeister et al., 2012].

The Fiego Landslide

The site under examination is located along the A3 motorway, near the south gateway of the Fiego I tunnel. It is part of a set of large translational landslides with rotational component. In particular, a large landslide was identified, which in the longitudinal and transverse directions (the latter parallel to the motorway route) has dimensions, respectively, of about 350 m and 170m. There is a principal large quiescent landslide body, over which are developed two active minor bodies.

One of these active bodies (Figure 7.6) is located

upstream of the motorway route and displays intense activity witnessed by numerous niches of secondary detachment, in addition to abundant and pervasive transverse and longitudinal crack.

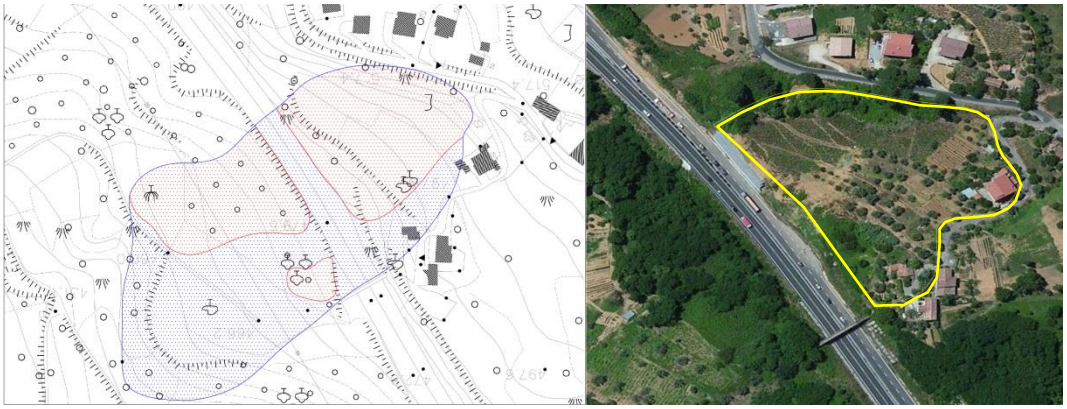

Figure 7.6: Landslide view: in blue the quiescent zone, in red the active minor bodies, in yellow the surveyed zone.

Geological investigations and survey were undertaken under the PON LEW, Landslide Early Warning.

The survey was aimed at creating a 3D model with high resolution, usable for geomorphological investigations and geotechnical analysis.

The survey was carried out in one day, performing two scans from two stations, with a resolution of 10 cm at a distance of 100 m. For the alignment of the scans cylindrical retroreflective targets were used, positioned so as to be easily visible from both scans.

Georeferencing of the survey, in the UTM-ETRF2000

system, was performed using the GNSS receiver and the magnetometer the laser scanner is equipped with, high precison not being necessary.

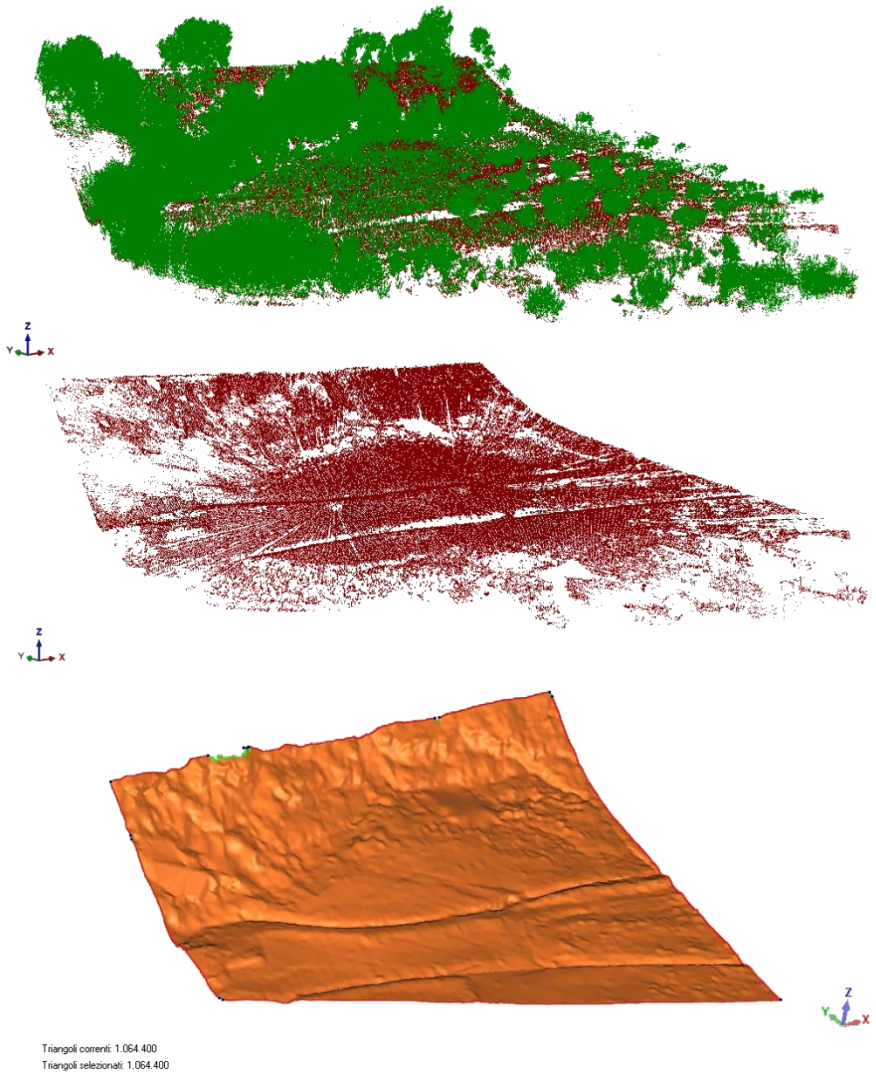

Figure 7.7: Screenshots during data processing

For the processing of point clouds it was used the software Riegl Riscan Pro®; for modeling the software Geomagic Studio® has been used.

For the reconstruction of the landslide the multi-target classification was first applied that eliminated several points of vegetation, and then the iterative tool for terrain filter, which allowed us to further eliminate those points that did not belong to the real ground surface.

Finally, the clouds were resampled using an octree procedure.

From the model geometric primitives were derived such as level curves and vertical profiles.

8

Dynamic measurements: the use of a laser pointer for monitoring bridge deflections

The possibility to perform fast and accurate image processing, thanks to the power of the most recent computers, allows us to make use of new exciting applications of this technology in several fields and, in particular, for the monitoring of large structures.

The bridges, due to their dimensions and great loads, are often monitored. To control the state of health of a bridge, static loads are applied to the structure, materialized by a convoy of heavy trucks parked on the

deck in known positions. The deflections of the beams are then measured by using levels or total stations. Dynamic measurements have been recently proposed, by using Micro Electro-Mechanical Systems [Yu et al., 2013] or Digital Image Correlation [Yoneyama and Ueda, 2012].

In the test described in the following, a very cheap instrumentation was used. The variation of the tangent to the elastic line was captured by using a laser pointer. A video of the oscillations of the laser footprint during the test was acquired. By analyzing the single frames, the variable position of the footprint centroid gives information about the inclination changes and, consequently, about the dynamic deflections.

The geometry of the test was set up in order to amplify the movements of the laser footprint and, consequently, to get a high precision.

In the following, the last test executed using this method is described.

The test layout

The University of Calabria is characterized by a South-North axis, along which the buildings of the Departments are sited. The axis is materialized by a

sequence of double-deck bridges: the upper deck can be used for vehicular traffic, while the lower one is reserved for pedestrians (Figure 8.1).

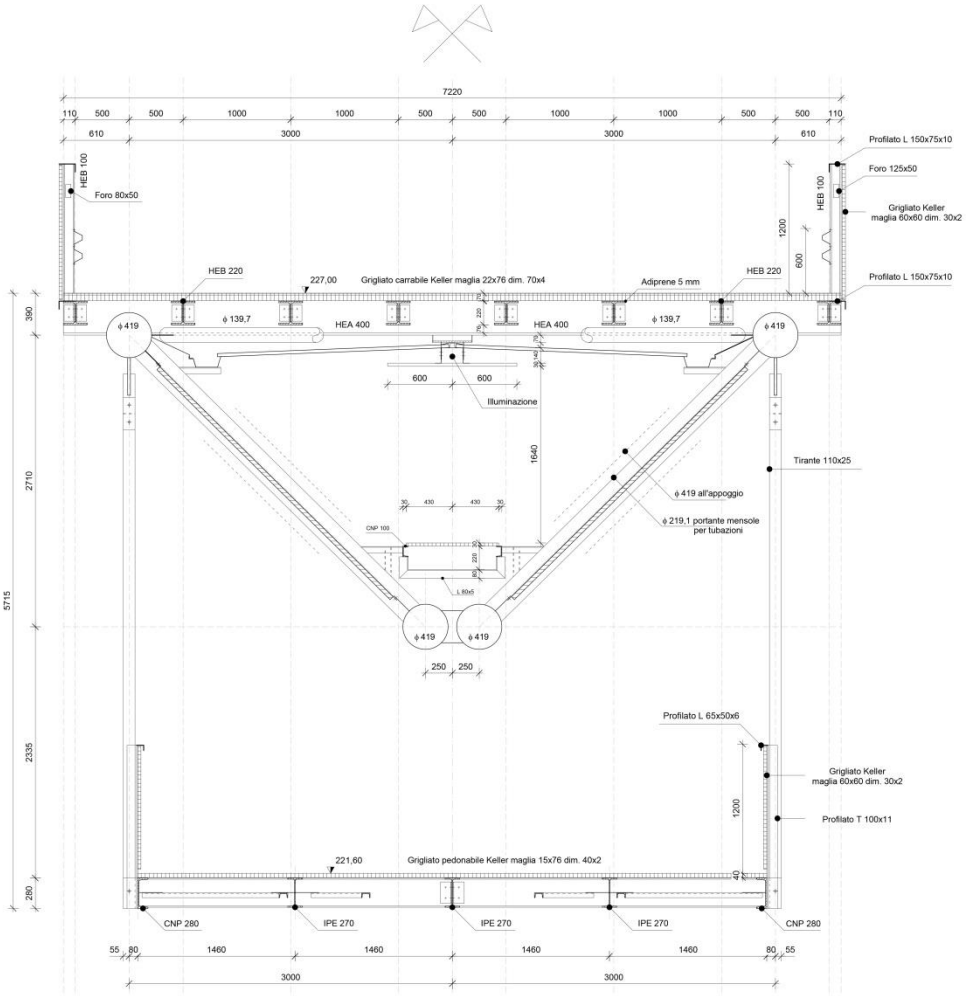

Figure 8.1: Cross section of the double-deck bridge at the University of Calabria.

The layout of the test is shown in figure 8.2. The

laser pointer is fixed to a tubular element of the truss beam of the bridge (figure 8.3, 8.4). The laser beam is projected onto a flat target fixed to a vertical wall of the north terminal abutment. To point exactly at the target, the pointer is mounted on a holder, usually used on optical tables, which allows precise horizontal and vertical movements. The holder is equipped with a strong magnetic base.

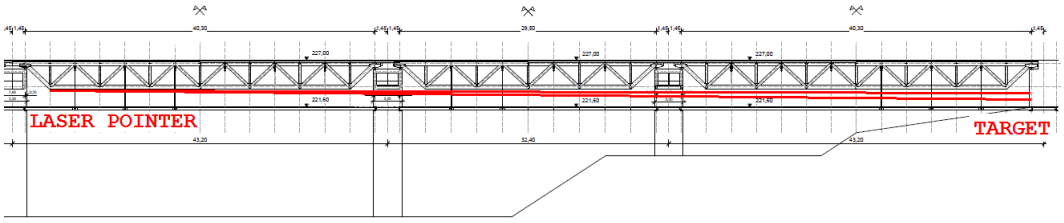

Figure 8.2: The layout of the test.

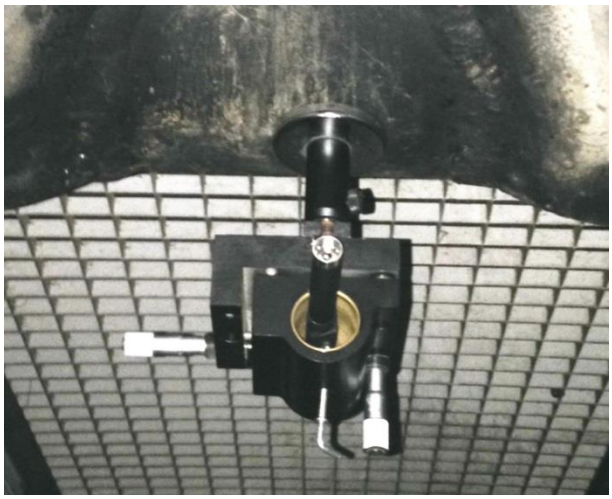

Figure 8.3: The laser pointer and the holder.

Figure 8.4: The pedestrian deck: the target is on the front wall.

The camera used to obtain the video was positioned on a robust tripod, slightly lateral with respect to the laser beam path.

The instruments used and the expected precision

The main characteristics of the laser pointer used are as follows:

- Wavelenght 532 nm (Green)
- Beam diameter 2.0 mm
- Beam divergence 0.8 mrad
- Power 100 mW (Gaussian Beam)
- Pointing stability < 0.05 mrad

The video was shot using a NIKON D610 camera with a 55 mm NIKKOR (previously calibrated) lens. The distance to the target was chosen so that the medium scale of the frames was 1 pixel=0.2 mm. Taking into account the maximum pointing stability of the laser pointer, a more detailed scale of the frame would be useless. Given that the distance from the laser pointer to the target was 115.7 m, we obtained a beam footprint of 95 mm and a maximum pointing instability of 5.8 mm (23 pixels).

The correlation techniques allowed us to determine the centroid of the footprint with an accuracy of one pixel, so almost the total expected error in the measurements of the beam inclination was due to the laser pointer instability and can be evaluated as 0.05 mrad.

The Test and the Results

The test was carried out during the movements of a truck elevator, used for work on the façade of a building alongside the bridge (Figure 8.5). The weight of the truck was about 260 kN.

The video was shot when the truck left the bridge. Due to the limited space, the truck performed some forward and backward movements to reach the optimal alignment before the final reverse run.

Figure 8.5: The truck elevator on the upper deck of the bridge.

In Figure 8.6, we can observe two frames obtained during the test. The ISO sensitivity and the aperture were chosen in order to execute automatically a

radiometric cut off, thus achieving two goals: a better defined shape of the laser beam footprint was obtained and the saturation of the image in the center zone of the footprint avoided. This allows a more accurate determination of the centroid.

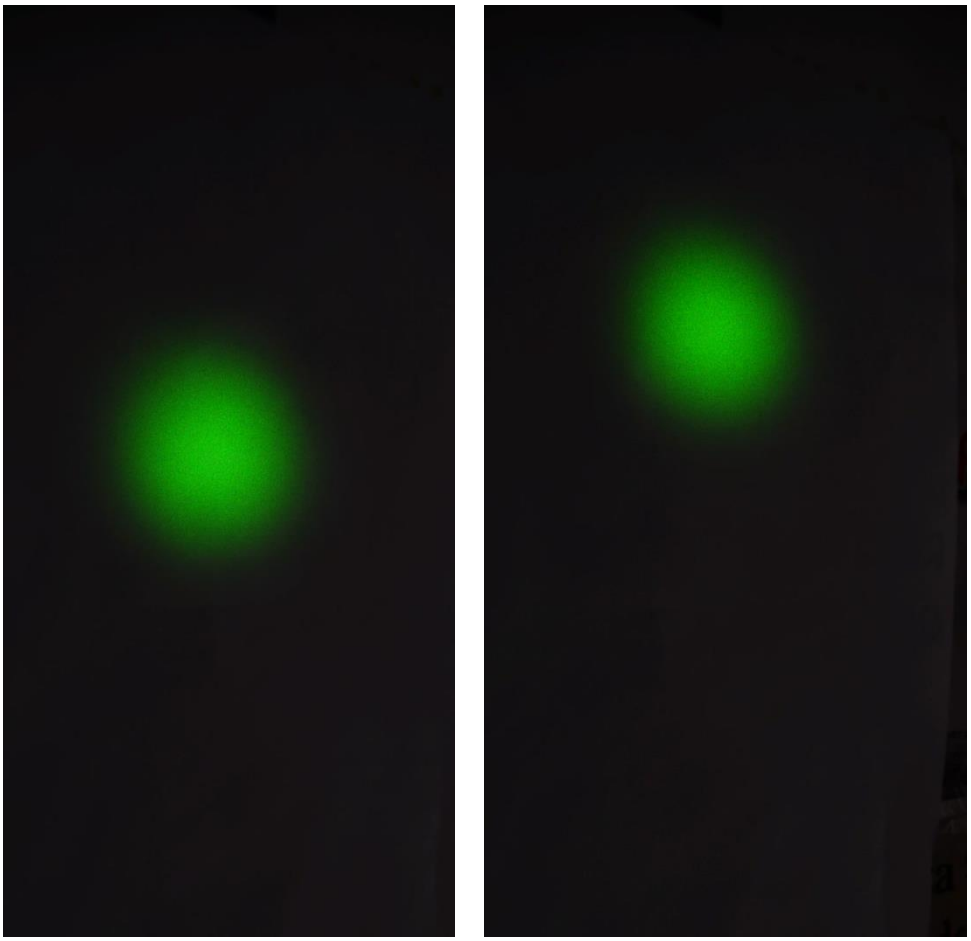

Figure 8.6: two frames acquired at the beginning and at the end of the test: after the truck left the bridge, the footprint is higher.

The frames were processed by using a code in Matlab® expressly realized. The position of the centroids (rows, columns) is given in pixels.
In figure 8.7 below, the position of the centroid during the test is shown.

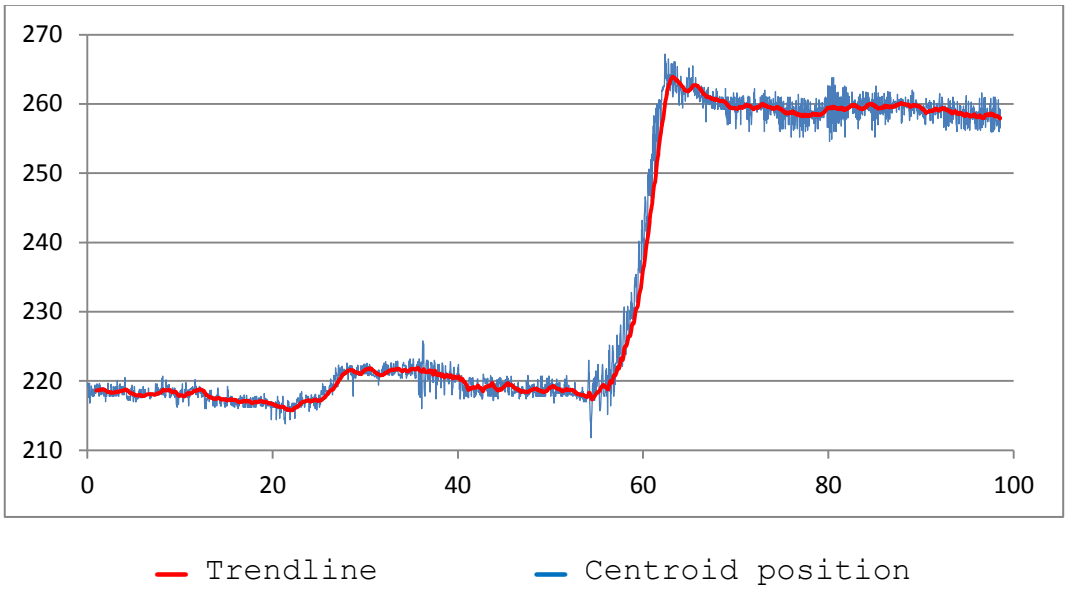

Figure 8.7: The vertical position of the centroid of the footprint during the test.

The origin of ordinates is at the bottom of the frame. The values have been transformed in mm. The scale of the frames was obtained by measuring a known length on a rectified frame. Abscissae are in seconds.

A sudden variation is evident, equal to about 40 mm, corresponding to an inclination change of 0.346 mrad. A rough estimation of the deflection can be made by

considering the laser positioned in correspondence to a bearing and a constant section of the truss beam. In this case the above inclination variation implies a deflection variation of the laser beam of about 6.9 mm at a distance of 20 m (middle of the span). Thus, it is possible to evaluate the variation of the truss beam deflection in 4.6 mm.

It is also possible to observe that the pointing stability was less than 0.05 mrad.

From a qualitative point of view, we can observe that the forward-backward movements of the truck are clearly reflected in the movements of the laser beam. Furthermore, some oscillations are recognizable after the truck left the bridge.

In conclusion, this method seems to be promising for bridge monitoring. A camera with a high frame rate could allow the study of the frequencies, but the problem of pointing stability needs to be considered.

A further refining should be made if a 3D model were available, in order to execute a FEM study and to compare theoretical and experimental results.

9

Dinamic measurements: the use of TLS and GNSS for monitoring the elastic line of a bridge

For the surveying of the bridges, laser scanning is by now a consolidated technique. The comparison of several scans acquired at different times, allows us to obtain, for example, the deviations between corresponding points of the bridge surface under different conditions. The laser scanner can thus be used for monitoring purposes.

The very high acquisition rate of this instrument is exploited to perform mobile mapping [Schwarz et al.,

1993; Tao and Li, 2007]. For this aim, the laser scanner is mounted on a vehicle: a mobile instrument is used to map a static object (land).

One can think, however, of using this instrument in a reverse way: a fixed instrument can be used to survey a mobile object. In particular, the deflections of the superstructure of a bridge could be dynamically measured in near real time.

In the following, a method is described for the dynamic surveying of the elastic line of a bridge, along with the first experimental tests.

The method

The method consists of placing a laser scanner, set up as line-scanner, under the superstructure of a bridge and acquiring continuously a line parallel to the axis of the deck.

The displacements with respect to the line surveyed under static conditions and without loads, allow us to obtain the elastic line. It is possible, in this way, to extract an elastic line for each scanned line; that is, up to several dozens of lines per second.

The accuracy achievable depends on the instrument used. At present, several laser scanners reach precisions of about 1 mm for distances up to 200 m; if

the required range is higher, then more powerful models could be used, at the cost, however, of lesser accuracy.

The operating mode is also important for the precision of the result. The best performances are obtained when the sampling rate is low: this lowers some effects, like, for example, the vibrations of the rotating mirror axis.

Furthermore, we must consider that the goal is to reconstruct a line, obtained starting from a series of points. The best fitting line has in general an accuracy rather better than each single point, so the final result could reach a precision higher than that declared for the instrument used.

First Test: The Cannavino Bridge at Celico

The Cannavino bridge (Figure 9.1) is characterized by a cantilever prestressed concrete structure. A cantilever collapse occurred during its realization in 1972, and it was subjected to of several studies, [Wittfoht, 1983].

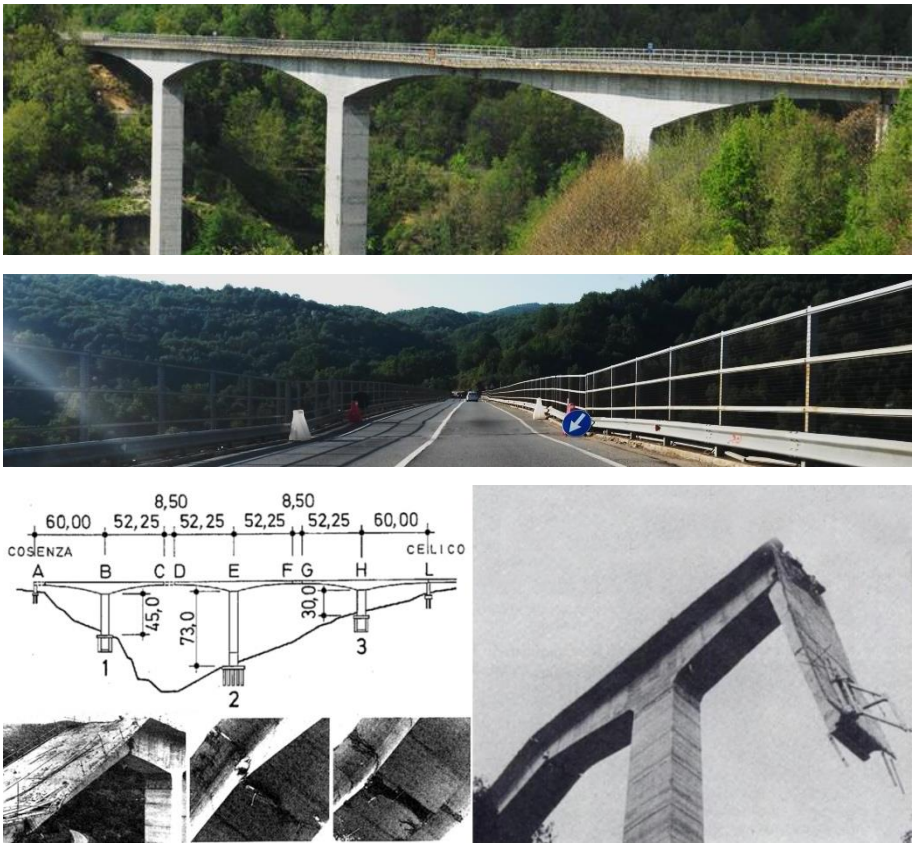

Figure 9.1: The Cannavino bridge. The present situation, a quoted elevation and photo of collapse (1972)

In recent years, the end of the cantilevers have showed noticeable deflections; for this reason, a periodic monitoring with total station is performed by the technicians of ANAS, the Italian National Autonomous Roads Corporation.

The instrument used for the test is a Riegl VZ1000 Laser Scanner, as described above. In this case, the

laser scanner was used in the line scan configuration. The function *timestamp* was used, so that for each measured point the instant of acquisition was recorded; to this aim, the GPS receiver integrated in the laser scanner was used.

The instrument was placed under the deck, near a pile, and a longitudinal path continuously acquired along the sidewalk. The scans were performed during a normal traffic period.

A scan rate of 110,000 points per second was selected.

The data acquired were processed with the RiSCAN PRO® software. A text file was obtained, containing the coordinates of the measured points, along with the timestamp. This file was processed with a Matlab® code realized on purpose and the single lines were extracted. The evaluation of the displacements was obtained using a spreadsheet and a cad program.

The following remarks can be made:

The row data generate very close lines that can be grouped in three curves groups. This can be caused by vibrations of the axis of the scanning mirror. To obviate this problem, the convergence of all lines at a point at the beginning of the cantilever was imposed.

Figure 9.2 shows the layout of the test and some results. The trendlines obtained diverge going to the end of the cantilever; the distance reaches a value of

about 6 mm. This result is reasonable for normal traffic loads.

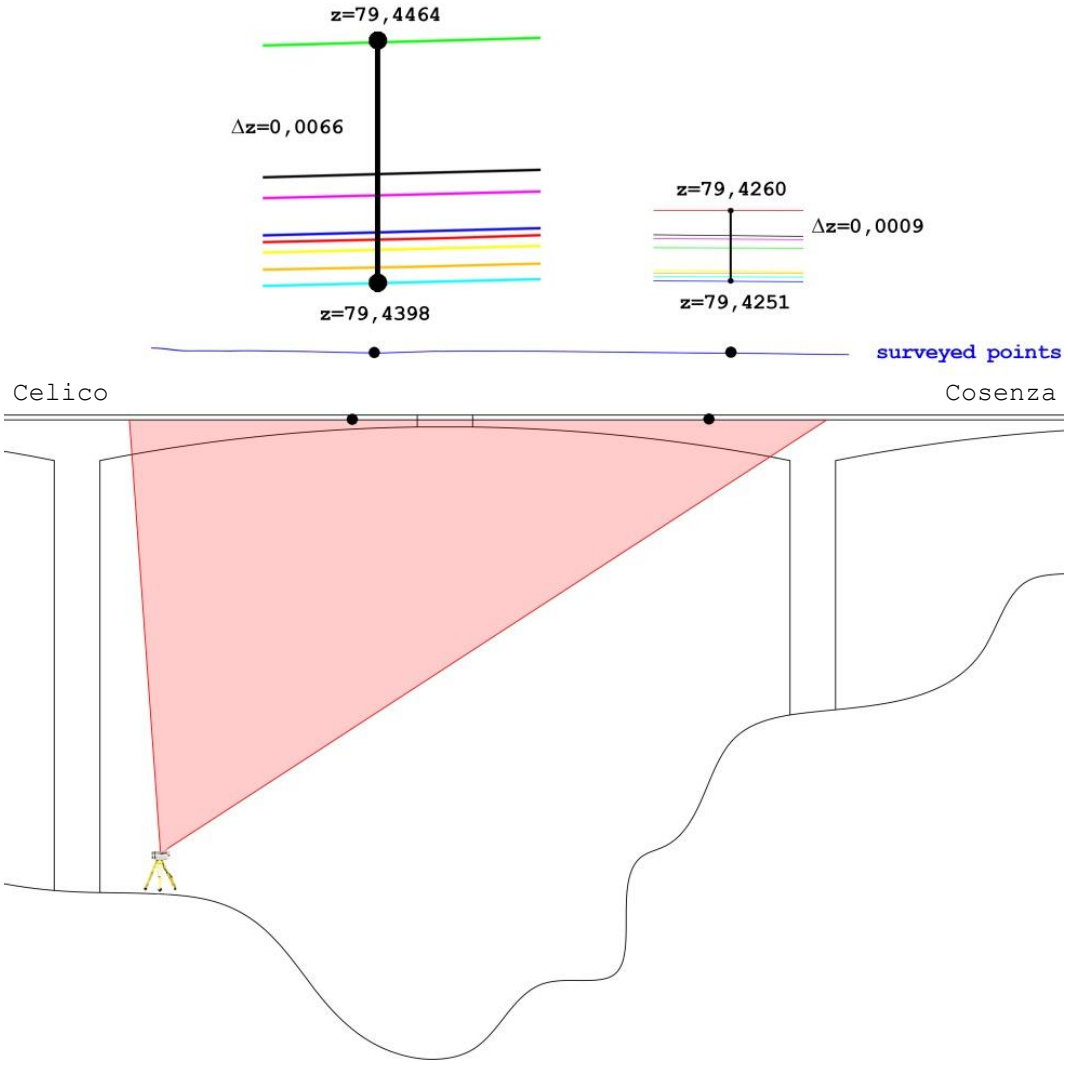

Figure 9.2: The layout of the test.

The Second Test: The Bridge at University of Calabria

The double-deck bridges at the University of Calabria (Figure 9.3) have been described previously.

Figure 9.3: University of Calabria bridges.

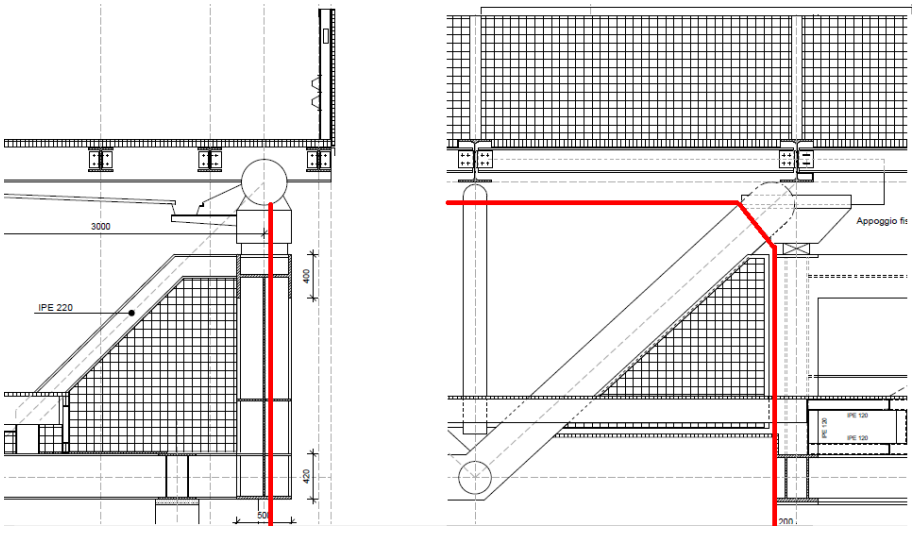

Figure 9.4: Cross section of the bridge at the bearing.

In Figure 9.4 the cross sections of the truss beam at the bearings are shown. The red line represents the path followed by the laser scanner during the acquisitions in line-scan mode.

The layout of the test is shown in figure 9.5. The laser scanner is positioned on a tripod under the bridge. The path followed for the scans corresponds to a generatrix of the highest tubular element of the truss beam.

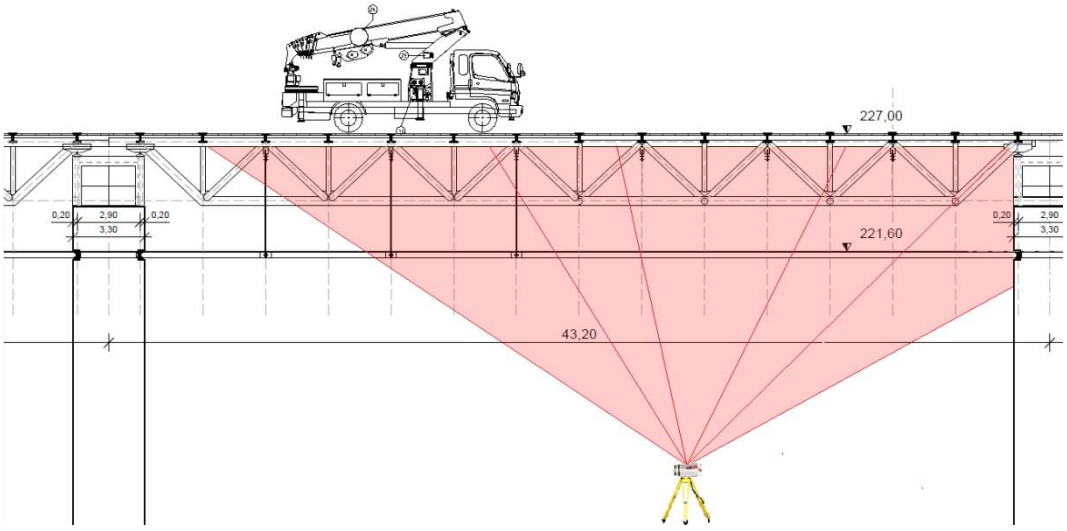

Figure 9.5: The layout of the test.

The acquisition rate was set to 70,000 points per second, which implies a slow rotation of the scan mirror.

During the test, a video was acquired from the last floor, and the truck movements were recorded. The

video was synchronized to the scan acquisitions.

The data acquired were processed with the software RiSCAN PRO® and the same procedure of the test on Cannavino bridge was followed.

The results are shown in the following figures.

It is possible to observe that the lines obtained at the beginning and at the end of the test are coincident on the bearing (Figure 9.6), while a height difference of about 2 mm is present in the middle zone of the span (Figures 9.7, 9.8).

This value is in full agreement with the results obtained using the laser pointer.

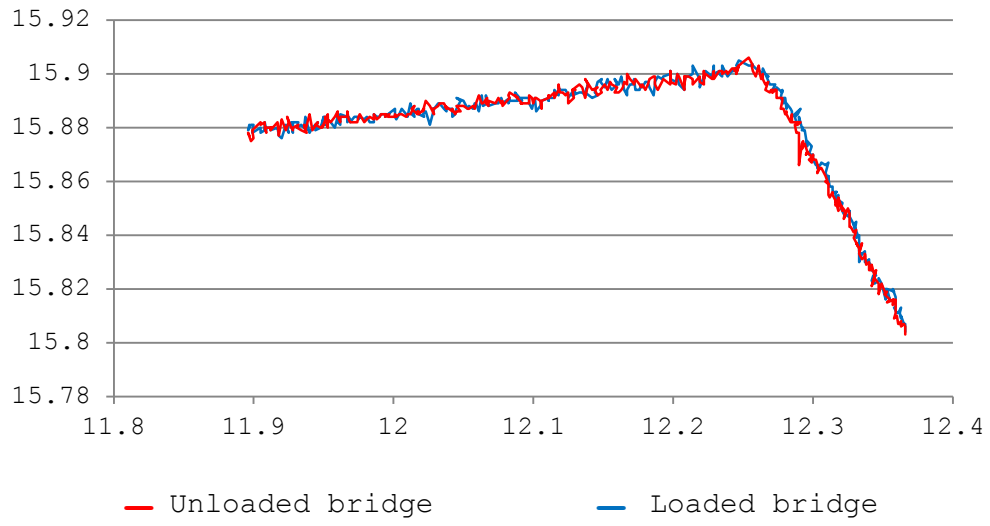

Figure 9.6: The profiles of loaded and unloaded bridge at the bearing.

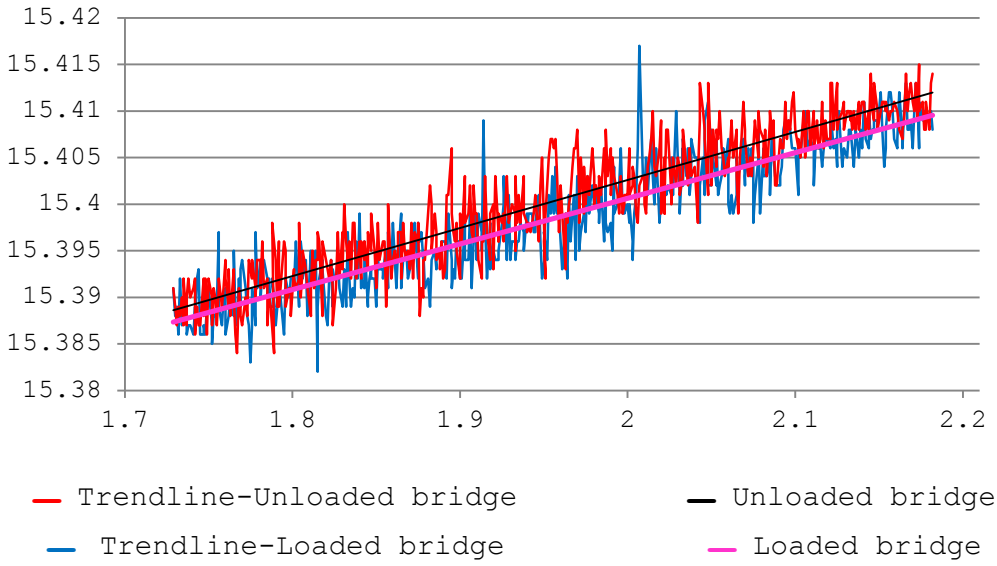

Figure 9.7: The profiles of the tubular beam at the north zone of the span.

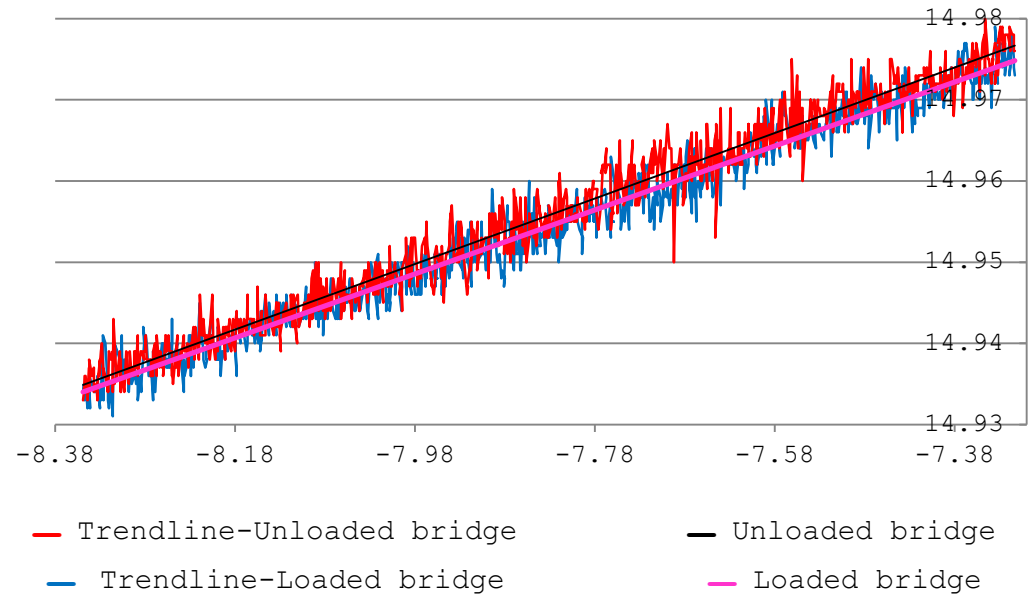

Figure 9.8: The profiles of the tubular beam at the south zone of the span.

To study the dynamic behavior of a bridge effectively, the obtained elastic lines should be related to the moving loads at the moment of the single scan (load intensity, position, speed). To reach this goal, several problems should be faced; first of all, the synchronization of the laser scanner and of the instruments used to detect the position of the moving loads. These aspects will be dealt with during the next experimental tests.

10

Conclusions and ideas for future developments

The work of this PhD thesis has consisted in the application of geomatic techniques for Survey, Diagnosis and Monitoring of Structures and Land.

After a preliminary overview of the geomatic techniques, some aspects, in particular laser scanner and digital image correlation, have been thoroughly investigated.

A series of applications were performed.

The first of these regarded a historic building in Cosenza, the Cavalcanti Palace. A survey with the total station was carried out to check the verticality of the main façade and to control some cracks.

Laser scanner and thermal camera were used for the

survey of the Escuelas Pias Church in Valencia. The result of the work was a very detailed 3D model, used for verifying historical hypotheses about the original design of the dome and the building procedure. The research of the deviation from the vertical of the axis of symmetry allowed us to detect a break point and two distinct directions for dome axis and lantern axis. Other interesting results were obtained with regard to the deviation between the theoretical shape and best fitting internal surface of the dome; the maximum deviations evidence a lowering of a dome slice in correspondence to a crack, highlighted in the 3D model textured with the thermal image.

Another survey was carried out by using total station and thermal camera, to detect some hidden windows in the façade of the ancient church of Santa Maria dei Longobardi, in San Marco Argentano, whose present aspect derives from the union of two adjacent churches.

Laser scanner and GNSS were used for the surveying of some bridges. In particular, the 3D model was obtained of a reinforced concrete arch bridge, cast-in-place. The model was used to perform a FEM analysis and allowed us to find the principal modes of vibration. Furthermore, the 3D model of a bridge of roman age was realized.

Digital Image Correlation and thermal camera were used for a laboratory test of some composite material

specimens. After a calibration procedure, the results obtained using this technique were compared with the test machine outcomes. A good agreement between test machine and DIC results was found: the differences are less than 2%.

Laser scanner and GNSS were used for modeling two landslides. By exploiting full waveform technology, the vegetation was eliminated and very accurate 3D models obtained.

The first landslide system consists of two major landslides activated in 2010. The model realized was compared to a DTM of the area, obtained in 2008. The comparison between the terrain models allowed the detection of the two landslides, their real limits and the depletion and accumulation zones. Similar results were obtained for the second landslide, sited close to the A3 motorway.

Finally, two new applications for deflection measurement of bridges under dynamic load were carried out.

The first of these is based on a laser pointer fixed to a beam of the bridge superstructure. The footprint of the laser beam, projected on a flat target, was filmed by a camera. The variable position of the footprint centroid was used to obtain information about the inclination changes of the superstructure of the bridge and, consequently, about the dynamic

deflections. The test was carried out on the bridge of the University of Calabria, during the movements of a heavy truck elevator. The results were in agreement with the theoretically predictable values; the method seems to be promising for bridge monitoring.

A procedure to measure the dynamic deformation of a structure using laser scanner was tested on two bridges. The method consists of placing a laser scanner, set up as line-scanner, under the superstructure of a bridge and on continuously acquiring a line parallel to the axis of the deck.

The first test regarded a bridge characterized by a cantilever prestressed concrete structure, with a span of 100 m. The second test was carried out on the double-deck bridge at the University of Calabria: the deflections caused by the movements of a heavy truck were monitored. The results were in agreement with the theoretically predictable values and, for the second test, they fully agree with the results obtained using the laser pointer. This method can, thus, be suitable for dynamically monitoring bridges.

Ideas for future developments

Several critical issues must be faced for the development of a methodology suitable for effectively monitoring the dynamic behavior of a bridge.

First of all, the obtained elastic lines should be exactly related to the moving loads at the moment of the single scan (load intensity, position, speed). To reach this goal, the synchronization of the laser scanner and of the instruments used to detect the position of the moving loads should be guaranteed. Timestamp should be very useful for this aim.

If the laser pointer is used, a problem to face could be the positioning on the bridge, along with the synchronization of the camera.

Other problems are due to the powering of the instruments if a continuous monitoring should be performed.

References

ABAQUS 6.14 *Analysis User's Manual*.

Abdel, M. (2011). *3d laser scanners: history, applications, and future*. http://documents.mx/documents/3d-laser-scanner-article-review.html

ASEB NRC, (1995). *The global positioning system: a shared national asset* National Academy Press, pp 284.

Achilli, V., Anzidei, M., Baldi, P., Marsella, M., Salemi, G., & Vespe, F. (1993). *The TYRGEONET project*. In Permanent Satellite Tracking Networks for Geodesy and Geodynamics (pp. 81-94). Springer Berlin Heidelberg.

Achilli, V., Carrubba, P., Fabris, M., Menin, A., & Pavanello, P. (2015). *An archival geomatics approach in the study of a landslide*. Applied Geomatics, 1-11.

Altomare, C., Artese, S., Zinno, R. (2013 a). *Un GIS per la conservazione, il monitoraggio e l'adeguamento di manufatti in zona sismica riconosciuti come Beni Culturali* - Atti 17a Conferenza Nazionale ASITA 5-7 novembre 2013 Riva del Garda

Altomare, C., Artese, S., Zinno, R. (2013 b). *A gis for the protection of cultural heritage*. Proceedings of IV Conference "Diagnosis, Conservation and Valorization of Cultural Heritage" - Naples - 12/13 December 2013 - pp 211-221 - ISBN 978-88-908168-0-2

Amenta, N., Choi, S., Dey, T. K., & Leekha, N. (2000, May). *A simple algorithm for homeomorphic surface reconstruction.* In Proceedings of the sixteenth annual symposium on Computational geometry (pp. 213-222). ACM.

Amirante, G., & Pessolano, M. R. (2005). *Immagini di Napoli e del regno: le raccolte di Francesco Cassiano de Silva.* Edizioni scientifiche italiane.

Ansioso, F., Artese, S., Magarò, F., Miceli, A., Miceli, C., Talarico, P., Venneri, A., Zagari, G., Zinno, R. (2015). *Un GIS per la conservazione e la valorizzazione dell'antica via Annia-Popilia* - GIS Day Calabria 2015 VI Edizione - ISBN: 978-88-941338-0-6

Antologia dell'Archivio Selvaggi (online), *Santa Maria de' Longobardi, detta dell'ilici,* poesia di suor Clarice Selvaggi

Arbesser-Rastburg, B. (2006). *The GALILEO single frequency ionospheric correction algorithm.* Third European Space Weather Week, 13, 17.

Archivio di Stato di Cosenza, Fondo Genio Civile, *Serie Piante e disegni, busta 5*

Archivio di Stato di Cosenza, Fondo Genio Civile, *Serie Terremoti, busta 42*

Archivio di Stato di Cosenza, *Platea del Monastero delle Clarisse del 1632*

Archivio Storico Diocesi San Marco Argentano-Scalea, *Relationes ad limina dal 1590*

Artese, G., Perrelli, M., Artese, S., Manieri, F., & Principato, F. (2013, February). *The contribute of geomatics for monitoring the great landslide of Maierato, Italy.* In International Workshop" The Role of Geomatics in Hydrogeological Risk (pp. 27-28).

Artese, G., Perrelli, M., Artese, S., Meduri, S., & Brogno, N. (2015). *POIS, a Low Cost Tilt and Position Sensor: Design and First Tests.* Sensors, 15(5), 10806-10824.

Artese, S., Altomare, C., Lerma, J., L., Zinno, R. (2014). *Terrestrial laser scanning registration analysis and its effects on a masterpiece dome.* In: EUROMED 2014 Proceedings. Cyprus, 3-8 novembre 2014

Artese, S., Miceli, A., Talarico, P., Venneri, A., Zagari, G., Zinno, R. (2015). *Ponti antichi e moderni: utilizzo di tecniche geomatiche per il rilievo, la rappresentazione e la modellazione strutturale.* Atti 19a Conferenza Nazionale ASITA, 29-30 Settembre - 1 ottobre 2015, Lecco - Polo di Lecco del Politecnico di Milano - ISBN 978-88-941232-2-7

Azhar, S., Hein, M., & Sketo, B. (2008, April). *Building information modeling (BIM): Benefits, risks and challenges.* In Proceedings of the 44th ASC National Conference.

Basov, N. G., & Prokhorov, A. M. (1955). *Possible methods of obtaining active molecules for a molecular oscillator.* Sov. Phys. JETP, 1, 184.

Bédard, Y. (2008). *Geomatics. Encyclopedia of geographical information science.* SAGE Publications, 195-97.

Bédard, Y., Gagnon, P., & Québec, Q. (1987, March). *Modernizing surveying and mapping education the baccalaureate in geomatics at laval university.* In Technical Papers, ACSM-ASPRS Annual Convention (p. 123). American Congress on Surveying and Mapping.

Beraldin, J. A. (2004). *Integration of laser scanning and close-range photogrammetry-the last decade and beyond.* In International Society for Photogrammetry and Remote Sensing.

Beraldin, J. A., Blais, F., Cournoyer, L., Rioux, M., El-Hakim, S. H., Rodella, R., ... & Harrison, N. (1999). *Digital 3D imaging system for rapid response*

on remote sites. In 3-D Digital Imaging and Modeling, 1999. Proceedings. Second International Conference on (pp. 34-43). IEEE.

Beraldin, J. A., Cournoyer, L., Rioux, M., Blais, F., El-Hakim, S., & Godin, G. (1997). *Object model creation from multiple range images: acquisition, calibration, model building and verification.*

Beraldin, J. A., Rioux, M., Cournoyer, L., Blais, F., Picard, M., & Pekelsky, J. (2007, January). *Traceable 3D imaging metrology*. In Electronic Imaging 2007(pp. 64910B-64910B-11). International Society for Optics and Photonics.

Bergevin, R., Soucy, M., Gagnon, H., & Laurendeau, D. (1996). *Towards a general multi-view registration technique.* Pattern Analysis and Machine Intelligence, IEEE Transactions on, 18(5), 540-547.

Bernardini, F., & Rushmeier, H. (2002, June). *The 3D model acquisition pipeline.* In Computer graphics forum (Vol. 21, No. 2, pp. 149-172). Blackwell Publishers Ltd.

Bernardini, F., Bajaj, C. L., Chen, J., & Schikore, D. R. (1999). *Automatic reconstruction of 3D CAD models from digital scans.* International Journal of Computational Geometry & Applications, 9(04n05), 327-369.

Bertolotti, M. (1985). *Twenty-five Years of the Laser.* Journal of Modern Optics,32(9-10), 961-980.

Besl, P. J., & McKay, N. D. (1992, April). *Method for registration of 3-D shapes.* In Robotics-DL tentative (pp. 586-606). International Society for Optics and Photonics.

Biagi, L. (2009). *I fondamentali del GPS.* Geomatics Workbooks, Vol. 8.

Biometric Data Interchange Formats-*Part 6"Iris Image Data Safety of Laser Products -Part-I Equipment Classification and User's Guide*, IEC 60582-1, (2001).

Blais, F. (2004). *Review of 20 years of range sensor development.* Journal od Electronic Imaging, 13(1).

Blais, G., & Levine, M. D. (1995). *Registering multiview range data to create 3D computer objects.* Pattern Analysis and Machine Intelligence, IEEE Transactions on, 17(8), 820-824.

Boehler, W., Vicent, M. B., & Marbs, A. (2003). *Investigating laser scanner accuracy.* The International Archives of Photogrammetry, Remote Sensing and Spatial Information Sciences, 34(Part 5), 696-701.

Bolitho, M., Kazhdan, M., Burns, R., & Hoppe, H. (2007, July). *Multilevel streaming for out-of-core surface reconstruction.* In Symposium on geometry processing (pp. 69-78).

Bolitho, M., Kazhdan, M., Burns, R., & Hoppe, H. (2009). *Parallel poisson surface reconstruction.* In Advances in Visual Computing (pp. 678-689). Springer Berlin Heidelberg.

Bornaz, L. (2006). *Principi di funzionamento e tecniche di acquisizione.* In F. Crosilla. S. Dequal Eds. - Laser scanning terrestre. (pp. 1–18). ISBN: 88-85137-19-9. UDINE: CISM (ITALY)

Bratus, A. (2015). *Monitoraggio di dissesti franosi con metodologia integrata basata sull'uso di sistema radar interferometrico terrestre (GBSAR).* ***Tesi di Dottorato.***

Bruck, H. A., McNeill, S. R., Sutton, M. A., & Peters Iii, W. H. (1989). *Digital image correlation using Newton-Raphson method of partial differential correction.* Experimental Mechanics, 29(3), 261-267.

Burrough, P. A., & McDonnell, R. A.(2011). *Principles of geographical information Systems* (Vol. 19988). Oxford University Press.

California State Department of Transportation (2011). Caltrans - *Surveys Manual "Terrestrial laser scanning specifications"*.

Cannarozzo, R., Cucchiarini, L., & Meschieri, W. (1998). *Misure, rilievo, progetto*. Zanichelli.

Carr, J. C., Beatson, R. K., Cherrie, J. B., Mitchell, T. J., Fright, W. R., McCallum, B. C., & Evans, T. R. (2001, August). *Reconstruction and representation of 3D objects with radial basis functions.* In Proceedings of the 28th annual conference on Computer graphics and interactive techniques (pp. 67-76). ACM.

Castellazzi G., D'Altri A.M., Bitelli G., Selvaggi I. and Lambertini A. (2015), *From laser scanning to finite element analysis of complex buildings by using a semi-automatic procedure*, Sensors, 15(8), 18360-18380.

Chen, Y., & Medioni, G. (1991, April). *Object modeling by registration of multiple range images.* In Robotics and Automation, 1991. Proceedings., 1991 IEEE International Conference on (pp. 2724-2729). IEEE.

Chías, P., Abad, T., Echeverría, E., Da Casa, F., & Celis, F. (2006). *A GIS in Cultural Heritage based upon multiformat databases and hypermedial personalized queries.* ISPRS Archives, 36(5), 222-226.

Chillemi, M., Giacobbe, L. (2007). *L'allineamento delle scansioni laser scanner mediante l'implementazione di un insieme ridondante di sistemi risolutivi.* 11a conferenza nazionale ASITA, 6-9 novembre 2007, Torino, Numero ISBN 978-88-903132-0-2.

Chu, T. C., Ranson, W. F., & Sutton, M. A. (1985). *Applications of digital-image-correlation techniques to experimental mechanics.* Experimental mechanics, 25(3), 232-244.

Cina, A. (2000). *GPS. Principi, modalità e tecniche diposizionamento (Vol. 1, pp. 1-126).* Celid.

Cliff, G. (1996). *Digital Photogrammetry: An Addendum to the Manual of Photogrammetry.* American Society for Photogrammetry and Remote Sensing, Bethesda, Maryland.

Cosser, E., Roberts, G. W., Meng, X., & Dodson, A. H. (2003, May). *Measuring the dynamic deformation of bridges using a total station.* In Proceeding of the 11th FIG Symposium on Deformation Measurements, Santorini, Greece (pp. 25-28).

Crosilla, F., & Beinat, A. (2003). *Tecniche avanzate di allineamento di scansioni laser. La tecnica del laser scanning: teoria e applicazioni".* International Centre for Mechanical Sciences (CISM), Udine, 75-99.

Crosilla, F., Galetto, R. (2003) *La tecnica del laser scanning. Teoria ed applicazioni*, CISM International Centre for Mechanical Sciences Udine.

Cruden, D. M., & Varnes, D. J. (1996). *Landslides: investigation and mitigation. Chapter 3-Landslide types and processes.* Transportation research board special report, (247).

Cruilles, V. S., & Monserrat, M. D. (1876). *Guía urbana de Valencia: antigua y moderna.*

Curless, B., & Levoy, M. (1996, August). *A volumetric method for building complex models from range images.* In Proceedings of the 23rd annual conference on Computer graphics and interactive techniques (pp. 303-312). ACM.

Curless, B., & Levoy, M. (1996, August). *A volumetric method for building complex models from range images.* In Proceedings of the 23rd annual conference on Computer graphics and interactive techniques (pp. 303-312). ACM.

Davis, J., Marschner, S. R., Garr, M., & Levoy, M. (2002, June). *Filling holes in complex surfaces using volumetric diffusion.* In 3D Data Processing

Visualization and Transmission, 2002. Proceedings. First International Symposium on (pp. 428-441). IEEE.

De Agostino, M., Lingua, A., & Piras, M. (2012). *Rock face surveys using a LiDAR MMS.* Ital. J. Remote Sens, 44, 141-151.

Delingette, H., Hebert, M., & Ikeuchi, K. (1991, June). *Shape representation and image segmentation using deformable surfaces.* In Computer Vision and Pattern Recognition, 1991. Proceedings CVPR'91., IEEE Computer Society Conference on (pp. 467-472). IEEE.

Detchev, I., Habib, A., & El-Badry, M. (2011, May). *Case study of beam deformation monitoring using conventional close range photogrammetry.* In ASPRS 2011 Annual Conference. Milwaukee, Wisconsin.

Dey, T. K., & Giesen, J. (2003). *Detecting undersampling in surface reconstruction.* In Discrete and Computational Geometry (pp. 329-345). Springer Berlin Heidelberg.

Di Salvo, A. F., Giuffrè, O., & Brutto, D. M. L. (2014). *Il laser scanner terrestre e la tecnologia full waveform per la modellazione tridimensionale in ambito geologico.* Tesi di Dottorato.

Dorai, C., Weng, J., & Jain, A. K. (1997). *Optimal registration of object views using range data.* Pattern Analysis and Machine Intelligence, IEEE Transactions on, 19(10), 1131-1138.

Eastman, C., Teicholz, P., Sacks, R., & Liston, K. (2011). *BIM handbook: A guide to building information modeling for owners, managers, designers, engineers and contractors.* Wiley. com.

Ebner, H., Fritsch, D., & Heipke, C. (1991). *Digital photogrammetric systems* (p.344). Wichmann.

Edelsbrunner, H. (1998). *Shape reconstruction with Delaunay complex.* In LATIN'98: Theoretical Informatics (pp. 119-132). Springer Berlin Heidelberg.

Eggert, D. W., Fitzgibbon, A. W., & Fisher, R. B. (1998). *Simultaneous registration of multiple range views for use in reverse engineering of CAD models.* Computer Vision and Image Understanding, 69(3), 253-272.

Einstein, A. (1917). *Zur quantentheorie der strahlung.* Physikalische Zeitschrift,18, 121-128.

El-Hakim, S. F., Beraldin, J. A., & Blais, F. (1995, December). *Comparative evaluation of the performance of passive and active 3D vision systems.* In Digital Photogrammetry and Remote Sensing'95 (pp. 14-25). International Society for Optics and Photonics.

El-Hakim, S. F., Beraldin, J. A., Picard, M., & Godin, G. (2004). *Detailed 3D reconstruction of large-scale heritage sites with integrated techniques.* Computer Graphics and Applications, IEEE, 24(3), 21-29.

Fabado, S., Seguí, A. E., Cabrelles, M., Navarro, S., García-De-San-Miguel, D., & Lerma, J. L. (2013). *3DVEM Software Modules for Efficient Management of Point Clouds and Photorealistic 3d Models.* ISPRS-International Archives of the Photogrammetry, Remote Sensing and Spatial Information Sciences, 1(2), 255-260.

Fabris, M., Menin, A., & Achilli, V. (2011). *Landslide displacement estimation by archival digital photogrammetry*. Italian Journal of Remote Sensing, 43(2), 23-30.

Ferrero A. M., Migliazza M., Roncella R., Rabbi E. (2011). *Rock slopes risk assessment based on advanced geo structural survey techniques*. Landslides, 8: 221-231.

Fidler, J. (1980). *Non-destructive surveying techniques for the analysis of historic buildings.* Transactions of the Association for

Studies in the Conservation of Historic Buildings, 5, 3-10.

Fleishman, A. I. (1978). A method for simulating non-normal distributions.Psychometrika, 43(4), 521-532.

Fuchs, P.A., Washer, G.A., Chase, S.B., and Moore, M. (2004), *Applications of Laser-Based Instrumentation for Highway Bridges*, Journal of Bridge Engineering , ASCE, November/December, pp. 541-549.

Gagnon, P., & Coleman, D. J. (1990). *La géomatique: une approche systémique intégrée pour répondre aux besoins d'information sur le territoire*. Journal of the Canadian Institute of Surveying and Mapping, 44(4), 377-389.

Gairns, C. (2008). *Development of a semi-automated system for structural deformation monitoring using a reflectorless total station*. In Masters Abstracts International (Vol. 48, No. 06)

George P.L., Borouchaki H. (1998), *Delaunay triangulation and Meshin*, Paris, Editions Hermes.

Ghilani, C. D., & Wolf, P. R. (2011). *Elementary Surveying: An Introduction to Geomatics.* ISBN-10, 132554348.

Gili, J. A., Corominas, J., & Rius, J. (2000). *Using Global Positioning System techniques in landslide monitoring.* Engineering Geology, 55(3), 167-192.

Glabsch, J., Heunecke, O., & Schuhbäck, S. (2009). *Monitoring the Hornbergl landslide using a recently developed low cost GNSS sensor network.* Journal of Applied Geodesy, 3(3), 179-192.

Godin, G., Beraldin, J. A., Rioux, M., Levoy, M., & Cournoyer, L. (2001). *An assessment of laser range measurement of marble surfaces.* Proc. Fifth Conference on optical 3-D measurement techniques, Vienna, 2001

Gomarasca, M. A. (2009). *Basics of geomatics.* Springer Science & Business Media.

Gomes, J., & Faugeras, O. (2000). *Reconciling distance functions and level sets.* Journal of Visual Communication and Image Representation, 11(2), 209-223.

Gomes, L., Bellon, O. R. P., & Silva, L. (2014). *3D reconstruction methods for digital preservation of cultural heritage: A survey.* Pattern Recognition Letters,50, 3-14.

Gómez, J. B. (1987). *Los comienzos de la arquitectura académica en Valencia: Antonio Gilabert.*

Gopi, S. (2007). *Advanced Surveying: Total Station, GIS and Remote Sensing.* Pearson Education India.

Gordon, J. P., Zeiger, H. J., & Townes, C. H. (1955). *The maser—new type of microwave amplifier, frequency standard, and spectrometer.* Physical Review,99(4), 1264.

Gressin, A., Mallet, C., & David, N. (2012). *Improving 3D Lidar point cloud registration using optimal neighborhood knowledge.* ISPRS Annals of Photogrammetry, Remote Sensing and Spatial Information Sciences I-3, 111-116.

Gressin, A., Mallet, C., Demantké, J., & David, N. (2013). *Towards 3D lidar point cloud registration improvement using optimal neighborhood knowledge.* ISPRS Journal of Photogrammetry and Remote Sensing, 79, 240-251.

Grinzato, E. (2012, April). *IR thermography applied to the cultural heritage conservation.* In 18th World Conference on Nondestructive Testing.

Guidi, G., Russo, M., & Beraldin, J. A. (2010). *Acquisizione 3D e modellazione poligonale.* McGraw-Hill, pp 480.

Hammoudi, K., & Dornaika, F. (2010). *A featureless approach to 3D polyhedral building modeling from aerial images.* Sensors, 11(1), 228-259.

Haralick, R. M., Joo, H., Lee, C. N., Zhuang, X., Vaidya, V. G., & Kim, M. B. (1989). *Pose estimation from corresponding point data. S*ystems, Man and Cybernetics, IEEE Transactions on, 19(6), 1426-1446.

Highland, L. (2004). *Landslide types and processes* (No. 2004-3072).

Hild, F., & Roux, S. (2006). *Digital image correlation: from displacement measurement to identification of elastic properties – a review.* Strain, 42(2), 69-80.

Hill, C. D. and Sippel, K. D. (2002). *Modern Deformation Monitoring: A Multi Sensor Approach.* FIG XXII International Congress, Washington DC, USA, pp.

Hoffmann-Wellenhof, B., Lichtenegger, H., & Collins, J. (1994). *GPS: theory and practice.* 3rd ed. Springer-Verlag, New York.

Hoffmeister, D., Tilly, N., Curdt, C., Aasen, H., Ntageretzis, K., Hadler, H., ... & Bareth, G. (2012). *Terrestrial laser scanning for coastal geomorphologic research in Western Greece.* Int Arch Photogramm Remote Sens Spat Inf Sci,39(B5), 511-516.

Horn, B. K. (1987). *Closed-form solution of absolute orientation using unit quaternions.* JOSA A, 4(4), 629-642.

Horn, B. K., Hilden, H. M., & Negahdaripour, S. (1988). *Closed form solutions of absolute orientation using orthonormal matrices.* Journal of the Optical Society A, 5(7), 1127-1135.

Hornung, A., & Kobbelt, L. (2006, June). *Robust reconstruction of watertight 3D models from non-uniformly sampled point clouds without normal information.* In Symposium on Geometry Processing (pp. 41-50).

Hug, C., Ullrich, A., & Grimm, A. (2004). *Litemapper-5600-a waveform-digitizing LiDAR terrain and vegetation mapping system.* International Archives of

Photogrammetry, Remote Sensing and Spatial Information Sciences, 36(Part 8), W2.

Hum-Hartley, S. (1978). *Nondestructive Testing for Heritage Structures.* Bulletin of the Association for Preservation Technology, 4-20.

Javan, A., Bennett Jr, W. R., & Herriott, D. R. (1961). *Population inversion and continuous optical maser oscillation in a gas discharge containing a He-Ne mixture.* Physical Review Letters, 6(3), 106.

Jaw, J. J., & Chuang, T. Y. (2008). *Registration of ground-based LiDAR point clouds by means of 3D line features.* Journal of the Chinese Institute of Engineers, 31(6), 1031-1045.

Johnson, A. E., & Kang, S. B. (1997, May). *Registration and integration of textured 3-D data.* In 3-D Digital Imaging and Modeling, 1997. Proceedings., International Conference on Recent Advances in (pp. 234-241). IEEE.

Kaplan, E., & Hegarty, C. (Eds.). (2005). *Understanding GPS: principles and applications.* Artech house.

Karbacher, S., Laboureux, X., Schön, N., & Häusler, G. (2001). *Processing range data for reverse engineering and virtual reality.* In 3-D Digital Imaging and Modeling, 2001. Proceedings. Third International Conference on (pp. 314-321). IEEE.

Kasperski, J., Delacourt, C., Allemand, P., Potherat, P., Jaud, M., & Varrel, E. (2010). *Application of a terrestrial laser scanner (TLS) to the study of the Séchilienne Landslide (Isère, France).* Remote Sensing, 2(12), 2785-2802.

Kazhdan, M., Bolitho, M., & Hoppe, H. (2006, June). *Poisson surface reconstruction.* In Proceedings of the fourth Eurographics symposium on Geometry processing (Vol. 7).

Kemp, K. (2008). *Encyclopedia of geographic information science.* Sage.

Kersten, T. P., & Lindstaedt, M. (2012). *Image-based low-cost systems for automatic 3D recording and modelling of archaeological finds and objects.* In: Progress in cultural heritage preservation (pp. 1-10). Springer Berlin Heidelberg.

Kimura, H., & Yamaguchi, Y. (2000). *Detection of landslide areas using satellite radar interferometry.* Photogrammetric Engineering and Remote Sensing, 66(3), 337-344.

Klobuchar, J. (1987). *Ionospheric time-delay algorithm for single-frequency GPS users.* Aerospace and Electronic Systems, IEEE Transactions on, (3), 325-331.

Kolluri, R., Shewchuk, J. R., & O'Brien, J. F. (2004, July). *Spectral surface reconstruction from noisy point clouds.* In Proceedings of the 2004 Eurographics/ACM SIGGRAPH symposium on Geometry processing, pp. 11-21. ACM.

Kraus K., 1994. Photogrammetry Vol. I, Fundamentals and Standard Processes, Dümmler/Bonn, ISBN 3-427-78684-6.

Kuhlmann, H. and Glaser, A. (2002). *Investigation of New Measurement Techniques for Bridge Monitoring.* 2nd Symposium on Geodesy for Geotechnical and Structural Engineering, Berlin, Germany, pp.123-132.

Leick, A. (2004). *GPS satellite surveying.* John Wiley & Sons, 2004 – pp. 435.

Lerma, J. L., Navarro, S., Cabrelles, M., & Villaverde, V. (2010). *Terrestrial laser scanning and close range photogrammetry for 3D archaeological documentation: the Upper Palaeolithic Cave of Parpalló as a case study.* Journal of Archaeological Science, 37(3), 499-507.

Li Z., Zhu Q., Gold C. (2010), *Digital Terrain Modeling: principles and methodology*. CRC Press, Boca Raton. ISBN 0203486749, 9780203486740.

Li, Z., Chen, J., & Baltsavias, E. (Eds.). (2008). *Advances in photogrammetry*. Remote sensing and

spatial information sciences: 2008 ISPRS congress book(Vol. 7). CRC Press.

Lichti, D. D., & Harvey, B. R. (2002). *The effects of reflecting surface material properties on time-of-flight laser scanner measurements.* Symposium on Geospatial Theory, Processing and Applicatons.tc,2, 1.

Lingua, A., Piatti, D., & Rinaudo, F. (2008). *Remote monitoring of a landslide using an integration of GB-INSAR and LIDAR techniques.* The international archives of the photogrammetry, remote sensing and spatial information sciences, 37, 133-139.

Lorensen, W. E., & Cline, H. E. (1987, August). *Marching cubes: A high resolution 3D surface construction algorithm.* In ACM siggraph computer graphics (Vol. 21, No. 4, pp. 163-169). ACM.

Low, K. L. (2004). *Linear least-squares optimization for point-to-plane icp surface registration.* Chapel Hill, University of North Carolina.

Lubowiecka, I.; Armesto, J.; Arias, P.; Lorenzo, H. (2009) *Historic bridge modelling using laser scanning, ground penetrating radar and finite element methods in the context of structural dynamics.* Engineering Structures, 31, 2667-2676.

Magarò, F., Ietto, F., Ponte, M. (2012), *Studio di un versante in frana in località "Vermicelli" di Rende (CS)*. Tesi di laurea Università della calabria A.A. 2011-2012

Maiman, T. H. (1960). *Stimulated optical radiation in ruby.*

Mallet, C., & Bretar, F. (2009). *Full-waveform topographic lidar: State-of-the-art.* ISPRS Journal of photogrammetry and remote sensing, 64(1), 1-16.

Masuda, T., Sakaue, K., & Yokoya, N. (1996, August). *Registration and integration of multiple range images for 3-D model construction.* In Pattern

Recognition, 1996., Proceedings of the 13th International Conference on (Vol. 1, pp. 879-883). IEEE.

Meli, A. P., Giuffrè, O., & Brutto, D. M. L. (2014). *La ricostruzione 3d in ambito archeologico e possibile utilizzo nel campo delle infrastrutture stradali: analisi delle potenzialita'delle tecniche image-based.* (Tesi di dottorato, Università degli Studi di Palermo, 2014).

Mikhail, E. M., Bethel, J. S., & McGlone, J. C. (2001). *Introduction to modern photogrammetry (Vol. 1).* John Wiley & Sons Inc.

Monti, C., Guerra, F., Balletti, C., & Miniutti, D. (1999). *Geometric operations in digital images.* In Proceedings of XVI International Symposium CIPA. Olinda, Brazil.

Neugebauer, P. J. (1997). *Reconstruction of real-world objects via simultaneous registration and robust combination of multiple range images.* International journal of shape modeling, 3(01n02), 71-90.

Ohtake, Y., Belyaev, A., Alexa, M., Turk, G., & Seidel, H. P. (2005, July). *Multi-level partition of unity implicits.* In ACM SIGGRAPH 2005 Courses (p. 173). ACM.

Pacichelli, G. B. (1702). *Il Regno di Napoli in prospettiva* (No. 150). A. Forni.

Pan, B., Qian, K., Xie, H., & Asundi, A. (2009). *Two-dimensional digital image correlation for in-plane displacement and strain measurement: a review.* Measurement science and technology, 20(6), 062001.

Paradis, M. (1981). *De l'arpentage à la géomatique (From Surveying to Geomatics).* The Canadian Surveyor, 35(3), 262-268.

Pavlopoulos K., Evelpidou N., Vassilopoulos A. (2009), *Mapping geomorphological environments.* Springer, Berlino. ISBN 978-3-642-01950-0.

Pentland, A., & Sclaroff, S. (1991). *Closed-form solutions for physically based shape modeling and recognition.* IEEE Transactions on Pattern Analysis & Machine Intelligence, (7), 715-729.

Pfennigbauer, M., & Ullrich, A. (2008, April). *Three-dimensional laser scanners with echo digitization.* In SPIE Defense and Security Symposium (pp. 69500U-69500U). International Society for Optics and Photonics.

Pike R. J., Evans I. S., Hengl T. (2009), *Geomorphometry: a brief guide*, in Hengl T., Reuter H. I. (a cura di), Geomorphometry: concepts, software, applications, Elsevier, Amsterdam: 3-30. ISBN 0123743451, 780123743459.

Pirotti, F., Guarnieri, A., & Vettore, A. (2013). *State of the art of ground and aerial laser scanning technologies for high-resolution topography of the earth surface.* European Journal of Remote Sensing, 46, 66-78.

Pirotti, F., Guarnieri, A., & Vettore, A. (2013). *Vegetation filtering of waveform terrestrial laser scanner data for DTM production.* Applied Geomatics, 5(4), 311-322.

Pulli, K. (1999). *Multiview registration for large data sets.* In 3-D Digital Imaging and Modeling, 1999. Proceedings. Second International Conference on (pp. 160-168). IEEE.

Remondino, F. (2003). *From point cloud to surface. International Workshop on Visualization and Animation of Reality-Based 3D Models*. 24-28 February 2003, Tarasp-Vulpera.

Remondino, F., & El-Hakim, S. (2006). *Image-based 3D Modelling: A Review.* The Photogrammetric Record, 21(115), 269-291.

Remondino, F., & Fraser, C. (2006). *Digital camera calibration methods: considerations and comparisons.* International Archives of Photogrammetry, Remote

Sensing and Spatial Information Sciences, 36(5), 266-272.

Remondino, F., Gruen, A., von Schwerin, J., Eisenbeiss, H., Rizzi, A., Girardi, S., ... & Richards-Rissetto, H. (2009, October). *Multi-sensor 3D documentation of the Maya site of Copan.* In 22nd CIPA Symposium, Kyoto, Japan (131-1).

Remondino, F., Guarnieri, A., & Vettore, A. (2005, January). *3D modeling of close-range objects: photogrammetry or laser scanning.* In Electronic Imaging 2005, pp. 216-225. International Society for Optics and Photonics.

Rocchini, C., Cignoni, P., Ganovelli, E., Montani, C., Pingi, P., & Scopigno, R. (2001, May). *Marching intersections: an efficient resampling algorithm for surface management.* In Shape Modeling and Applications, SMI 2001 International Conference on. pp. 296-305. IEEE.

Romsek, B. R. (2008). *Terrestrial laser scanning: Comparison of time-of-flight and phase based measuring systems*. MSc Dissertation AAI1469768 Purdue University.

Roth, G. (1999). *Registering two overlapping range images.* NRC Publications Archive (NPArC)

RUDOLF, S. (2011). *10 years of terrestrial laser scanning-technology,systems and applications.* ИНТЕРЭКСПО ГЕО-СИБИРЬ.

Ruggiero, C., Gallo, A., Lio, A., Zappani, A., Fortunato, G., & Muzzupappa, M. (2012). *An Integrated Methodology for the Digitization, Survey and Visualization of Santa Maria Patirion's Church.* International Journal of Heritage in the Digital Era, 1(Supplement 1), 21-26.

Russo, M., Remondino, F., & Guidi, G. (2011). *Principali tecniche e strumenti per il rilievo tridimensionale in ambito archeologico.* Archeologia e Calcolatori, 22, 169-198.

Rüther, H., Held, C., Bhurtha, R., Schroeder, R., & Wessels, S. (2014). *From Point Cloud to Textured the Zamani Laser Scanning Pipeline in Heritage Documentation.* South African Journal of Geomatics, 1(1), 44-59.

S. Cristofaro (1932), *Cronistoria della città di San Marco.*

Saastamoinen, J. (1972). *Atmospheric correction for the troposphere and stratosphere in radio ranging satellites.* The use of artificial satellites for geodesy, 247-251.

Sagawa, R., & Ikeuchi, K. (2008). *Hole filling of a 3D model by flipping signs of a signed distance field in adaptive resolution.* Pattern Analysis and Machine Intelligence, IEEE Transactions on, 30(4), 686-699.

Saygi, G., Agugiaro, G., Hamamcıoğlu-Turan, M., Remondino, F. (2013). *Evaluation of GIS and BIM roles for the information management of historical buildings.* XXIV International CIPA Symposium.

Scaioni M., Alba M. (2010), *Understanding changes and deformations on multi temporal rock face point clouds.* International Archives of Photogrammetry and Remote Sensing, 38 (3A): 67-72.

Scaioni, M., Feng, T., Barazzetti, L., Previtali, M., Lu, P., Qiao, G., ... & Li, R. (2014). *Some applications of 2-D and 3-D photogrammetry during laboratory experiments for hydrogeological risk assessment*. Geomatics, Natural Hazards and Risk, (ahead-of-print), 1-24.

Schawlow, A. L., & Townes, C. H. (1958). *Infrared and optical masers.* Physical Review, 112(6), 1940.

Schutz, C., Jost, T., & Hugli, H. (1998, August). *Multi-feature matching algorithm for free-form 3D surface registration.* In Pattern Recognition, 1998. Proceedings. Fourteenth International Conference on (Vol. 2, pp. 982-984). IEEE.

Schwarz, K. P., Martell, H. E., El-Sheimy, N., Li, R., Chapman, M. A., & Cosandier, D. (1993, October). *VIASAT-A mobile highway survey system of high accuracy.* In Vehicle Navigation and Information Systems Conference, 1993., Proceedings of the IEEE-IEE (pp. 476-481). IEEE.

Selvini, A. (1988). *Principi di fotogrammetria*. Clup.

Sgrenzaroli, M., & Vassena, G. (2007). *Tecniche di rilevamento tridimensionale tramite laserscanner.* Brescia, Starrylink Editrice.

Slob S., Hack R., Van Knappen B., Kemeny J. (2004), *Automated identification and characterization of discontinuity sets in outcropping rock masses using 3D terrestrial laser scan survey techniques*. EUROCK 2004 & 53rd Geomechanics Colloquium, 7-9 ottobre, Salisburgo: 439-443.

Smith, D. K., & Tardif, M. (2012). *Building information modeling: a strategic implementation guide for architects, engineers, constructors, and real estate asset managers.* John Wiley & Sons.

Soprintendenza B.A.P. delle Province di Cosenza, Catanzaro e Crotone, *Progetti e disegni*.

Soucy, M., & Laurendeau, D. (1995). *A general surface approach to the integration of a set of range views.* Pattern Analysis and Machine Intelligence, IEEE Transactions on, 17(4), 344-358.

Spaans, J. A. (1984). *Navigation by satellite timing and ranging: Global Positioning System (GPS) NAVSTAR.* NASA STI/Recon Technical Report N,86, 20467.

Stiros, S. C., Vichas, C., & Skourtis, C. (2004). *Landslide monitoring based on geodetically derived distance changes.* Journal of surveying engineering, 130(4), 156-162.

Stoddart, A. J., & Hilton, A. (1996, August). *Registration of multiple point sets.* In Pattern Recognition, 1996., Proceedings of the 13th International Conference on (Vol. 2, pp. 40-44). IEEE.

Sui, L., Wang, X., Zhao, D., & Qu, J. (2008). *Application of 3D laser scanner for monitoring of landslide hazards.* The International Archives of the Photogrammetry, Remote Sensing and Spatial Information Sciences, 37.

Tao, C. V., & Li, J. (Eds.). (2007). *Advances in mobile mapping technology.* CRC Press.

Tarchia, D., Casagli, N., Fanti, R., Leva, D. D., Luzi, G., Pasuto, A.,... & Silvano, S. (2003). *Landslide monitoring by using ground-based SAR interferometry: an example of application to the Tessina landslide in Italy.* Engineering Geology, 68(1), 15-30.

Terzopoulos, D., Witkin, A., & Kass, M. (1988). *Constraints on deformable models: Recovering 3D shape and nonrigid motion.* Artificial intelligence, 36(1), 91-123.

Trainer, M. (2010). *The 50th anniversary of the laser.* World Patent Information,32(4), 326-330.

Tsai, Z. X., You, G. J. Y., Lee, H. Y., & Chiu, Y. J. (2012). *Use of a total station to monitor post-failure sediment yields in landslide sites of the Shihmen reservoir watershed, Taiwan.* Geomorphology, 139, 438-451.

Tsui, J. B. Y. (2000). *Fundamentals of global positioning system receivers.* Wiley-Interscience.

Turk, G., & Levoy, M. (1994, July). *Zippered polygon meshes from range images.* In Proceedings of the 21st annual conference on Computer graphics and interactive techniques (pp. 311-318). ACM.

Ullrich, A., Studnicka, N., Hollaus, M., Briese, C., Wagner, W., Doneus, M., & Mücke, W. (2007, December). *Improvements in DTM generation by using full-waveform airborne laser scanning data.* In 7Th International Conference On Laser Scanning and Digital Aerial Photography. Today And Tomorrow, Moscow, Russia (Vol. 6, pp. 2007-07).

Van der Marel, D. H. (2000). *US Discontinue Intentional Degrading of GPS.* GIM International, June, 51-53.

Van Sickle, J. (2008). *GPS for land surveyors.* Crc Press.

Varnes, D. J. (1978). *Slope movement types and processes.* Transportation Research Board Special Report, (176).

Vendroux, G., & Knauss, W. G. (1998). *Submicron deformation field measurements: Part 2.* Improved digital image correlation. Experimental Mechanics, 38(2), 86-92.

Verdú, R. S. (1996, September). *Cúpulas en la arquitectura valenciana de los siglos XVI a XVIII.* In Actas del Primer Congreso Nacional de Historia de la Construcción (Vol. 19, p. 21).

Verdú, R. S., Pérez, L. P., & Chapapría, J. E. (1995). *La cúpula en la arquitectura moderna valenciana, siglos XVI a XVIII, metodologías de estudios previos para las arquitecturas de sistemas abovedados.* Universidad Politécnica de Valencia.

Voegtle, T., Schwab, I., & Landes, T. (2008, July). *Influences of different materials on the measurements of a terrestrial laser scanner (TLS).* In Proc. of the XXI Congress, The International Society for Photogrammetry and Remote Sensing, ISPRS2008 (Vol. 37, pp. 1061-1066).

Voltolini, F., Rizzi, A., Remondino, F., Girardi, S., & Gonzo, L. (2007). *Integration of non-invasive techniques for documentation and preservation of complex architectures and artworks.* In Proc. Proc. of 2nd ISPRS International Workshop 3D-ARCH.

Vosselman, G., Gorte, B. G., Sithole, G., & Rabbani, T. (2004). *Recognising structure in laser scanner point clouds.* International archives of photogrammetry, remote sensing and spatial information sciences, 46(8), 33-38.

Wells, D. (1987). *Guide to GPS positioning, Canadian GPS Associates, New Brunswick, Canada.* For many years the only text for GPS.

Wheeler, M. D., Sato, Y., & Ikeuchi, K. (1998, January). *Consensus surfaces for modeling 3D objects from multiple range images.* In Computer Vision, 1998. Sixth International Conference on (pp. 917-924). IEEE.

Wheeler, M. D., Sato, Y., & Ikeuchi, K. (1998, January). *Consensus surfaces for modeling 3D objects from multiple range images.* In Computer Vision, 1998. Sixth International Conference on (pp. 917-924). IEEE.

Whitaker, R. T. (1998). *A level-set approach to 3D reconstruction from range data.* International journal of computer vision, 29(3), 203-231.

Wittfoht, H. (1983). *Ursachen für den Teil-Einsturz des" Viadotto Cannavino" bei Agro di Celico.* Beton- und Stahlbetonbau, 78(2), 29-36.

Yilmaz, H. M., Yakar, M., Gulec, S. A., & Dulgerler, O. N. (2007). *Importance of digital close-range photogrammetry in documentation of cultural heritage.* Journal of Cultural Heritage, 8(4), 428-433.

Yoneyama, S., & Ueda, H. (2012). *Bridge deflection measurement using digital image correlation with camera movement correction.* Materials Transactions, 53(2), 285-290.

Yu, Y., Liu, H., Li, D., Mao, X., & Ou, J. (2013). *Bridge deflection measurement using wireless mems inclination sensor systems.* International Journal on Smart Sensing & Intelligent Systems, 6(1).

Zhang, Z. (1994). *Iterative point matching for registration of free-form curves and surfaces.* International journal of computer vision, 13(2), 119-152.

Zhang, Z. (2000). *A flexible new technique for camera calibration.* Pattern Analysis and Machine Intelligence, IEEE Transactions on, 22(11), 1330-1334.

Zogg, H.M., and Ingensand, H. (2008), *Terrestrial Laser Scanning for Deformation Monitoring –Load Tests on the Felsenau Viaduct (CH).* The International Archives of the Photogrammetry, Remote Sensing and Spatial Information Sciences, Volume XXXVII, Part B5, pp. 555-562.

http://www.correlatedsolutions.com/vic-2d/-(accessed 15-11-2015)

http://www.gps.gov/ -(accessed 15-11-2015)

http://www.gps.gov/systems/gps/control/-(accessed 15-11-2015)

http://www.gsa.europa.eu/ -(accessed 15-11-2015)

http://www.navipedia.net/index.php/GLONASS_Ground_Segment - accessed 15-11-2015 -(accessed 15-11-2015)

https://www.glonass-iac.ru/ - (accessed 15-11-2015)

MLA style: "The Nobel Prize in Physics 1964". Nobelprize.org. Nobel Media AB 2014. Web. 23 Oct *2015.http://www.nobelprize.org/nobel_prizes/physics/laureates/1964/-(accessed 15-11-2015)*

MLA style: "The Nobel Prize in Physics 1981". Nobelprize.org. Nobel Media AB 2014. Web. 24 Oct *2015.http://www.nobelprize.org/nobel_prizes/physics/laureates/1981/-(accessed 15-11-2015)*

Riegl Laser Measurement Systems GmbH (2012a), Training materials - Terrestrial scanning. *http://www.riegl.com/members-area/training-materials/terrestrial-scanning//-(accessed 15-11-2015)*

Acknowledgement

I would like to express my thanks to my Supervisor, Prof. Ing Raffaele Zinno for giving me this great opportunity. His support and assistance made it possible to achieve my goal. I would also like to thank SMARTLab (Structural Monitoring, Structural Advanced Materials, Structural Rehabilitation, Structural Testing) at the University of Calabria, for giving me technical and scientific support, for the valuable help of all provided during my research and specially for theor friendship. I would like to thank Ing. PhD Chiara Altomare for the collaboration during the survey of the the Escuelas Pias Church; Ing. Angela Miceli, Paolo Talarico, and Assunta Venneri for the realization of FRC specimens and collaboration during the survey; the mechanics laboratory of Unical for the tests; Ing. PhD Giuseppe Zagari for the finite element modeling of the Caprovidi bridge; Dott. Chiara Miceli for the historical research on the church of Santa Maria dei Longobardi and Dott. Floriana Magarò for the geological investigations on the Vermicelli Landslide.

I would like to express my gratitude to Prof. Josè Luis Lerma Garcìa and to GIFLE (Grupo de Investigación en Fotogrametría y Láser Escáner) for hosting, advice and software development at the Polytechnic University of Valencia, as well as Prof. Juan B. Aznar and Father Antonio for managing the survey inside the Escuelas Pias church.

Thanks to Geom. Antonio Gervasi, for his help during the survey of Cannavino Bridge.

Thanks to Prof. Michael Cronin, my English teacher, for the language support.

Thanks to the 3DReshaper, Hexagon Group, and the VIC-2D™, Correlated Solutions, for the temporary license given to me.

Thanks to Michele Perrelli and Sebastiano Meduri for their unvaluable work with Matlab®, as well as Spring Research (Giuseppe Artese, Sebastiano Meduri, Francesco Muto, Michele Perrelli, Andrea Solano) for outstanding help given to me as partners and as friends.

Thanks to Ingeos Consulting for their kindness and comprehension.

Special thanks to Mom and Dad, my Sister and Davide, my grandparents, Valentino, without whom I am nothing, and my friends for their support and for always believing in me.